Design of Fixed Order Nonsmooth Robust H_∞ MIMO Wide Area Controller for Damping of Inter Area Oscillations in Power Grids

Von der Fakultät für Ingenieurwissenschaften,
Abteilung Elektrotechnik und Informationstechnik
der Universität Duisburg-Essen

zur Erlangung des akademischen Grades

Doktor der Ingenieurwissenschaften (Dr.-Ing.)

genehmigte Dissertation

von

Mahshid Maherani
aus
Esfahan, Iran

1. Gutachter: Prof. Dr.-Ing. habil. Gerhard Krost
2. Gutachter: Prof. Dr.-Ing. S. X. Ding
Tag der mündlichen Prüfung: 21.10.2019

ABSTRACT

Oscillatory stability control for power systems has become more important since low frequency inter area oscillations are often poorly damped due to increasing load demand and growing penetration levels of renewable energy sources, during transient and dynamic conditions. Undesirable power system states such as tripping of transmission lines, generation sources and loads, can lead to cascaded outages and blackouts in interconnected grid. The developed robust control theories in one side and wide-area measurement technologies in the other side make the wide area real time feedback control potentially promising for cascade outages prohibition. This research is to develop a systematic procedure of designing damping control system for interconnected power grid by applying Wide Area Measurement (WAM) and robust control techniques while putting emphasis on several practical considerations.

The following objectives of research are achieved in this thesis:

- Design of fixed order wide area damping controller:

This thesis presents the design of Multi Input, Multi Output (MIMO) fixed order non-smooth robust H_∞ wide area damping controller for supressing power oscillations and stabilizing the multi machine power system. Due to the restricted accuracy of classical local damping controllers to a neighbourhood of the operating point, robust controllers are considered. In order to reduce the computational complexity of the control design and the order of the synthesized controller, instead of reduction of the number of states, this research focused on design of fixed order controller that does not need to reduce the order of controller later. Fixed order is a restricted structural constraint on the controller. The proposed method is based on shaping of the open loop transfer function in the frequency domain. Nonsmooth optimization techniques are used to H_∞ synthesis problem under additional structural constraints (fixed order) on the controller. This approach avoids using Lyapunov variables and therefore leads to moderate size optimization programs even for very large systems.

- Consideration on power system uncertainties:

Because of different uncertainties in power system like variant generation and consumption, grid topology, load patterns and load type (dynamic, static), neglected high frequency dynamics and invalid assumptions made in the modelling process, robust controllers are used to damp power oscillations. These uncertainties directly determine the stability margin of the operating point. Power system model with these types of uncertainties is named multi model. The effect of uncertainties is considered by unstructured uncertainty. The unstructured uncertainty is considered as a weighting function. The weighting function is a fixed stable transfer function,

which contains the features of the highlighted range of frequency for multi model. In this research, rang of inter-area frequency (less than 1 Hz) will be considered for uncertain weighting function. Furthermore, wide area controls have communication links, which cause time delay uncertainty, which is considered as parametric uncertainty.

- Proper controller architecture:

Centralized and decentralized architectures were implemented to evaluate the efficient and reasonable performance and stability of controllers. In this work, the selection of the nominal model and the application of specific stability and performance criteria play an important role in the definition of the correct controller structure.

- Reserved input and output channels for centralized controller:

This study deals with centralized controller, which has some reserve input and output channels to deal with possible communication dropouts. The proposed controller can damp oscillations while some input or/and output signals are interrupted.

ABSTRAKT

Die Kleinsignalstabilität elektrischer Übertragungsnetze wird zunehmend wichtiger, da niederfrequente inter-area modes aufgrund eines steigenden Lastbedarfs und eines zunehmenden Durchdringungsgrades erneuerbarer Energiequellen, während transienter und dynamischer Bedingungen, oft schlecht gedämpft werden. Unerwünschte Systemzustände elektrischer Übertragungsnetze, die zum Auslösen der Schutzeinrichtungen von Übertragungsleitungen, Erzeugungsanlagen und Lasten führen, können im Verbundnetz kaskadiert auftreten und damit zum Systemzusammenbruch dem sogenannten Blackout führen. Die Methoden der Robusten Regelung auf der einen Seite und die Verfügbarkeit von Wide-Area-Measurement (WAM) Feld-Messdaten auf der anderen Seite, ermöglichen den Einsatz im Feld gewonnener Messdaten zur Bildung geschlossener Regelkreise. Diese Arbeit stellt ein systematisches Verfahren zum Entwurf eines Wide Area Damping Control (WADC) Systems für elektrische Übertragungsnetze unter Verwendung von Wide Area Measurement Messdaten und einer Robusten Regelung, unter Berücksichtigung mehrerer praktischer Überlegungen vor.

In dieser Arbeit werden folgende Forschungsziele erreicht:
- Entwurf eines „Wide Area Damping“ Reglers mit fester Ordnung:
Diese Dissertation präsentiert das Design eines robusten non-smooth Multi-Input Multi-Output (MIMO) H_∞ WADC zur Dämpfung niederfrequenter inter-area Modes in elektrischen Übertragungsnetzen. Aufgrund der eingeschränkten Genauigkeit klassischer lokaler Dämpfungsregler auf eine Umgebung des Arbeitspunktes werden robuste Regler berücksichtigt. Um die rechnerischen Aufwand des Reglerentwurfs und die Ordnung des synthetisierten Reglers zu reduzieren, anstatt die Anzahl der Zustände des Systems zu reduzieren, konzentrierte sich diese Arbeit auf das Design eines Reglers mit fester Ordnung, um später die Ordnung Reihenfolge des Controllers nicht reduzieren zu müssen. Eine feste Ordnung des Reglers ist eine strukturelle Einschränkung für den Regler. Das hier vorgeschlagene Verfahren basiert auf der Gestaltung der Übertragungsfunktion im offenen Regelkreis im Frequenzbereich. Non-smooth Optimierungstechniken werden verwendet, um das Problem der Synthese von H_∞-Reglern unter zusätzlicher struktureller Bedingungen (feste Ordnung) zu lösen. Dieser Ansatz vermeidet die Verwendung von Lyapunov-Variablen und führt daher zu Optimierungsprogrammen mittlerer Größe selbst für sehr große Systeme.
- Berücksichtigung von Unsicherheiten in Übertragungsnetzen:
Unterschiedliche Unsicherheiten im Stromnetz wie variable Erzeugung bzw. Verbrauch, mögliche Netztopologie-Änderungen, unvorhersehbare Lastverläufe und Lastarten (dynamisch, statisch), vernachlässigte hochfrequente Vorgänge in der Netzdynamik und ungültige

Annahmen im Modellierungsprozess erfordern den Einsatz Robuste Regler zur WADC. Diese Unsicherheiten bestimmen direkt die Stabilitätsgrenzen des Arbeitspunktes. Ein Energiesystemmodell mit diesen Arten von Unsicherheiten wird als Multimodel bezeichnet. Die Auswirkung der oben beschriebenen Unsicherheiten wird als unstrukturierte Unsicherheit berücksichtigt, und als Gewichtungsfunktion betrachtet. Diese Gewichtungsfunktion ist eine stabile Übertragungsfunktion fester Ordnung, die die Merkmale des hervorgehobenen Frequenzbereichs für Multi Models enthält. Bei dieser Untersuchung wird der Bereich der inter-area Frequenz (< 1 Hz) für eine unsichere Gewichtungsfunktion berücksichtigt. WADC verfügen außerdem über Kommunikationsverbindungen, die eine unsichere Zeitverzögerung beinhalten, die hier als parametrische Unsicherheit betrachtet wird.

-WADC Architektur:

Zur Bewertung der Leistungsfähigkeit und der Angemessenheit der Stabilitätsgrenzen wurden zentrale und dezentrale Architekturen implementiert. In dieser Arbeit spielen die Auswahl des nominal models und die Anwendung spezifischer Stabilitäts- und Performance- Kriterien eine wichtige Rolle bei der Definition der richtigen Regler Struktur.

- Reservekanäle in zentraler WADC:

Dieser Teil beschäftigt sich mit der zentralen WADC, die über einige Reserve-Eingangs- und Ausgangskanäle verfügt, um mögliche Kommunikationsausfälle zu bewältigen. Die vorgeschlagene WADC kann Schwingungen dämpfen, auch wenn einige Eingangs- und / und Ausgangssignale unterbrochen werden.

ACKNOWLEDGMENT

I would like to express my profound gratitude and sincere thanks to my supervisor, Prof. Dr.-Ing. habil.Gerhard Krost for his guidance, support, invaluable advice and continuous encouragement throughout my tenure as a Ph.D. student.

I would like to express my sincere and profound gratitude to Univ. Prof. Dr.-Ing. habil.István Erlich, who gave me an opportunity as his PhD student to conduct unique research in a highly challenging and interesting area. I will always hold his memory in the highest esteem.

I would like to thank all of EAN staff members especially Dr.-Ing. Fekadu Shewarega for his technical and fatherly support, which helped me on many occasions. I would also like to express my thanks to Jens Denecke, Duc Thanh Do, and Bader Sager for technical discussions and advices, Ms. Hannelore Treutler for her help in countless issues, Ralf Dominik for his support regarding computer related technical issues and for helping me improve my German language proficiency and Rüdiger Reißig for his help regarding technical issues.

My warmest thanks and appreciation goes to my parents for their infinite and unconditional love, for all the hardship they went through to enable me fulfil my dreams, and for their continuous encouragement during the long and at times tough years of my studies. Also, my endless thanks to my sister, and my brother for their support and love.

Last but not least, I would like to express my heartfelt thanks to many other people, who directly and indirectly contributed to my success.

TABLE OF CONTENTS

LIST OF FIGURES

Abbreviations

PSS	Power System Stabilizer
FACTS POD	Flexible AC Transmission System Power Oscillation Damping
PMU	Phasor Measurement Unit
GPS	Global Positioning System
PCM	Probabilistic Collocation Method
WADC	Wide Area Damping Controller
WAMS	Wide Area Measurement System
SG	Synchronous Generators
IM	Induction Motor
HVDC	High Voltage Direct Current
PV	Photovoltaic Plant
DFIG	Doubly Fed Induction Generator
AVR	Automatic Voltage Regulator
VSC	Voltage Source Converter
AC	Alternating Current
DC	Direct Current
VOC	Voltage Oriented Control
SRIG	Slip Ring Induction Generator
LSC	Line Side Converter
MSC	Machine Side Converter
CR	Crowbar
CH	Chopper
MPPT	Maximum Power Point Tracking
LFIO	Low Frequency Inter-area Oscillations
SCADA	Supervisory Control And Data Acquisition
AAF	Anti-Aliasing Filter
PLO	Phase Locked Oscillator PLO
DFT	Discrete Fourier Transform
SE	State Estimation

KF	Kalman Filter
ESPRIT	Estimation of Signal Parameters by Rotational Invariance Technique
HHT	Hilbert–Huang Transform
WT	Wavelet Transform
RASSI	Recursive Adaptive Stochastic Subspace Identification
SVC	Static Var Compensator
DAE	Differential Algebraic Equations
LQG	Linear Quadratic Gaussian
SDP	Semi Definite Programming
LTI	Linear Time Invariant
PLC	Power Line Cable
LM	Large Motor
MM	Medium Industrial Motor
TP	Trip Motors
CWADC	Centralized WADC
DWADC	Decentralized WADC
COI	Center Of Inertia
TFM	Transfer Function Matrix
RG	Renewable Based Generation
DG	Distributed Generation
LQR	Linear Quadratic Regulator
WG	Wind Generator
EM	Electromechanical
EDFLR	Extended Desensitized Four Loop Regulator
TCSC	Thyristor Controlled Series Capacitor
TCPAR	Thyristor Controlled Phase Angle Regulator
PID	Proportional–Integral–Derivative
RGA	Relative Gain Array
LMI	Linear Matrix Inequalities
LPV	Linear Parameter Varying

RTDS	Real Time Domain Simulation
USP	Unified Smith Predictor
HSV	Hankel Singular Values
LF	Low-Frequency
SPC	System Protection Center
LPC	Local Protection Center

CHAPTER 1. INTRODUCTION

1.1. Motivation

Small signal oscillations are one of the major threats for the stable operation of the power systems since they are often poorly damped due to increase in energy interchanges between interconnected areas. Advent of renewable energy with unpredictable behavior can cause uncertain amount of transferred electricity and pushes the power system to behave closer to operational boundaries. Furthermore, high penetration of renewable energy and decrease of percentage of synchronous generators in electrical grid cause the general decline of inertia and raise the risk of instability. Variation of generation and demand and high fluctuation of operating point make power systems more uncertain. Keeping the system stable under different changes that are applied to the system, is a serious challenge to avoid happening of blackouts and critical situations. According to all challenges, necessity of appropriate measurement, monitoring and protective control for reliability and good performance for safe and continuous energy supply is given dramatically. Heavy power transfers across weak tie lines between different components of large interconnected electrical power grids as well as high gain exciters get arise rotor angle instability and cause oscillations of groups of machines relative to each other. This problem causes frequency of oscillations between 0.1 to 1 Hz, which are called inter-area frequencies. Generally, there are two kinds of power oscillation damping controllers in power systems: Power System Stabilizer (PSS) and Flexible AC Transmission System Power Oscillation Damping (FACTS POD) controllers. The overall system damping cannot be improved by using the traditional approach such as PSS that provide supplementary control action through the generator excitation systems. Supplementary control signals are required to be added to these devices to achieve more damping. Traditional controllers usually use local inputs and cannot always be effective to solve the problem. It is known that the system dynamic performance improvement can be achieved if wide area signals of the power system from one or more distant locations are used to the damping controller design. The wide area measurement technologies under development based on Phasor Measurement Unit (PMU) with Global Positioning System (GPS) make wide area control of power system practical.

Because of variations in generation and load patterns and changes in transmission networks, power systems experience changes in operating conditions which are considered as uncertainty, that inter-area frequencies are sensitive to this uncertainty.

The importance of the load characteristics on inter-area oscillations is well documented. Static and dynamic load components with a composite load model are reported to provide more accurate oscillation damping results than with simpler load models. In few post analyses of the blackouts, simpler load models showed more damping than that observed through the measurements. However, on changing the load model to a more complex form, the simulations were able to match the damping obtained from the measurements. Due to its natural complexity and uncertainty, load dynamics, in general, may be never known completely in operation and control. The lack of knowledge about the dynamic characteristic of each individual component due to poor measurements, modeling, and exchange information, as well as the uncertainties in components/customers behaviors via switching events contribute to load uncertainties.

Wind and solar power sources are uncertain renewable energy sources. Power generation of uncertain renewable generation sources has basic characteristics of uncertainty, such as intermittence, randomness, and fluctuations. This type of uncertainty threatens the safety and stability of the power grid and is not conducive to the power balance. The negative impact of power uncertainty on the power grid is closely related to the fraction of the grid comprising with these sources. The impact of small penetration amounts of renewable energy sources to the power grid is ignorable, but the effect is evident if the amount is large. This uncertain renewable source effects directly on inter-area frequencies and is motivated to suppress their oscillation.

In addition, some uncertainty in power system model due to inaccurate approximation of power system parameters, neglected high frequency dynamics and invalid assumptions made in the modeling process exist.

Different techniques have been investigated to damp uncertain power system oscillations. The developed robust control theory and wide area control system technologies offer a great potential to overcome the shortages of conventional local controllers.
The order of the controller is considered as a key factor since the controller is implemented in computers and devices that have limited memory and computing power. Implementing a high order controller both in hardware and software is a challenging task and leads to numerical problems. Even though there are some methods to reduce the order of the controller, they do not guarantee that the reduced controller will achieve the requirements of stability and

performance. Structural constraints can be applied to standard robust control synthesis and design fixed order (as low as possible order for controller) control. These constrains have nonsmooth and nonconvex behavior that are solved by proper optimization method.
To study the effect of uncertainties in power model parameters on inter-area oscillations and on fault clearing time in time domain simulations Probabilistic Collocation Method (PCM) has been used. In general, the parameterized model fails to describe the plant because the plant (with different dynamic, in different size and number of component) will always have dynamics that are not represented in model, which is described by parametrized model. In this research, uncertainty of general model is considered as unstructured uncertainty. Unstructured uncertainty is described with uncertain weighting function which is shown with transfer function in the desired inter-area range of frequency. This weighting function accompanies with appropriate, uncertain linear, time invariant objects are used to represent unknown dynamic objects whose only known attributes are bounds on their frequency response. This combination is lumped to nominal model and named multi model with uncertainty.

Time delay is considered in controller structure to compensate distance between measurements and actuators with controller. These distances will be presented by parametric uncertain time delay in propagated and fixed types. Designing procedure will be considered as time delay to compensate its negative oscillations.

Two architectures will be considered to design of Wide Area Damping Controller (WADC). Intention of considering centralized and desterilized types is to compare performance and accessibility and reliability of them together for better implementation.

1.2. Literature Review on Wide Area Damping Control for Power Systems

Inter-area oscillations are a part of the nature of interconnected power systems. Large power systems being connected by weak ties transmitting heavy power flows tend to exhibit such modes. These oscillations are a result of the swing between groups of machines in one area against groups of machines in another area, interacting via the transmission system. [1]

Control of power system oscillations became feasible with the advent of PMUs, which are a solution to increase observability in traditional monitoring systems and provide additional insight of power system dynamics.

The WAMS project was founded in 1995 [2] . The measurement devices used in WAMS are GPS time synchronized PMUs, which provide high sample rate voltage and current phasor measurements.

Analysis of inter-area oscillations

Analysis of inter-area oscillation is conducted using: (i) model based and (ii) measurement based approaches.

Modal analysis is the most used method to determine the nature of inter-area oscillation modes for wide-area damping controller systems [3] - [6] .

Some methods used for oscillation detection using measurement based approaches include:

- Kalman Filter (KF) is an optimal recursive method, which can be used to estimate oscillation contents in a power system [7] .
- Prony method [8] is an extension of Fourier analysis method. It can directly estimate frequency, damping and phase of a recorded signal by using a summation of complex exponentially damped signals to the observed one [9] .
- Hilbert-Huang Transform (HHT) is a nonlinear analysis technique, which can extract time-varying oscillations characteristics of the measured signal, i.e., frequency, amplitude and damping ratio [10] .

Recently new techniques have been proposed to identify inter-area oscillation modes such as system identification (SI) methods, Estimation of Signal Parameters by Rotational Invariance Technique (ESPRIT) [11] , Yule–Walker algorithm [12] , Wavelet Transform (WG) [13] , Recursive Adaptive Stochastic Subspace Identification (RASSI) [14] .

Controller devices to damp inter-area oscillations

PSSs are the most common damping control devices in power systems. They are the most cost effective devices to damp electromechanical oscillations. Originally, the PSSs usually rely on local information (such as generator rotor speed or electric power) and are effective in damping local modes [15] . However, many researchers extended their capabilities to damp inter-area oscillation modes like, hybrid PSSs [16] - [18] .

Power electronics controlled devices provide solutions for damping of inter-area oscillations. Controllers are used mainly to improve the utilization capacity of the existing transmission systems. They not only enhance transient stability and control the voltage but also improve oscillations damping [19] . However, both FACTS controller and PSS devices indirectly damp oscillations by controlling voltage and reactive power flow.

High Voltage, Direct Current (HVDC) systems are widely used to interconnect regional grids. They have inherent advantage to prevent flowing of the disturbances. In addition, they show great ability to damp oscillations [20] due to their fast response, direct control of active power, good controllability and large adjustable capacity. Moreover, HVDC systems locations as inter-ties between various system areas give them the ability to directly and significantly damp inter-area oscillation modes.

The trend of using sustainable energy, especially wind power, increases nowadays. With high penetration of wind, many aspects of the power system operation and control might be affected. Recent research studies have investigated the impact and control of wind power plants (WPPs) on damping electromechanical power system oscillations using Doubly Fed Induction Generator (DFIG) (type-3) or full converter interfaced generators (type-4) [21] ,[22] .

Modeling of devices

General models are developed for some devices such as power system stabilizers for small signal stability studies [26] . Some devices have no general models such as HVDC systems. In general, valve switching can be neglected for power electronics controlled devices with electromechanical oscillation studies [24] . Hence, injection model [27] is used for representation of series connected power electronics controlled devices e.g. VSC-HVDC [23] -[25] . This model is valid for load flow and angle stability analysis, i.e., phasor model [27] .

Control techniques used

A variety of different strategies has been proposed in recent literature to design effective WADCs applications from simple gain control method [28] , [29] to advanced robust [30] -[34] and fuzzy logic controllers [35] , [36] .

Robust control techniques: using such techniques can help achieving robustness for a power system under a wide range of operating conditions [37] . Different robust controller methods are considered like: H_2, H_∞, H_∞ loop shaping, and μ synthesis [30] -[34] , [38] for designing a robust controller for power systems. The solution to control design problem is based on the Riccati equation approach. Moreover, these techniques can handle modeling errors and uncertainties in the studied system [37] , [39] . H_∞ is a robust control technique, which maintains system robustness in presence of model uncertainties. H_2 can handle stochastic aspects such as measurement noise, random disturbance and capture of the cost control [39] . Hence, the mixed H_2/H_∞ multi-objective controller is commonly used in wide area damping control system [37] , [38] , [39] . The main challenges with H_2 and custom H_∞ approaches are that they depend

heavily on the proper selection of some weight filters, and the plant model needs to be reduced. Most of these designs are based on nominal operating point.

Fuzzy logic (FL) control method: this method is used in power system control due to its robustness against variations of input signals and system operating conditions. It can be considered as another solution for nonlinear control problem. Applications of wide area damping control systems can be found in [35] , [36] .

Neural Network (NN): NN is also used in designing wide area damping control systems [40] . The main advantage of this method is its adaptive characteristics with changing of the operating point in power systems. The requirement of massive training data is the main drawback of this method especially in case of using it for large power systems [35] .

Wide area challenges

Applications of using remote signals in control systems face many challenges i.e.

- latency
- choosing input signals
- measurements noise
- signal loss and centralized controller optimal location.

There are several reasons for time delay in wide area based signals [41] . Measuring equipment (voltage transducers and current transducers) are sources of delays of the signals. Also, the required sampling rate for phasors computation and PMU processing time to convert samples into phasors are important factors in increasing delays. The time delay can be ideally represented as $e^{-s\tau}$ in the Laplace domain. Researchers transformed $e^{-s\tau}$ by a finite dimension rational approximation in the frequency domain using Padé approximations [41] . Another technique to include the delay in the controller design is Unified Smith Predictor (USP) approach. Reference [42] used such method to design a dead time power system. Padé approximation and USP are effective techniques for constant time delay representation.

Selection of control input signals to each control agent is an important stage in case of using wide area scheme. Transfer function residue method (modal control theory) is widely used for selection of remote signals [23] , [43] , [44] , [45] . The residue is a complex conjugate pair for oscillatory mode. Geometric method (joint controllability/observability method) depends on geometric measures of controllability and observability [43] . Hankel Singular Values (HSV) can relate input output combinations with internal states of the system [46] .

Evaluation of the controller performance

The final step in designing a controller is evaluating its performance. In this step, the control technique can be proved to be effective at damping inter-area oscillations. Usually, researches start with root-locus plots for oscillation modes before and after applying of control system to verify obtaining targeted damping of critical modes under linear analysis, feedback gain is changed from 0 (open loop) to 1 (closed loop) [47] . Then, time domain simulations under several of events are performed to ensure nonlinear performance validation of the control system.

In this research, modal analysis is used to determine inter-area oscillation modes for design of wide area damping controller systems. The order of the controller is important while the controller is implemented in computers and devices that have limited memory and computing power. Some methods are proposed with reduced order of designed controller, which can make high risk for stability. Furthermore, there is a specific fixed order controller design for parametric models which use Laguerre parameters and consider quadratic controller type which has same number of input and outputs[48] . The Multi Input, Multi Output (MIMO) fixed order nonsmooth robust H_∞ wide area damping controller is proposed in this work for supressing power oscillations and stabilizing the multi machine power system. Time delay is represented with Padé approximations, geometric method is selected to control input signals to each control agent and time domain simulations under several of events are performed to ensure nonlinear performance validation of the control system.

1.3.Objective

Wide area damping control system is still in its infancy because many issues remain unresolved in the design and implementation of such systems. Some of them are listed as follows:

- Control system architecture – which structure is suitable, centralized or decentralized?
- Measurement types and locations – what kind of measurements are suitable for stabilizing signals? Where and how can these signals be measured?
- Control devices and locations – what devices should be controlled and what are best control sites?
- Time delay – How to design a controller that can handle a range of time delay?

- System uncertainties – when designing a controller, how to deal with all kinds of uncertainties produced in the system modeling process?
- Controller design and implementation – how to design a controller to meet the robust and performance requirements for inter-area oscillations damping? How and where to implement such a controller?

The objective of this research is to propose a systematic procedure of designing a wide area damping control system for power system inter-area oscillations, with particular attention to several practical issues like time delays, and robust stability and performance.

1.4. Contributions of this Dissertation

The following contributions have been made and are reported in this document:

- Proposed a procedure to design the wide area damping control systems with centralized and decentralized architectures, and it is proved that both of them are effective to damp out inter-area oscillations. It is proved that decentralized has better performance than centralized controller.
- The proposed WADC is stable for stable and unstable plant models by providing remote measurements to the controller and control actions through generator excitation systems without conventional PSS.
- The controller design technique can use the full order system as well as reduced order system since the order of the controller is fixed.
- The proposed method is based on shaping of the open loop transfer function in the frequency domain.
- Nonsmooth robust fixed order controller as structural robust control uses first order steepest descent optimization method because of its nonsmoothness.
- This approach avoids using Lyapunov variables and therefore leads to moderate size optimization programs even for very large systems.
- The effects of time delays on wide area damping control systems are considered as parametric (structured) uncertainty, which is approximated as first order Padé approximation and is considered as fixed and propagated types.

- Model uncertainties because of variation in generation, penetration of renewable energy, in some cases different grid topology and loads patterns, which happen in grids are considered as unstructured uncertainty or frequency dependent ones.
- The robustness of the designed controller is tested by evaluating the damping control system performance under different operating conditions and the system response to various disturbances using time domain simulation based on nonlinear power system models.
- The performance of controller is tested for small and larger electrical power grid under small and large disturbances and shows noticeable damping in both cases.
- This type of controller also applies for grids with high penetration of renewable energy.
- The centralized architecture controller considerers some reserve input and output channels to deal with probable communication dropouts.

1.5. Outline of this Dissertation

This dissertation consists of nine chapters.

Chapter 1. The introduction describes the motivation, objectives and contributions. A literature review is also given in this chapter that summarizes others' work in the field of wide area damping control for inter-area oscillations.

Chapter 2. 'Modeling' gives the detailed power system component dynamic models that are used in this research.

Chapter 3. The necessity of wide area damping control system design according to power system stability is described as damping of low frequency inter-area oscillations. Modal analysis of linearized power system models is outlined.

Chapter 4. The synthesis of the robust controller is defined as a nonsmooth robust fixed order controller, which uses first order steepest descent optimization method.

Chapter 5. Presentation of uncertainty on power grid, modelling of uncertainty as transfer function and effect of it on frequency domain are focused in this chapter.

Chapter 6. Steps of control procedure like selection of architecture, input and output signals, nominal model and multi model with considering defined uncertainties in chapter 5, will be discussed.

Chapter 7. Case studies are considered with only conventional energy sources as generators. Designed controller will be tested with different faults and uncertainties to evaluate its robustness and performance.

Chapter 8. Case studies are considered with converter based energy sources as well as conventional generators to evaluate operation of controller.

Chapter 9. Conclusions and Future Work summarizes the findings of this research and lists several topics for the future work.

CHAPTER 2. POWER SYSTEM MODELLING

2.1. Introduction

This chapter briefly describes models of the main components of the power system. This includes Synchronous Generators (SG), Induction Motors (IM), excitation control systems, PSS, High Voltage Direct Current (HVDC) transmission line, Photovoltaic plant (PV), wind turbine equipped DFIG and dynamic and static loads.

2.2. Power System Modelling

2.2.1. Synchronous Generator Model

A 6th order state space model for the electrical part and a 2nd order model for the mechanical part, represent the synchronous generator model used in this study. The electrical model of the machine is depicted in Figure 2. **1** with $z = r + jx$, $x = \omega l$,

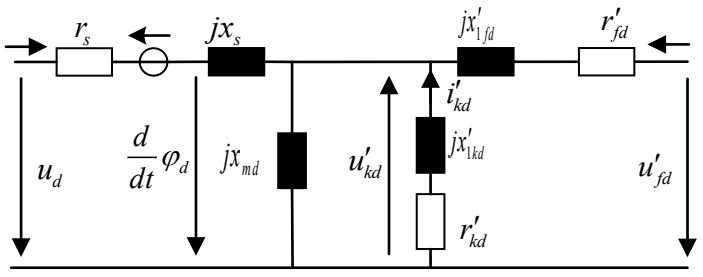

a) d-axis

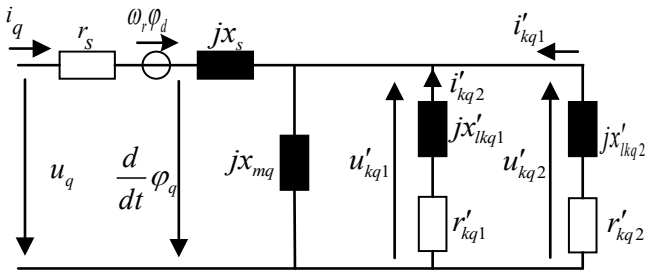

b) q-axis

Figure 2. 1. d and q-axis equivalent circuits

The model takes into account the dynamics of the stator, field, and damper windings. The equivalent circuit of the model is represented in the rotor reference frame (dq frame) [1] . All rotor parameters and electrical quantities are viewed from the stator.

With the following equations.

$$u_d = r_s i_d + \frac{\mathrm{d}}{\mathrm{d}t}\varphi_d - \omega_r \varphi_q \quad \varphi_d = l_d i_d + l_{md}(i'_{fd} + i'_{kd}) \tag{2.1}$$

$$u_q = r_s i_q + \frac{\mathrm{d}}{\mathrm{d}t}\varphi_q + \omega_r \varphi_d \quad \varphi_q = l_q i_q + l_{mq} i'_{kq} \tag{2.2}$$

$$u'_{fd} = r_{fd} i'_{fd} + \frac{\mathrm{d}}{\mathrm{d}t}\varphi_{fd} \quad \varphi'_{fd} = l'_{fd} i'_{fd} + l_{fd}(i_d + i'_{kd}) \tag{2.3}$$

$$u'_{kd} = r'_{kd} i'_{kd} + \frac{\mathrm{d}}{\mathrm{d}t}\varphi'_{kd} \quad \varphi'_{kd} = l'_{kd} i'_{kd} + l_{md}(i_d + i'_{kd}) \tag{2.4}$$

$$u'_{kq1} = r'_{kq1} i'_{kq1} + \frac{\mathrm{d}}{\mathrm{d}t}\varphi'_{kq1} \quad \varphi'_{kq1} = l'_{kq1} i'_{kq1} + l_{mq} i_q \tag{2.5}$$

$$u'_{kq2} = r'_{kq2} i'_{kq2} + \frac{\mathrm{d}}{\mathrm{d}t}\varphi'_{kq2} \quad \varphi'_{kq2} = l'_{kq2} i'_{kq2} + l_{mq} i_q \tag{2.6}$$

Mechanical part of the machine represents swing equations as follow:

$$\frac{\mathrm{d}}{\mathrm{d}t}\delta = \omega_0 \Delta\omega_r \tag{2.7}$$

$$\frac{\mathrm{d}\Delta\omega}{\mathrm{d}t} = \omega_0 (T_m - T_e - K_d \Delta\omega_r)/2H \tag{2.8}$$

The parameters of equations is shown in Table 2. 1.

Table 2. 1. Parameters of synchronous generator

r_s	stator resistance	i_d	d-axis current
r'_{fd}	field resistance	i_q	q-axis current
r'_{kq1}	damper winding resistance	ω_r	Rotor angle velocity
r'_{kq2}	damper winding resistance	i_{fd}	field current
r'_{kd}	damper winding resistance	i_{kq1}	damper winding current

x_s	stator reactance	i_{kq2}	damper winding 1 current q-axis
x_m	magnetizing reactance	i_{kd}	damper winding 2 current q-axis
x'_{lkq1}	leakage reactance	T_m	mechanical torque
x'_{lkq2}	leakage reactance	T_e	electrical torque
x'_{kd}	leakage reactance	$\Delta\omega$	rotor speed deviation
x'_{1fd}	field reactance	H	inertia constant of the motor
φ_d	magnetic flux, d axis	u_d	d-axis voltage
φ_q	magnetic flux, q axis	u_q	q-axis voltage
K_d	damping factor	δ	angular speed deviation

2.2.1.1. Excitation System Model

Excitation systems supply direct current to the synchronous machine field winding as the main task. The field voltage as well as field current through the excitation system is controlled by the Automatic Voltage Regulator (AVR). The control functions response is the control of voltage and reactive power flow, and the enhancement of system stability. Excitation system types DC, AC, and static are listed in [49] . DC exciter is used in this research.

2.2.1.2. Power System Stabilizer Model

The main function of a PSS is to add damping to the generator rotor oscillations by controlling its excitation [49] . This is achieved by modulating the generator excitation so as to develop a component of electrical torque in phase with rotor speed deviations. The PSS adds appropriate phase compensation to account for phase lag between the exciter input and the electrical torque. This is performed by adding a supplementary PSS signal to the AVR summation input along with terminal and reference voltages. The PSS block diagram is shown in Figure 2. 2 [1] . Shaft speed, real power, and terminal frequency are used as input signals to the PSS [50] . In this work, the rotor speed deviation is used as the input signal to the PSS.

The PSS structure contains different parts, which will be described by details and is shown in Figure 2. 2.

- The phase compensation blocks: provide the appropriate phase lead characteristics to compensate for the phase lag between the exciter input and the generator rotor speed.
- The PSS gain, KPSS: is used for amplification and its value is set for maximum amount of damping.
- The signal washout: is used to prevent steady changes in speed from modifying the generator terminal voltage.
- The high pass, low pass filter: are used to allow signals associated with rotor oscillations to pass unchanged.
- Limiter: The output of the stabilizer must be limited to prevent damping signals from saturating the excitation system and thereby defeating the voltage regulation function [50] . The positive output limit of the stabilizer is set at a relatively large value in the range of 0.1 to 0.2 p.u. This allows a high level of contribution from the PSS during large swings. The negative output limit of the stabilizer, usually in the range of -0.05 to -0.1 pu, is to allow sufficient control range while providing satisfactory transient response and also to prevent unit trip in case of PSS output being held at the negative limit because of a failure of the stabilizer.

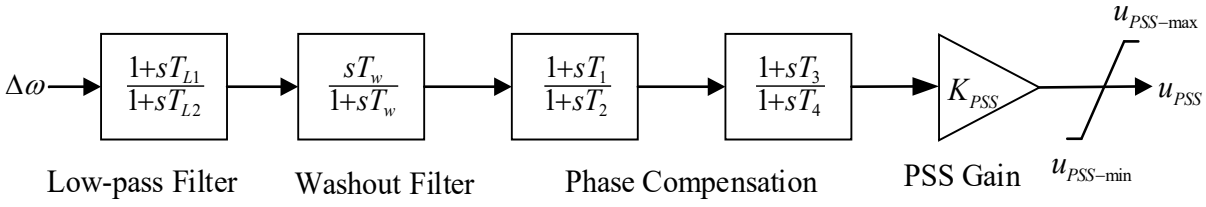

Figure 2. 2. The PSS block diagram [1]

2.2.2. Induction Motor (IM) Model

The models discussed below are built based on physical components and their mathematical interpretation. A simplified induction motor model can be obtained from the scheme in Figure 2. 3.

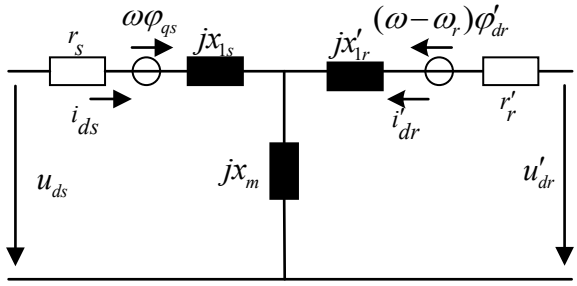

a) d-axis

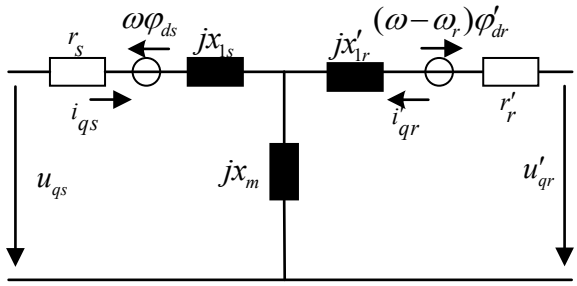

b) q-axis

Figure 2. 3. Model of induction motor

The 3rd order equivalent model for an induction motor is described in [1] , and is widely used in dynamic load modelling [51] , [52] . This model can be described with equations (2.9)- (2.15):

$$u_{qs} = r_s i_{qs} + d\varphi_{qs} / dt + \omega\varphi_{ds} \tag{2.9}$$

$$u_{ds} = r_s i_{ds} + d\varphi_{ds} / dt - \omega\varphi_{qs} \tag{2.10}$$

$$u'_{qr} = r'_r i'_{qr} + d\varphi'_{qr} / dt + (\omega - \omega_r)\varphi'_{dr} \tag{2.11}$$

$$u'_{dr} = r'_r i'_{dr} + d\varphi'_{dr} / dt - (\omega - \omega_r)\varphi'_{qr} \tag{2.12}$$

$$\frac{d\omega}{dt} = -\frac{1}{2H}(T_e - F\omega_m - T_m) \tag{2.13}$$

$$T_e = 1.5p(d\varphi_{ds} i_{qs} - \varphi_{qs} i_{ds}) \tag{2.14}$$

$$\frac{d\theta_m}{dt} = \omega_m \tag{2.15}$$

The parameters of equations are shown in Table 2. 2.

Table 2. 2. Parameter of induction machine

r_s	stator resistances	s	slip of the motor
r'_r	rotor resistances	i_{ds}	d-axis stator current
x_s	stator reactance	i_{qs}	q-axis stator current
x'_r	rotor reactance	u_{ds}	d-axis stator voltage
x_m	magnetizing reactance	u_{qs}	q-axis stator voltage
ω_m	angular velocity of the rotor	H	inertia constant of the motor
ω_r	electrical angular velocity	θ_m	rotor angular position
T_e	electromagnetic torque	θ_r	electrical rotor angular position
T_m	mechanical torque (≈ 1pu)	J	combined rotor and load inertia coefficient.
p	number of pole pairs	F	combined rotor and load viscous friction coefficient

2.2.3. HVDC Transmission Line

HVDC transmission has advantages over AC transmission in special situation. The following are the types of applications for which HVDC transmission has been used:

1. Underwater cables longer than about 30 km. AC transmission is impractical for such distance of the cable requiring intermediate compensation stations.
2. Asynchronous link between two AC systems where AC tie would not be feasible because of system stability problems or a difference in nominal frequencies of the two systems.
3. Transmission of large amounts of power over long distances by overhead lines. HVDC transmission is a competitive alternative to AC transmission for distances in excess of about 600 km.[1]

HVDCs systems have the ability to rapidly control the transmitted power. Therefore, they have a significant impact on the stability of the associated AC power systems. Voltage Source Converter (VSC) based is an important technology that is suited to strengthen the weak transmission and distribution systems. It not only achieves efficient power transmission, but also to provides dynamic reactive power support for the linked AC systems. VSC-HVDC technology is state of the art application of power electronics, and also a key technology for smart grid systems. A point to point VSC-HVDC transmission scheme is shown in Figure 2. 4, which consists of two VSCs interconnected on the DC side via a DC transmission line and

connected to two different AC grids on the AC side. A passive or active AC network can be connected on the AC side of the VSC. If the VSC is connected to a passive network on its AC side, the power flow can be only from the DC input side towards the passive load on the AC side. However, if the AC side is connected to an active AC network, the power flow can be in both directions by controlling the AC voltage output of the VSC.

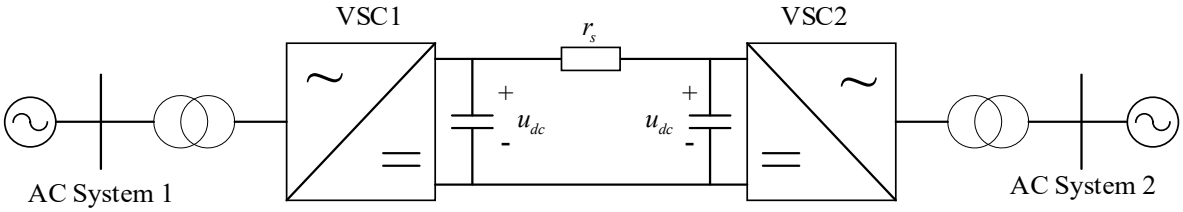

Figure 2. 4. VSC-HVDC transmission line

HVDC system modelling can range in complexity from full detail models, which include valve switching to simple models, which are only acceptable when the HVDC system is remote and has no significant impact on the stability analysis. This research is concerned with electromechanical oscillations and so the operation of the power electronics within the HVDC converter stations is neglected. As such the converter stations is presented simply as sinks and sources of active and reactive power.

2.2.3.1.VSC-HVDC Injection Model

The VSC-HVDC converter stations are modeled as coupled injections of active and reactive power [53] . As the power system phenomena of interest are electromechanical oscillations (with typical frequency of 0.2–2 Hz) the fast time constants associated with the switching operations of the power electronics can be neglected [53] , [54] . The converters are represented simply as controlled equivalent generator buses connected to the AC system across a reactance, x, which practically represents the converter transformer Figure 2. 5.

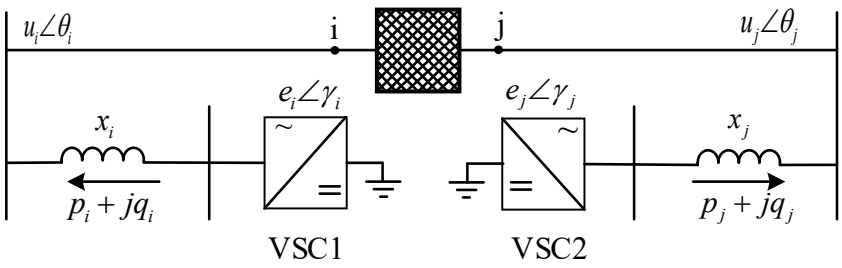

Figure 2. 5. Injection model for an HVDC line in parallel with an AC line

Converter station controllers and DC line dynamics are utilized to determine the expected flow into and out of the VSC-HVDC system. The equivalent generator bus voltage and angle are then simply varied to produce the desired power flow as follows:

$$p = eu\sin(\gamma - \theta)/x \tag{2.16}$$

$$q = [e^2 - eu\cos(\gamma - \theta)]/x \tag{2.17}$$

DC line dynamics are represented by a simple π-model in this study, as in Figure 2. 6, described mathematically by (2.18)- (2.20) where c_{dc}, l_{dc} and r_{dc} represent the capacitance, inductance and resistance of the HVDC line.

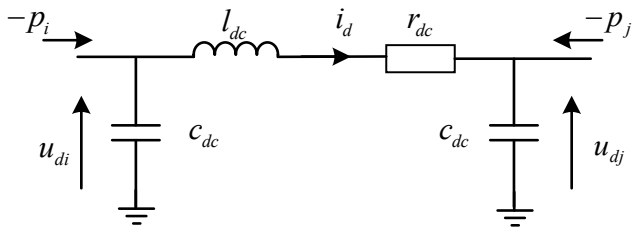

Figure 2. 6. HVDC line model based upon power injection

$$du_{di}/dt = (-P_i/u_{di} - i_d)/c_{dc} \tag{2.18}$$

$$du_{dj}/dt = (-P_j/u_{dj} - i_d)/c_{dc} \tag{2.19}$$

$$di_d/dt = (-i_d r_{dc} + u_{di} - u_{dj})/l_{dc} \tag{2.20}$$

The control of VSC-HVDC largely follows the dq frame and contains of two parts:

- Inner current control loop,
- Outer loop control.

The equivalent block diagram of the current controller is depicted in Figure 2. 7. H(s) is a low pass filter.

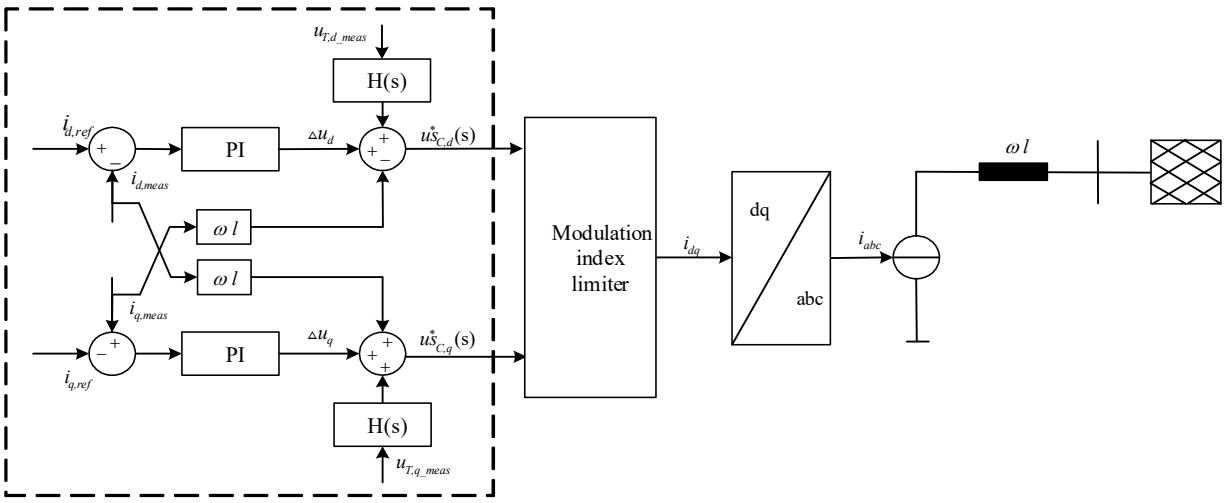

Figure 2. 7. Inner current control loop

A common outer control loop scheme is used with one converter station maintaining DC voltage and the other regulating active power. Reactive power control is independent at each converter station and maintained at zero for the duration of this study. Controllers are PI or integral regulators as shown in Figure 2. 8

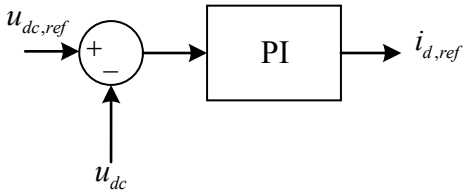

a)

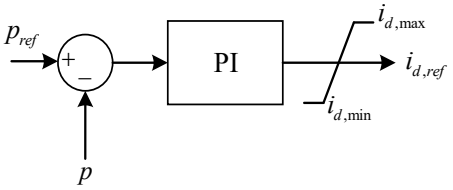

b)

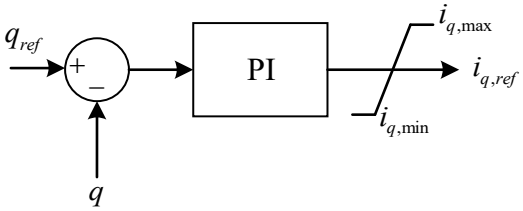

c)

Figure 2. 8. a) DC voltage, b) active power and c) reactive power controllers for VSC-HVDC injection model.

Each complete VSC-HVDC model is defined using line equations (2.18)- (2.20) with one converter operating with control schemes a) and c) from Figure 2. 8, and the other with control schemes b) and c) from Figure 2. 8 [23] , [24] .

2.2.4. Wind Turbine, Doubly Fed Induction Generator (DFIG) and Control

Figure 2. 9 shows the DFIG based wind turbine generation model [55] . Mechanical power is converted to electrical power through rotor and stator of the wind turbine which are connected by transformer to grid. The main parts of the DFIG system contains

- The Slip Ring Induction Generator (SRIG) with three phase stator and rotor windings,
- The back to back converter.

Variable rotor speed following speed-power characteristic curve guarantees efficient power conversion by pitch control. The Line Side Converter (LSC) and the Machine Side Converter (MSC) are two control loops that separately control DFIG. The MSC

- Operates at slip frequency,
- Controls active and reactive power at the generator stator terminals.

The LSC

- Maintains the DC voltage.
- Impact reactive power exchange with the grid.

The protection devices Crowbar (CR) and Chopper (CH) are essential in disturbances.

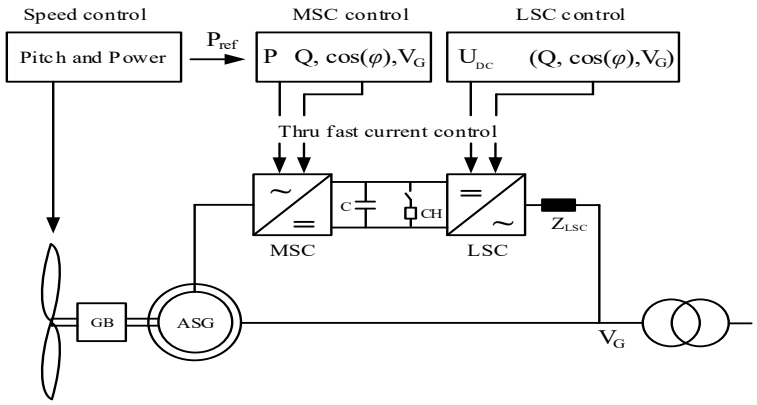

Figure 2. 9. Basic concept of a DFIG based wind turbine generator

The control structure of MSC based on the space phasor coordinates with orthogonal direct (d) and quadrature (q) axis is depicted in Figure 2. 10. In this way, the stator voltage is selected as

the reference frame enabling the decoupled control of P (d control channel) and Q (q control channel). Thus, independent control of active and reactive power of the generator can be achieved through the MSC. Moreover, damping control is also embedded into the speed control structure [56] . Current control parameter of DFIG is shown at Table 2. 3.

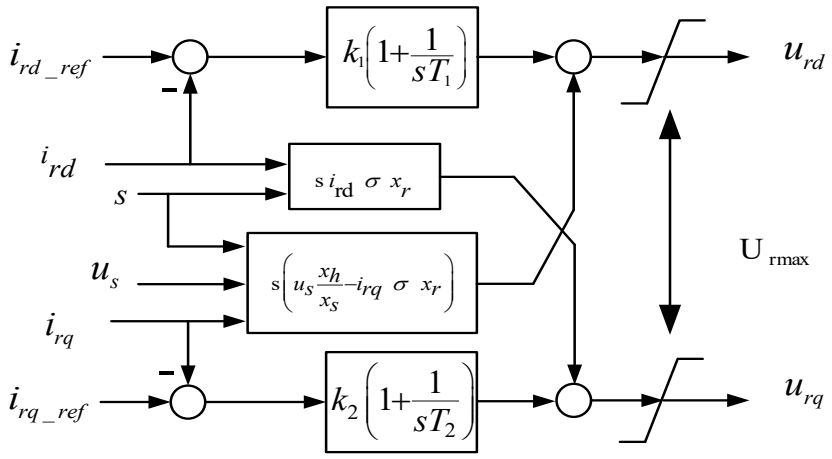

Figure 2. 10. Structure of MSC current controller

Table 2. 3. Current control parameter of DFIG

σ	leakage factor	i_{rd}	d-axis component of the rotor current
u_S	stator voltage	i_{rq}	q-axis component of the rotor current
x_r	rotor reactance	u_{rd}	d-axis component of the rotor voltage
x_h	main field reactance	u_{rq}	q-axis component of the rotor voltage
s	slip	T	Time constant

2.2.5. Photovoltaic Plant (PV) and Control

The configuration of a grid connected PV system is shown in Figure 2. 11 [57] . Generated DC current by conventional PV system greatly depends on the solar irradiation and the voltage at the terminals of the PV system. The DC current produces DC power, which is transformed by means of a PV inverter. Some elements such as a grid connection filter, a grid monitor or interaction unit are responsible for synchronization, measurements, anti-island detection, etc. Low-Frequency (LF) transformer (which is optional depending on local regulations, the converter topology and the modulation used to control it [57]). An intermediate DC-DC power converter between the PV modules and the grid tied inverter is optional. This optional part

decouples the PV system operating point from the PV inverter grid control. Additionally, it can boost the PV system DC output voltage if required, or provide galvanic isolation and perform the Maximum Power Point Tracking (MPPT) control.

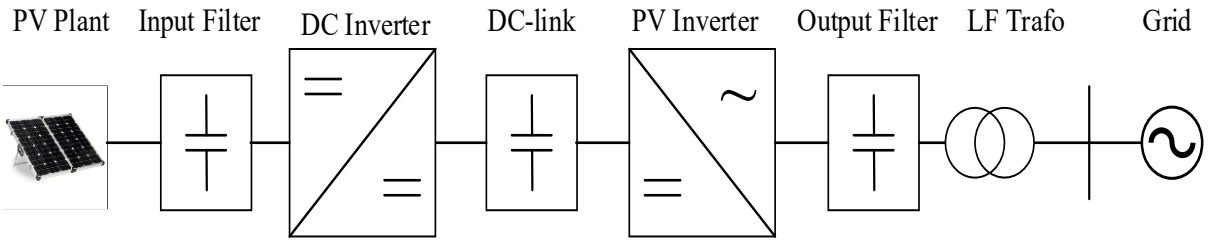

Figure 2. 11. Grid connected PV system

As seen from Figure 2. 12, there are two main components contributing to the dynamic behaviour of the PV:

- PV array
- VSC converter

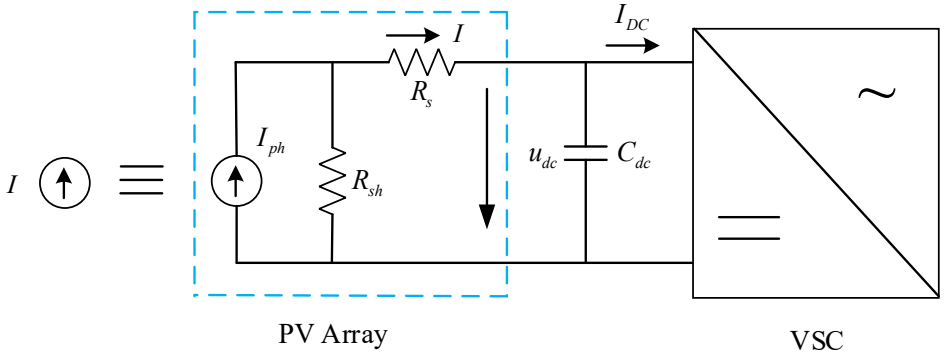

Figure 2. 12. Block diagram of PV with converter

PV cells are represented as current source whose value is almost equal to their short circuit current as long as the load impedance is small. As the load impedance increases, the initial change in current is small, however, as the load impedance increases further, the cell starts to act like a voltage source with a fast declining current when the voltage reaches the open circuit voltage.

The cell is shown Figure 2. 12 and is modeled [58] as a current source, I_{ph} which is the generated current from photovoltaic. R_s is the series resistance which is mainly the body resistance of the cell, electrode resistance, the conductor resistance and the surface resistance. R_{sh} is the parallel resistance which makes up for the surface leakage current along the edge of the cell and the leakage current along the micro cracks and grains. In this research, the cell is considered as simple current source. VSC control for PV plant is modelled like VSC-HVDC.

2.2.6. Load Models Considered

The mathematical representation of load modelling is measured voltage and/or frequency at a load bus. Loads consume active and reactive power. According to the main goal, there are many alternatives for load representation. The main and practical classification in this research is static and dynamic load models. The dynamic load is described as a function of voltage and frequency corresponding at any instant of time while static load is not depending on time and characterized with the relation of active and reactive power with voltage and/or frequency [60] .

2.2.6.1. Static Load Model

Static load can be presented with:

- *ZIPF model or polynomial model*

The ZIPF static load model characteristic is shown by three possibilities

- Constant power,
- Constant current,
- Constant impedance.

The ZIPF model, equations (2.21) and (2.22), is a polynomial model that represents the sum of these three categories:

$$P_{static} = P_0[a_1(\frac{u}{u_0})^2 + a_2(\frac{u}{u_0}) + a_3](1 + K_{pf}\Delta f) \quad (2.21)$$

$$Q_{static} = Q_0[a_4(\frac{u}{u_0})^2 + a_5(\frac{u}{u_0}) + a_6](1 + K_{qf}\Delta f) \quad (2.22)$$

Where u_0, P_0 and Q_0 are the nominal values of the loads, Δf is the frequency deviation, and K_{pf} and K_{qf} are the frequency sensitive parameters, and the coefficients a_1 to a_6 are the parameters of the model.

- *Exponential Load Model*

Equations (2.23) and (2.24) express the power dependence, as a function with a non-integer exponent

$$P_{static} = P_0(\frac{u}{u_0})^{n_p}(1 + K_{pf}\Delta f) \quad (2.23)$$

$$Q_{static} = Q_0 (\frac{u}{u_0})^{n_q} (1 + K_{qf} \Delta f) \quad (2.24)$$

The exponents n_p, n_q, of the model for different load components are included in Table 2. 4. P_0 and Q_0 are the values of the active and reactive power at the initial conditions. Δf is the frequency deviation, and K_{pf} and K_{qf} are the frequency sensitive parameters [51] .

Table 2. 4. Voltage dependency of load components

Load Component	n_p	n_q	**Load Component**	n_p	n_q
Air Conditioner	0.5	2.50	Pumps, fans other motors	0.08	1.60
Resistance Space Heater	2	0	Large industrial motors	0.05	0.50
Fluorescent Lighting	1	3	Small industrial motors	0.10	0.60

2.2.6.2. Dynamic Load Models

Dynamic load models can be classified into three groups:

- Physical dynamic load models,
- Input, output dynamic load models,
- Dynamic load models for specific applications.

In this research, physical dynamic load model is used.

- *Physical dynamic load model*

The physical dynamic load model is considered as a simplified induction motor that was described in part (2.2.2) completely.

2.2.6.3. Composite Load Model

A composite dynamic load is a combination of static and dynamic load, which are usually connected in parallel. References [61] , [62] build their composite load models with a combined structure of ZIP load (constant power, constant current, constant impedance) plus an induction motor load. This was also applied in this work.

CHAPTER 3. POWER SYSTEM STABILITY AND ANALYSIS

3.1. Power System Stability

Power system stability is an important problem for secure system operation. Originally, power system contains some synchronous machines, which work synchronously. It is necessary that these generators operate under all steady states conditions in synchronism. When a disturbance occurs in the system, the system develops to become stable or back to normal. Many major blackouts are caused by power system instability. For dealing with instability, first it should be better defined and different type of power system instabilities classified. Then the appropriate way and technology to control them should be found.

3.1.1. Definition and Classification of Power System Stability

Power system stability is the ability of an electric power system, for a given initial operating condition, to either regain a new state of operating equilibrium or return to the original operating condition (if no topological changes occurred in the system) after being subjected to a physical disturbance, with most system variables bounded so that practically the entire system remains intact [1] .

Classification:

- Makes stability analysis easier as well as effective understanding of different power system instabilities
- Identifies key factors easily that lead to instability
- Can be devised some methods for improving power system stability.

Power system stability can be classified into different categories and subcategories as shown in Figure 3. 1.

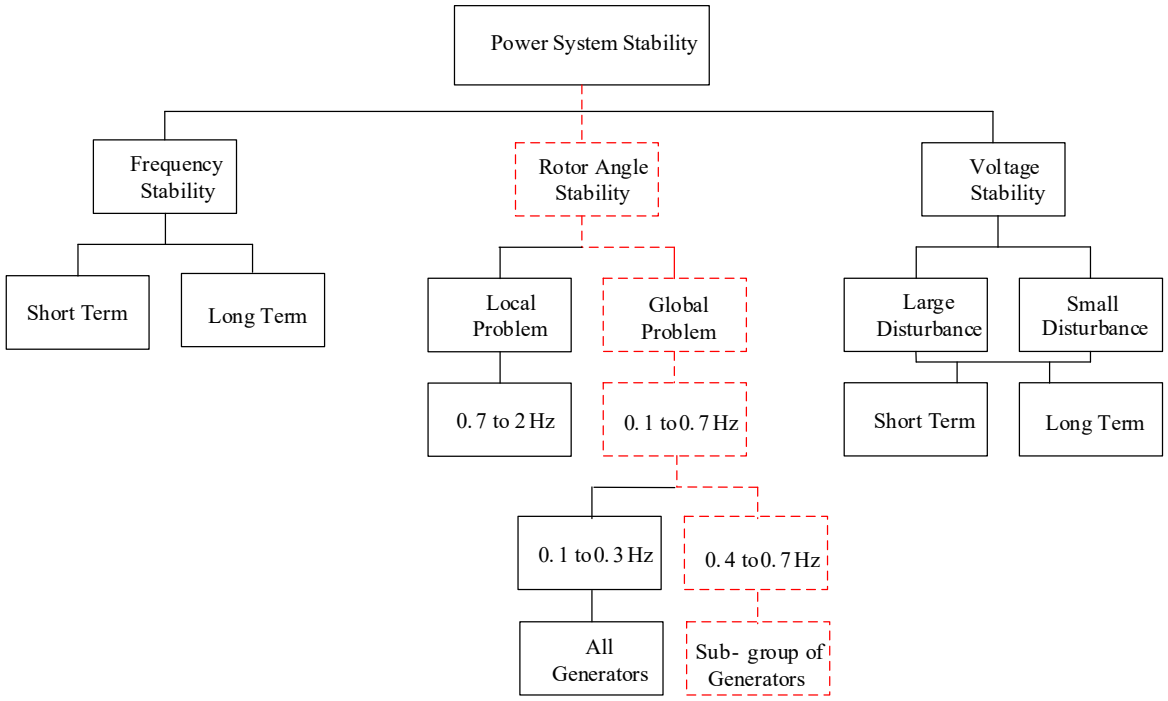

Figure 3. 1. Classification of power system stability

3.1.2. Voltage Stability

- The ability of a power system to maintain steady by all the voltages of all the buses in the system after a disturbance from a given initial operational condition refers to voltage stability.
- This ability mainly depends on maintain/restore equilibrium between reactive load demand and load supply from the power system.
- Voltage instability may occur in the form of a fall or rise of voltages of some buses, whereas, the most common form of voltage instability is the progressive drop in bus voltages. A possible outcome of voltage instability is loss of load in an area, or tripping of transmission lines and other elements by their protective systems leading to cascading outages. Loss of synchronism of some generators may result from these outages or from operating conditions that violate field current limit [63] .

3.1.3. Frequency Stability

- The ability of power system to maintain steady frequency within a nominal range.

- Following a severe system upset resulting in a significant imbalance between generation and load refers to frequency stability [64] .
- It depends on the ability to maintain/restore equilibrium between system generation and load, with minimum unintentional loss of load.
- Instability that may result occurs in the form of sustained frequency swings possibly leading to tripping of generating units and/or loads. Generally, frequency stability problems are associated with inadequacies in equipment responses, poor coordination of control and protection equipment, or insufficient generation reserve [64] -[66] .

3.1.4. Rotor Angle Stability

- Rotor angle stability refers to the ability of synchronous machines of an interconnected power system to remain synchronous after being subjected to a disturbance.
- It depends on the ability to maintain/restore equilibrium between electromagnetic torque (generator output) and mechanical torque (generator input) of each synchronous machine in the system.
- Instability that may result occurs in the form of increasing angular excursions of some generators leading to their loss of synchronism with other generators.
- The change in electromagnetic torque (ΔT_e) of a synchronous machine following a perturbation can be resolved into two components:

1. Synchronizing torque component, in phase with rotor angle deviation ($\Delta\delta$),
2. Damping torque component, in phase with the speed deviation ($\Delta\omega$).

Mathematically, this can be expressed as follows:

$$\Delta T_e = T_s \Delta\delta + T_D \Delta\omega \tag{3.1}$$

Where $T_s\Delta\delta$ is the synchronizing torque component of torque change. T_s is the synchronizing torque coefficient. $T_D\Delta\omega$ is the damping torque component of torque change. T_D is the damping torque coefficient.

System stability depends on the existence of both components of torque for each of the synchronous machines. Lack of sufficient synchronizing torque causes an increase in rotor angle through a non-oscillatory or a periodic mode. This form of instability is known as aperiodic or non-oscillatory instability. Lack of damping torque causes rotor oscillations of

increasing amplitude. This form of instability is known as oscillatory instability. Rotor angle stability can be classified into the following two subcategories:

- Large disturbance rotor angle stability or transient stability
- Small disturbance (or small signal) rotor angle stability

3.1.4.1. Large Disturbance Rotor Angle Stability or Transient Stability

- The ability of the power system to maintain synchronism when subjected to a severe disturbance, such as a short circuit, is large disturbance rotor angle stability or transient stability.
- The initial operating state of the system and the severity of the disturbance will impact on large disturbance rotor angle. Usually, the system is altered so that the post disturbance steady state operation differs from that prior to the disturbance.
- Instability is usually in the form of aperiodic angular separation due to insufficient synchronizing torque, manifesting as first swing instability [63] .
- Most of the time, large disturbance rotor angle does not accrue as the first swing instability. The time frame of interest in transient stability studies is usually 3 to 5 seconds following the disturbance [1] . It may extend to 10–20 seconds for very large systems with dominant inter-area swings [63] .

3.1.4.2. Small Disturbance Rotor Angle Stability

The ability of the power system to maintain synchronism when subjected to a small disturbance. Small disturbance angle stability analysis uses the linearized model for powerful modal analysis, then refer disturbance should be small enough for this goal. In today's power systems, small-disturbance rotor angle stability problem is usually associated with insufficient damping of oscillations [63] . Small disturbance rotor angle stability problems may be either local or global in nature. The descriptions of these problems are given below:

- *Local problems*

In this case a small part of power system for instance, a single power plant (units at the generating station) against the rest of the power system is swinging. It is called local, because of the oscillations are localized at a small part or one station of power system. Stability (damping) of these oscillations depends on the strength of the transmission system as seen by

the power plant, generator excitation control systems and plant output [1] . When a generator is tied to a power system via a long radial line, it is susceptible to local mode oscillations [67] .

- *Global problems*

This type of problem comes from the nature of interconnected power systems. Large power systems being connected by weak tie transmission lines and heavy power transfer, are subjected to inter-area modes. As a result, inter-area oscillation experiences groups of machines in one area oscillates against groups of machines in another area, interacting via the transmission system. This may be caused by small disturbances such as changes in loads or may occur as an aftermath of large disturbances. This type of instability (small signal rotor angle instability) in interconnected power systems is mostly dominated by Low Frequency Inter-area Oscillations (LFIO). However, over a period of time, they may grow in amplitude and cause the system to collapse [68] . Incidents of inter-area oscillations have been reported for many decades.

Features of inter-area mode in large interconnected systems depend on

- the network configuration
- types of generator excitation systems and their locations.

The stability of inter-area modes depends on load characteristics [1] . In addition, the natural frequencies and damping of inter-area modes depend on the weakness of inter-area ties and on the power transferred through them. Characteristics of inter-area oscillations are analysed in [69] , [70] using modal analysis of network variables such as voltage magnitude and angle; these are quantities that can be measured directly by PMUs. The study gives a deeper understanding of how inter-area oscillations propagate in the power system network and propose an alternative for system oscillatory mode analysis and mode tracing by focusing on network variables. Power system oscillation damping has always been a major concern for the reliable operation of power systems. To increase damping, several approaches have been proposed; the most common ones being excitation control through PSS and/or supplementary damping control of HVDC, SVCs and other FACTS devices. In this research, we focus on wide area damping excitation control using control input signals derived from PMU data.

3.1.5. Wide Area Measurement and Control System

Wide area measurement and control systems have been discussed in last decades. Particularly, these concepts are based on collecting data and control the large interconnected power system by means of time synchronized phasor measurements [71] . Operating power system networks

under some severe conditions from one side and transferring more power over a limited transmission infrastructure because of deregulation from the another side, cause power systems drive closer to their capacity which may lead to system blackout. Because of recent shortage, it is necessary that power transfer capacity is high in means of maintaining high reliability. Inappropriate view of system dynamics from Supervisory Control And Data Acquisition (SCADA), and uncoordinated local actions are the main problems of the current energy management systems. WAMSs and WACSs based on synchronized phasor measurement propose a solution to these issues [71] .

3.1.6. Phasor Measurement Units

A PMU is an equipment to estimate the magnitude and phase angle of voltage or current as electrical phasor quantity in the interconnected grid using a common time source for synchronization. GPS provides time synchronization for synchronized real time measurements of multiple remote measurement points on the grid. Task of PMUs is capturing samples from a waveform and reconstruct the phasor quantity. The synchronized measurement is known as a synchrophasor. The frequency is measured as well as magnitude of measurement like voltage and current in the power grid. Synchrophasor measurements give a dynamic view of a power system. The integrated application design is shown in Figure 3. 2.

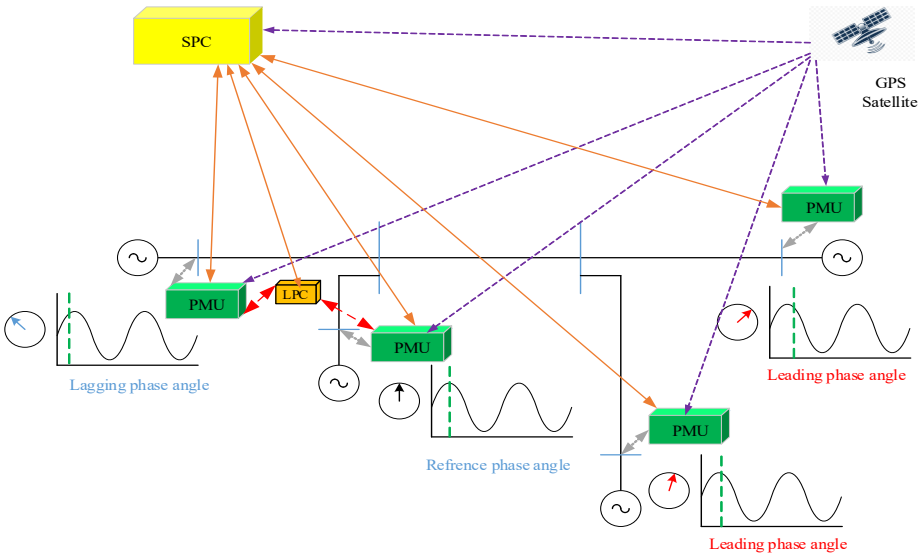

Figure 3. 2. Application design based on phasor measurement units

The data from different phasor measurement units are communicated with System Protection Center (SPC). SPC can control all the circuit breakers in the transmission network by sending

control pulses, and also we have a Local Protection Center (LPC) for local control applications. Figure 3. 3 shows the functional block diagram of a typical PMU; the different blocks of PMU are described as follows.

- Analog inputs: the voltages and currents in their analog form are derived and then fed to Anti-Aliasing Filter.
- Anti-Aliasing Filter (AAF): according to sampling theorem, sampling frequency must be greater than twice the maximum frequency of the signal to be sampled. If lower sampling rates are used, then the original signal's information may not be completely recoverable from the sampled signal and this may appear as aliases. So to avoid this effect, AAF is used which restricts the bandwidth of the signal to approximately satisfy the sampling theorem, for the fixed sampling frequency of the system[72] -[74] .
- Global Positioning System GPS: is a satellite based navigation system which gives account of information about location and time irrespective of atmospheric conditions.
- Phase Locked Oscillator (PLO): Usually in PMU, the pulse signals from the satellite are phase locked with the sampling clock. This job is accomplished by phase lock oscillator. The PLO system is analyzed in [75] .
- A/D Converter: The Analog to Digital converter digitizes the analog signal, from the AAF, at sampling instants defined by the sampling time signals from PLO. These digitized samples are then fed to the phasor microprocessor.
- Phasor Microprocessor: It is programmed to calculate the positive sequence components from the digitized sampled data by using a recursive algorithm which usually applies Discrete Fourier Transform (DFT) as described in [76] . This calculated phasor is time tagged. All the measured data are transmitted to the remote location through a proper communication channel using modems.

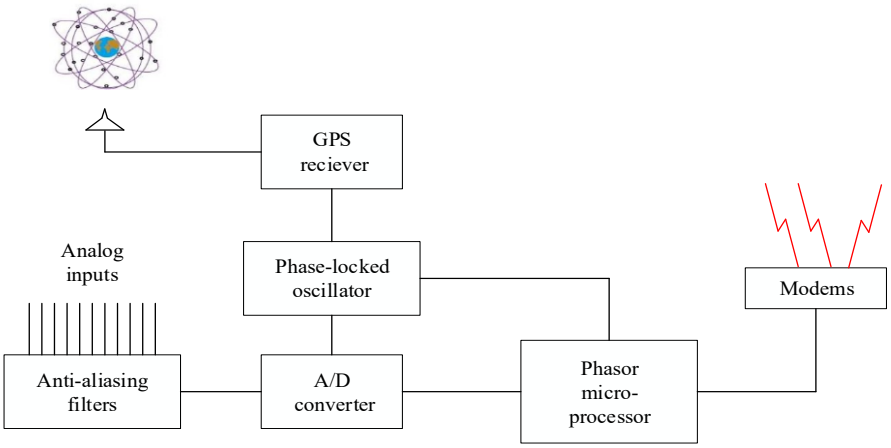

Figure 3. 3. Basic block diagram of PMU

3.1.7. Applications of PMUs and WAMS

With the emergence and development of synchrophasor technology, the potential applications of PMUs and WAMS in power system monitoring, operation, protection, and control were explored. The applications include

- Model validation,
- State Estimation (SE),
- Protection,
- Closed loop control.

Synchronized phasor measurements can provide a proper view at various sites of grid during disturbance to observe system oscillations. This is a big picture on system dynamics during disturbances with sufficient data for validating system models used in computer simulation programs. The other application of PMUs is the state estimation in case of system security from voltage collapse. PMUs are used as pilot points for the secondary voltage control of power system. This control is performed by decomposing the network into coherent regions and providing each of them with a single PMU.

Wide area protection and emergency control systems, using WAMS technology, can also be introduced in the power system to increase the power system transmission capability and/or power system reliability. Synchrophasor measurements for different protection problems including differential protection, adaptive out of step protection, and backup protection, etc. are solutions.

Local signals were used to control power system. The closed loop control is done based on mathematical model of the system without actual measurement of the system. The phasor measurements give possibility to control based on the remote measured values that will be less dependent on the model of the system. Furthermore, predictive control with phasor feedback can solve the nonlinear optimal control problem.

3.1.8. Wide Area Damping Control

The main goal of recent control of large interconnected power systems is to improve dynamic performance and to enhance transfer capacity in weak tie lines. Because of lack of observability of local measurement of inter-area modes, wide area control which uses wide area measurement was proposed in many studies to solve this problem that may be more effective than local control [77] -[79] . One promising application of WACS using global measurements is WADC.

The concept is to design controllers that use wide area measurements to improve power system oscillation damping [80] . WADC designing procedures are discussed in [81] -[84] . Closed loop field tests show a promising future for WADC. Design of WADCs uses different types of robust controller, predictive controller and different structures like centralized and decentralized ones. The WADCs were employed together with PSS controllers. The most important factors in consideration with WAMS, WACS, and WADC are communication, transmission, and end to end delays, and loss of remote control signals [81] . Time delays cause a phase lag, which can affect the control performance, and interactions among system dynamics, which is considered in the model design process. Time delay in control design with different algorithms in different studies is considered in [78] , [85] . The important delay period in WAMS is around 0.5–1.0 seconds, which happens between the measurement and the controller input signal arrival. An outlook for WADC is to implement it to improve damping of low frequency oscillation by means of robust fixed order control. This will allow achieving robustness and stability over a wide range of operating conditions. Although the concept has not yet been widely implemented in real power systems, it offers a promising solution for the future of damping control.

3.2. Tools for Analysis

Power system oscillation analysis has received considerable attention over the past decades. Features such as frequency and damping of the power system oscillations provide critical information for system operators. Analysis of such oscillations are conducted using: (i) model based and (ii) measurement based approaches. The former approach is based on the linearized differential equation of the system around a specific operating point which is used in this approach. Some of the well known methods used for oscillation detection using measurement based approaches include: Kalman Filter (KF) [15] , Estimation of Signal Parameters by Rotational Invariance Technique (ESPRIT) [11] , Hilbert–Huang Transform (HHT) [10] , Yule–Walker algorithm [12] , Wavelet Transform (WG) [13] , Recursive Adaptive Stochastic Subspace Identification (RASSI) [14] and Prony analysis method [8] .

3.2.1. Power System Linearization

Power systems, even in their simplest form, exhibit nonlinear and time varying behaviors. Moreover, different power system equipment such as:

- Synchronous Generators;
- Loads;
- Reactive power control devices like capacitor banks and shunt reactors;
- Power electronically switched devices such as static Var Compensators (SVC)s;
- Currently developed Flexible AC Transmission Systems (FACTS) devices;
- Series capacitors,

are characterized by complex dynamic behaviour. Accurate modelling of these electrical equipments plays an important role for analysis and simulation studies of the whole system.
The power system as a physical system and having large number of components showing nonlinear behaviour, is modelled using sets of nonlinear Differential Algebraic Equations (DAE)s. These equations describe the dynamic behaviour of the system in vector matrix format. Electro-Mechanical (EM) power oscillations are slow enough to consider the modelling in phasor domain and be accurate sufficiently. Due to this passive grid, element dynamics are neglected and are modelled as algebraic equations (steady state) instead of differential equations. Also, output variables which can be observed on the system may be expressed in terms of the state variables and the input variables as follows:

$$\dot{\boldsymbol{x}} = \boldsymbol{f(x,u)} \tag{3.2}$$

$$\boldsymbol{y} = \boldsymbol{g(x,u)} \tag{3.3}$$

Where

$$\dot{\boldsymbol{x}} = \begin{bmatrix} \dot{x}_1 & \dot{x}_2 & \dots & \dot{x}_n \end{bmatrix}^T \;,\; \boldsymbol{x} = \begin{bmatrix} x_1 & x_2 & \dots & x_n \end{bmatrix}^T$$

$$\boldsymbol{u} = \begin{bmatrix} u_1 & u_2 & \dots & u_m \end{bmatrix}^T \;,\; \boldsymbol{f} = \begin{bmatrix} f_1 & f_2 & \dots & f_n \end{bmatrix}^T \tag{3.4}$$

$$\boldsymbol{y} = \begin{bmatrix} y_1 & y_2 & \dots & y_p \end{bmatrix}^T \;,\; \boldsymbol{g} = \begin{bmatrix} g_1 & g_2 & \dots & g_p \end{bmatrix}^T$$

and n is the order of the system, m is the number of inputs, $\boldsymbol{x}$ is the state vector with its entries as state variables, $\boldsymbol{u}$ is the vector of inputs to the system, and $\boldsymbol{f}$ is a vector of n first order

nonlinear ordinary differential equations. p is the number of outputs, $\boldsymbol{y}$ is the vector of outputs, $\boldsymbol{g}$ is a vector of nonlinear functions relating state and input variables to output variables.

The derivatives $(\dot{x}_1, \dot{x}_2, \ldots, \dot{x}_n)$ are simultaneously zero at equilibrium points where all the variables are constant and unvarying with time. The system in this case is in steady state and is written as:

$$\dot{\boldsymbol{x}}_0 = \boldsymbol{f}(\boldsymbol{x}_0, \boldsymbol{u}_0) = \boldsymbol{0} \tag{3.5}$$

Where $\boldsymbol{x_0}$ and $\boldsymbol{u_0}$ are the state and input vectors, respectively, at to the equilibrium point. Assume the system is perturbed from its equilibrium point by small deviations of the following form

$$\boldsymbol{x} = \boldsymbol{x}_0 + \Delta\boldsymbol{x}, \;\; \boldsymbol{u} = \boldsymbol{u}_0 + \Delta\boldsymbol{u} \tag{3.6}$$

Where the prefix Δ denotes a small deviation, then (3.1) is written as:

$$\dot{\boldsymbol{x}} = \dot{\boldsymbol{x}}_0 + \Delta\dot{\boldsymbol{x}} = \boldsymbol{f}[(\boldsymbol{x}_0 + \Delta\boldsymbol{x}), (\boldsymbol{u}_0 + \Delta\boldsymbol{u})] \tag{3.7}$$

Which can be expressed in terms of Taylor's series expansion, truncated to first order, as follows:

$$\begin{aligned} &\dot{x}_i = \dot{x}_{i0} + \Delta\dot{x}_i = f_i[(x_0 + \Delta x), (u_0 + \Delta u)] = \\ &f_i(x_0, u_0) + \left[\frac{\partial f_i}{\partial x_1}\Delta x_1 + \cdots + \frac{\partial f_i}{\partial x_n}\Delta x_n\right] + \left[\frac{\partial f_i}{\partial u_1}\Delta u_1 + \cdots + \frac{\partial f_i}{\partial u_m}\Delta u_m\right] \end{aligned} \tag{3.8}$$

Since $\dot{x}_{i0} = f_i(x_0, u_0)$, (3.1) is written as:

$$\Delta\dot{x}_i = \left[\frac{\partial f_i}{\partial x_1}\Delta x_1 + \cdots + \frac{\partial f_i}{\partial x_n}\Delta x_n\right] + \left[\frac{\partial f_i}{\partial u_1}\Delta u_1 + \cdots + \frac{\partial f_i}{\partial u_m}\Delta u_m\right] \tag{3.9}$$

With $i = 1, 2, \ldots, n$. Similarly, (3.2) is written as:

$$\Delta y_j = \left[\frac{\partial g_j}{\partial x_1}\Delta x_1 + \cdots + \frac{\partial g_j}{\partial x_n}\Delta x_n\right] + \left[\frac{\partial g_j}{\partial u_1}\Delta u_1 + \cdots + \frac{\partial g_j}{\partial u_m}\Delta u_m\right] \tag{3.10}$$

With $j = 1, 2, \ldots, p$. The linearized form in state space representation, of the nonlinear equation (3.1), (3.2) to small perturbations from the equilibrium point is therefore expressed as:

$$\Delta\dot{\boldsymbol{x}} = \boldsymbol{A}\Delta\boldsymbol{x} + \boldsymbol{B}\Delta\boldsymbol{u} \tag{3.11}$$

$$\Delta\boldsymbol{y} = \boldsymbol{C}\Delta\boldsymbol{x} + \boldsymbol{D}\Delta\boldsymbol{u} \tag{3.12}$$

Where

$$\boldsymbol{A}=\begin{bmatrix} \frac{\partial f_1}{\partial x_1} & \cdots & \frac{\partial f_1}{\partial x_n} \\ \vdots & \vdots & \vdots \\ \frac{\partial f_n}{\partial x_1} & \cdots & \frac{\partial f_n}{\partial x_n} \end{bmatrix} \quad \boldsymbol{B}=\begin{bmatrix} \frac{\partial f_1}{\partial u_1} & \cdots & \frac{\partial f_1}{\partial u_1} \\ \vdots & \vdots & \vdots \\ \frac{\partial f_n}{\partial u_1} & \cdots & \frac{\partial f_n}{\partial u_m} \end{bmatrix} \tag{3.13}$$

$$\boldsymbol{C}=\begin{bmatrix} \frac{\partial g_1}{\partial x_1} & \cdots & \frac{\partial g_1}{\partial x_n} \\ \vdots & \vdots & \vdots \\ \frac{\partial g_n}{\partial x_1} & \cdots & \frac{\partial g_n}{\partial x_n} \end{bmatrix} \quad \boldsymbol{D}=\begin{bmatrix} \frac{\partial g_1}{\partial u_1} & \cdots & \frac{\partial g_1}{\partial u_1} \\ \vdots & \vdots & \vdots \\ \frac{\partial g_n}{\partial u_1} & \cdots & \frac{\partial g_n}{\partial u_m} \end{bmatrix}$$

Δ is the prefix, which shows a small deviation

$\boldsymbol{x}$ is the system state vector of dimension n,

$\boldsymbol{y}$ is the output vector of dimension p,

$\boldsymbol{u}$ is the input vector of dimension m,

The transfer function representation of the linearized system in Laplace transform of (3.10) and (3.11) and is as follows:

$$\boldsymbol{G(s)}=\frac{\boldsymbol{\Delta y(s)}}{\boldsymbol{\Delta u(s)}}=\boldsymbol{C(sI-A)^{-1}B+D}=\boldsymbol{C}\frac{\boldsymbol{adj(sI-A)}}{\boldsymbol{det(sI-A)}}\boldsymbol{B+D} \tag{3.14}$$

Where $det(s\boldsymbol{I}-\boldsymbol{A})$ is the characteristic polynomial of matrix $\boldsymbol{A}$. Its root are the eigenvalues of the system.

3.2.2. Modal Analysis

3.2.2.1. Eigenvalues and Eigenvectors

The eigenvalues of the $\boldsymbol{A}$ matrix determine the time response of the system to small perturbation and give valuable information about the stability and performance of the system given by the values of the scalar parameter λ to the equation,

$$\boldsymbol{A\phi} = \lambda\boldsymbol{\phi} \tag{3.15}$$

Where $\boldsymbol{\phi}$ is an $n \times 1$ vector. For any eigenvalue λ_i, the n column vector $\boldsymbol{\phi}$, which satisfies equation (3.14), is called the right eigenvector of $\boldsymbol{A}$ associated with the eigenvalue λ_i. Therefore, we have,

$$\boldsymbol{A\phi}_i = \lambda_i\boldsymbol{\phi}_i \quad ,i = 1,2,...,n \tag{3.16}$$

$$\boldsymbol{\phi}_i = \begin{bmatrix} \boldsymbol{\phi}_{1i} & \boldsymbol{\phi}_{2i} & \cdots & \boldsymbol{\phi}_{ni} \end{bmatrix}^T$$

Right eigenvector associated with a mode accounts for the mode shape. It has the same dimensions as the state variable and therefore is unit dependent. Each component of the right eigenvector contains information about the observability of the associated mode in the state variable corresponding to that component.

Similar to (3.15), the n row vector $\boldsymbol{\psi_i}$ which satisfies,

$$\boldsymbol{\psi}_i\boldsymbol{A} = \lambda_i\boldsymbol{\psi}_i \quad ,i = 1,2,...,n \tag{3.17}$$

$$\boldsymbol{\psi}_i = \begin{bmatrix} \boldsymbol{\psi}_{i1} & \boldsymbol{\psi}_{i2} & \cdots & \boldsymbol{\psi}_{in} \end{bmatrix}$$

Is called the left eigenvector associated with the eigenvalue λ_i. It has a direct effect on the amplitude of a mode excited by a specific input. Each component of the left eigenvector contains information about the controllability of the associated mode using the state variables corresponding to that component. The left and right eigenvectors corresponding to different eigenvalues are orthogonal. In other words, if λ_i is not equal to λ_j, then,

$$\boldsymbol{\phi}_i\boldsymbol{\psi}_j = \boldsymbol{0} \quad ,i \neq j \tag{3.18}$$

However, in the case of eigenvectors corresponding to the same eigenvalue,

$$\boldsymbol{\phi}_i\boldsymbol{\psi}_j = \boldsymbol{C}_i \tag{3.19}$$

Where C_i is a non zero constant. It is a common practice to normalise these vectors so that,

$$\boldsymbol{\phi}_i\boldsymbol{\psi}_j = 1 \tag{3.20}$$

The modal matrices $\boldsymbol{\phi}$ and $\boldsymbol{\psi}$ of right and left eigenvectors are formed from their individual corresponding vectors as follows:

$$\boldsymbol{\phi} = \begin{bmatrix} \boldsymbol{\phi}_1 & \boldsymbol{\phi}_2 & \cdots & \boldsymbol{\phi}_n \end{bmatrix}, \quad \boldsymbol{\psi}_i = \begin{bmatrix} \boldsymbol{\psi}_1^T & \boldsymbol{\psi}_2^T & \cdots & \boldsymbol{\psi}_n^T \end{bmatrix}^T$$

$$\boldsymbol{\psi\phi} = \boldsymbol{I}, \boldsymbol{\psi} = \boldsymbol{\phi}^{-1} \tag{3.21}$$

3.2.2.2. Solution of Differential Equations

Assuming zero input, the solution of each individual differential equation in (3.16) in terms of the eigenvalues, left and right eigenvectors are given by [1]

$$\Delta x_j(t) = \sum_{i=1}^{n} \phi_{ji} c_i e^{\lambda_i t} \tag{3.22}$$

Where $c_i = \psi_i \Delta x\ (0)$ is a scalar product that represents the magnitude of the excitation of the *i*th mode resulting from the initial conditions. Therefore, the free motion, or initial condition, response is given by a linear combination of *n* dynamic modes corresponding to the *n* eigenvalues of the state matrix.

As a result, the stability of the linear system is determined by the eigenvalues.

- A real eigenvalue, corresponding to a non-oscillatory mode, with a negative value represents a decaying mode. A positive real eigenvalue represents a periodic instability.
- Complex eigenvalues, which occur in conjugate pairs, correspond to oscillatory modes and are given by $\lambda = \sigma \pm j\omega$.

The real component gives the damping and the complex component gives the frequency of oscillation in rad/s. A negative real part represents a damped oscillation whereas a positive real part represents oscillation of increasing amplitude. To determine the rate of decay of the amplitude of the oscillation, a damping ratio is calculated using:

$$\zeta = \frac{-\sigma}{\sqrt{\sigma^2 + \omega^2}} \tag{3.23}$$

3.2.2.3. Participation Factors

The concept of participation factor was developed in [86] initially to measure the degree of participation of state variables in a mode. The participation factor for the *j*th state in the *i*th mode is calculated as follows.

$$p_{ji} = \phi_{ji} \psi_{ij} \tag{3.24}$$

Where ϕ_{ji} is the *j*th entry of the *i*th right eigenvector and ψ_{ij} is the *j*th entry of the *i*th left eigenvector. The right eigenvector element, ϕ_{ji}, measures the activity of the *j*th state in the *i*th

mode, the left eigenvector element, ψij, weighs the contribution of this activity to the mode, and thus the participation factor p_{ij} measures the net participation of the jth state in the ith mode. By using the left eigenvectors, the participation factors can be seen as right eigenvectors weighted by left eigenvectors. The participation factor is in fact a measure of the sensitivity of the ith eigenvalue to a change in the jth diagonal element of the $\boldsymbol{A}$ matrix. The participation factors are dimensionless and are associated exclusively with the mode. Since they deal only with state variables and do not include inputs and outputs, their use for PSS siting is considered necessary but not sufficient.

If the participation vector is defined as the vector containing all the participation factors for the ith mode, i.e. $p_{i=}[p_{1i}\ \ p_{2i}\ \ \ldots\ \ p_{ni}]$, then the participation matrix $\boldsymbol{P}$ is formed as follows

$$\boldsymbol{P} = \begin{bmatrix} p_1 & p_2 & \ldots & p_n \end{bmatrix}$$

3.2.3. Selection of Measurements and Control Locations

The selection of appropriate stabilizing signals and locations of control sites is an important consideration in the design of control systems.

There are two methods to select feedback signals and control sites for maximum damping effect:

- Controllability/observability analysis
- Damping torque analysis.

Controllability/observability analysis comes from modal control theory of linear time invariant systems [86] , [87] . Damping torque analysis [89] , [90] has more physical meaning to select stabilising signal and control sites.

Controllability/observability analysis is used in this study for selection of appropriate stabilizing signals and locations of control sites. The linearized state space MIMO model is presented with (3.10), (3.11). Residue R_k can be said to quantify the participation of mode k in the dynamics as seen between inputs and outputs. Residue matrix $\boldsymbol{R_k}$ associated with the kth natural mode is a $p \times m$ matrix and defined as the product of the mode's observability and controllability:

$$\boldsymbol{R_k} = \boldsymbol{C\Phi_k\Psi_k B} \tag{3.25}$$

When signals of a widely differing physical significance, such as power flow in a tie line (MW), bus frequency (Hz), shaft speed (rad/s), angle shift (deg.), etc. are involved in the output matrix simultaneously, the residue approach suffers a scaling problem. The validity of the relative measure can be ensured only when all outputs are of the same type. To overcome this shortcoming, geometric measures introduced by Hamdan [91] are used to evaluate the comparative strength of a signal and a control site with respect to a given model. The geometric measures of controllability $gm_{ci}(k)$ and observability $gm_{oj}(k)$ associated with the mode k are:

$$gm_{ci}(k) = cos(a(\boldsymbol{\Psi}_k, \boldsymbol{b}_i)) = \frac{|\boldsymbol{\Psi}_k \boldsymbol{b}_i|}{\|\boldsymbol{\Psi}_k\| \|\boldsymbol{b}_i\|} \tag{3.26}$$

$$gm_{oj}(k) = cos(\theta(\boldsymbol{\Phi}_k, \boldsymbol{c}_j^T)) = \frac{|\boldsymbol{c}_j \boldsymbol{\Phi}_k|}{\|\boldsymbol{\Phi}_k\| \|\boldsymbol{c}_j\|} \tag{3.27}$$

With $\boldsymbol{b}_i$ the ith column of input matrix $\boldsymbol{B}$ (corresponding to the ith input) and $\boldsymbol{c}_j$ the jth row of output matrix $\boldsymbol{C}$ (corresponding to the jth output). $|z|$ and $||z||$ are the modulus and Euclidean norm of z respectively; $\alpha\ (\boldsymbol{\psi_k}, \boldsymbol{b_i})$ is the geometrical angle between the input vector i and the kth left eigenvector, while $\theta\ (\boldsymbol{\phi_k}, \boldsymbol{c_j^T})$ is the geometrical angle between the output vector j and the kth right eigenvector. These equations show that the controllability measure is related to the angle between the left eigenvectors and the columns of the input matrix $\boldsymbol{B}$ and that the observability measure is related to the angle between the right eigenvectors and the rows of the output matrix $\boldsymbol{C}$.

If $gm_{ci}(k)=0$, then the mode k is uncontrollable from input i. If $gm_{oj}(k)=0$, then the mode k is unobservable from the output j. Being based on directional properties of the underlying column vectors in the system matrices, the geometrical measures remain effective classifiers, even for inputs and outputs of widely differing type.

CHAPTER 4. BACKGROUND OF NONSMOOTH FIXED ORDER CONTROLLER THEORY

4.1. Necessity of Robust Wide Area Control

The model used in power system oscillation is described by differential equations, difference equations, or statistical data; it means that the design of modern control systems is essentially based on model of the system. The mathematical model cannot describe the physical phenomena of a system completely. The model, in somehow, is so complicated to capture the main characteristic of the system. Furthermore, the physical system is not isolated from the outside world, it means the surrounding environment directly effects on the system. It is difficult to describe the external influence by models. This means that there is a gap between the actual system and its mathematical model that is called uncertainty. Furthermore, variations in generation, load patterns and changes in transmission networks, emersion of chaotic renewable power sources are causes that power systems experience changes in operating conditions which are considered as uncertainty. The purpose of robust control is to extract characteristics of model uncertainty and apply this information to the design of a control system, so as to enhance the performance of the actual control system to the limit. System with uncertainty is shown in Figure 4. 1.

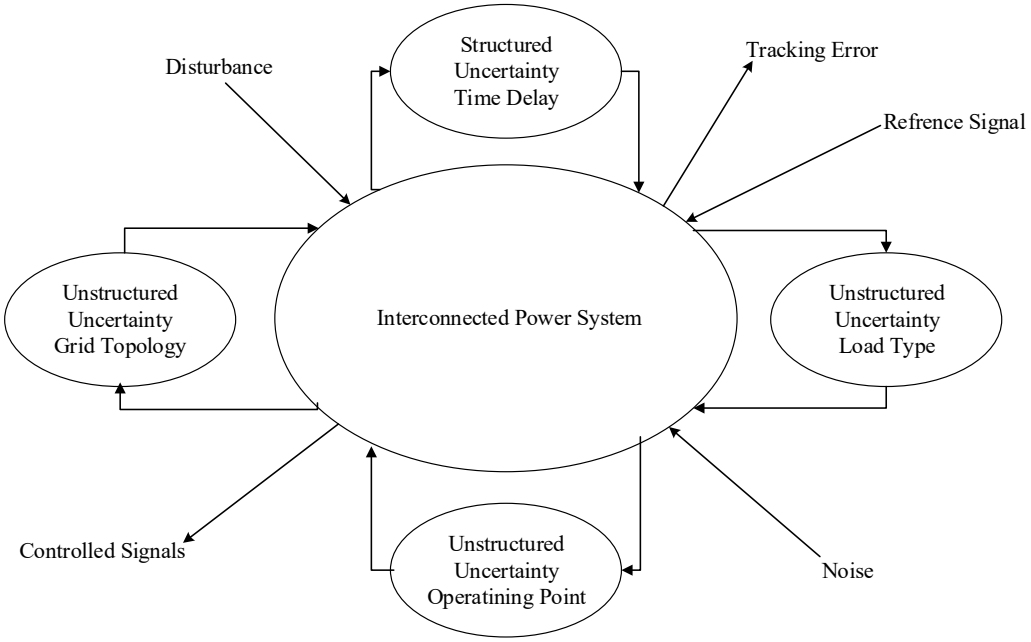

Figure 4. 1. Model with uncertainty

A controller is called robust, if it can also work well under a different set of assumptions except a particular nominal set of parameters. High gain is one of the good and simple examples for designing a robust controller. The effect of any parameter variation will be negligible. From the closed loop transfer function perspective, high open loop gain leads to substantial disturbance rejection in the face of system parameter uncertainty. Instability of closed loop by high gain robust controller is its disadvantage. There are other types of robust controllers like H_∞, H_2, μ synthesis and loop shaping which do not have high gain deficiency.

4.1.1. Robustness

A controller is called robust if it is insensitive to differences between the actual system and the model of the system, which is used to design the controller. These differences refer to model mismatch or model uncertainty.

Our approach to check whether the design specifications are satisfied for the ‘‘worst case’’ uncertainty is as follows:

- Define the uncertainty set: mathematical representation for model uncertainty is described.
- Check robust stability: determine whether the system remains stable for all plants in the uncertainty set.
- Check robust performance: if robust stability is satisfied, determine whether the performance specifications are met for all plants in the uncertainty sets.

To account for model uncertainty, it will be assumed that the dynamic behaviour of a plant is described not by a single linear time invariant model but by a set Π of possible linear time invariant models, sometimes denoted as the ‘‘uncertainty set’’:

- Π- set of possible perturbed plant models.
- $\boldsymbol{G(s)} \in \Pi$– nominal plant model (with any uncertainty).
- $\boldsymbol{G_p(s)}$ and $\tilde{\boldsymbol{G}} \in \Pi$– particular perturbed plant models.

It should be considered that, except the model uncertainty, it comes to concern of robustness by sensor and actuator failures, physical constraints, changes in control objective; the opening and closing of loops are big deals for robustness. Furthermore, if a control design is based on an optimization, then the robustness problem may also be caused by a mathematical objective

function not properly describing the real control problem. Also, the numerical design algorithms themselves may not be robust.

4.1.2. Consideration of Uncertainty

Uncertainty in the plant model may have several origins:

- The parameters in the linear model which are in error or only known approximately.
- The parameters in the linearized model vary due to change of the operating conditions and nonlinearities.
- Deficiency of measurement devices.
- Unknown behavior of model at high frequencies.
- Transforming a detailed model to simpler lower order nominal model and representing neglected dynamics as "uncertainty".
- The implemented controller may differ due to all of recently mentioned uncertainties origin, from the obtained by solving the synthesis problem.

The various sources of model uncertainty mentioned above may be grouped to two main classes:

- Parametric (real) uncertainty. Here the structure of the model (including the order) is known, but some of the parameters are uncertain.
- Dynamic (frequency dependent) uncertainty. Here the model is in error because of missing dynamics, usually at high frequencies, either through deliberate neglection or because of lack of knowledge of the physical process. Any model of power system will contain this source of uncertainty.

Parametric uncertainty is quantified by assuming that each uncertain parameter is bound within some region $[\alpha_{min}, \alpha_{max}]$. That is, we have parameter sets of the form:

$$\alpha_p = \bar{\alpha}(1 + r_\alpha \Delta) \tag{4.1}$$

Where $\bar{\alpha}$ is the mean parameter value, $r_\alpha=(\alpha_{max}-\alpha_{min})/(\alpha_{max}+\alpha_{min})$ is the relative uncertainty in the parameter, and Δ is any real scalar satisfying $|\Delta|\leq 1$.

Dynamic uncertainty is somewhat less precise and thus more difficult to quantify but it appears that the frequency domain is particularly well suited for this class. This leads to complex perturbation which we normalize such that $\|\boldsymbol{\Delta}\|_\infty \leq 1$.

Unstructured uncertainty is considered by weighting function on the special range of frequency on the Bode diagram of the system. Unstructured uncertainty is more important than parametric one because all models include uncertainty to take care of un-modelled dynamics.

To make the model uncertainty more simple, unstructured perturbations are used. A "full" complex perturbation matrix Δ is used to define unstructured uncertainty the dimension of which is compatible with that of the plant, where at each frequency any $\Delta(j\omega)$ is satisfying $\sigma(\Delta(j\omega)) \leq 1$. Common forms of unstructured uncertainty are shown in Figure 4. 2. Unstructured uncertainty is discussed as follows:

- Additive and inverse additive uncertainty
- Multiplicative and inverse multiplicative input uncertainty
- Multiplicative and inverse multiplicative output uncertainty.

Figure 4. 2. a), b), c) shows three feedforward forms: additive, multiplicative input, multiplicative output uncertainty where in all of them, neglection of high frequency dynamics and uncertain right half plane zeros are common deficiencies. Additive plant errors, input (actuators) errors and output (sensors) errors are considered by a), b), c) in order.

Figure 4. 2 d), e), f) shows three feedback forms, inverse additive, multiplicative input, multiplicative output uncertainty where in all of them: neglection of high frequency dynamics and uncertain right half plane poles are common deficiencies.

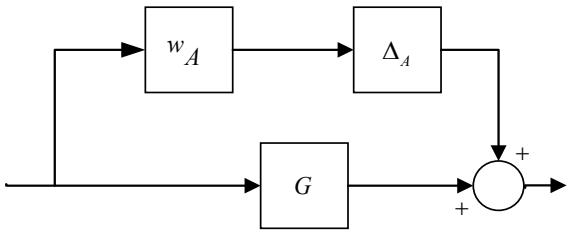

a)

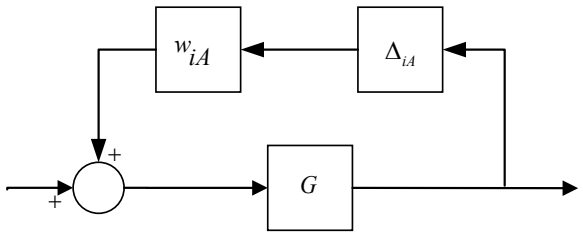

d)

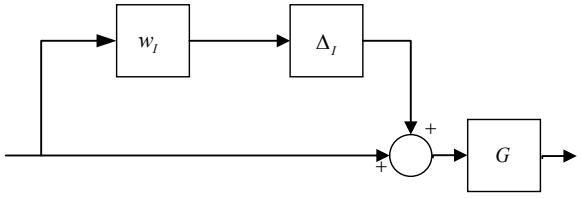

b)

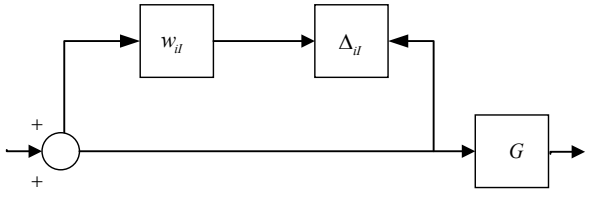

e)

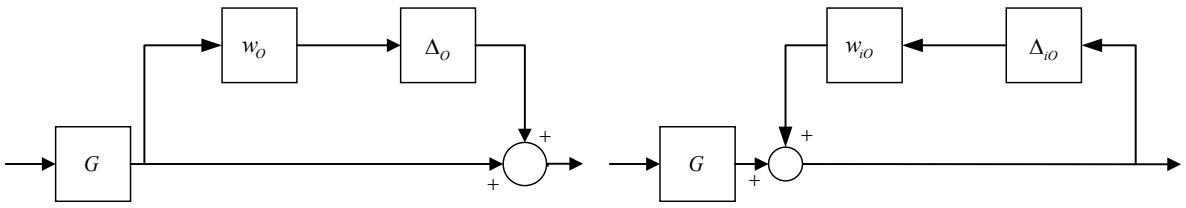

c) f)

Figure 4. 2. Unstructured uncertainty

Equations of the perturbed models with feedforward forms are

$$\Pi_A: \quad G_P = G + E_A; \quad E_A = w_A \Delta_A \tag{4.2}$$

$$\Pi_I: \quad G_P = G(I + E_I); \quad E_I = w_I \Delta_I \tag{4.3}$$

$$\Pi_O: \quad G_P = (I + E_O)G; \quad E_O = w_O \Delta_O \tag{4.4}$$

Equations of the perturbed models with feedback forms are

$$\Pi_{iA}: \quad G_p = G(I - E_{iA}G)^{-1}; \quad E_{iA} = w_{iA}\Delta_{iA} \tag{4.5}$$

$$\Pi_{iI}: \quad G_p = G(I - E_{iI})^{-1}; \quad E_{iI} = w_{iI}\Delta_{iI} \tag{4.6}$$

$$\Pi_{iO}: \quad G_p = (I + E_{iO})^{-1}G; \quad E_{iO} = w_{iO}\Delta_{iO} \tag{4.7}$$

Multiplicative input feedforward or/and feedback form will be used to design power oscillation damping controller, which considers high frequency dynamics, uncertain right half plane zeros and uncertain right half plane zeros as uncertainties at the same time[92] , [93] .

4.1.3. Introduction and Comparison of Different Types of Robust MIMO Control

Practical procedures for multivariable controller MIMO play an important role in industrial control. In industrial systems, which are SISO or loosely coupled, robust control approaches are easier applied and implemented. In our approach, the different robust control methods are categorized as follows:

- Linear Quadratic Gaussian (LQG) control

- H_2 control
- H_∞ control
- Mixed H_2/H_∞ control
- H_∞ loop shaping control
- μ synthesis

LQG control could be well defined and easily formulated as optimizations. Accurate plant models were frequently not available and the assumption of white noise disturbances was not always relevant or meaningful to practicing control engineers. As a result, LQG designs were sometimes not robust enough to be used in practice. For an LQG controlled system with a combined Kalman filter and Linear Quadratic Regulator (LQR) control law there are no guaranteed stability margins [92] , [94] .

Motivated by the shortcomings of LQG control there was a significant shift towards H_2, H_∞ optimization for robust control. Both H_2 and H_∞ require the solutions of two Riccati equations, they both give controllers of state dimension equal to that of the generalized plant, and they both exhibit a separation structure in the controller. It should be said that H_∞, H_2 algorithms, in general, find a suboptimal controller; to find an optimal H_∞ controller is numerically and theoretically complicated. This contrasts significantly with H_2 theory, in which the optimal controller is unique [93] .

A difficulty that sometimes arises with H_∞ control is the selection of weights such that the H_∞ optimal controller provides a good trade off between conflicting objectives in various frequency ranges. Thus, for practical designs it is sometimes recommended to perform only a few iterations of the H_∞ algorithm. The justification for this is that the initial design, after one iteration, is similar to an H_2 design, which does trade off over various frequency ranges [88].

Mixed H_2/H_∞ output feedback control is a prominent example of a multi objective design problem, where the feedback controller has to respond favourably to several performance specifications. Typically, in H_2/H_∞ synthesis, the H_∞ channel is used to enhance the robustness of the design, whereas the H_2 channel guarantees good performance of the system. Due to its importance in practice, mixed H_2/H_∞ control has been addressed in various ways over the years, and we briefly review the main trends [92] , [93] , [94] .

H_∞ loop shaping is a design technique that incorporates loop shaping methods to obtain

performance/robust stability tradeoffs and a particular H_∞ optimization to guarantee closed loop stability and a level of robust stability at all frequencies. It is easy to apply and works very well in practice, that it can be applied for MIMO plants [92] , [93] .

μ synthesis is a powerful tool for explaining succinctly the robust performance problem as well as the robust stability problem with multiple uncertainties. D-K iteration is the most common method to solve this problem. One of the main drawbacks of D-K iteration is that it does not guarantee convergence to a global or even local minimum, which leads to non-optimality of the resulting controller [95] .

Several methods and techniques for robust controller design were described, but the emphasis has been on H_∞ loop shaping which is easy to apply.

The order of the controller is considered as a key factor since the controller is implemented in computers and devices that have limited memory and computing power. Implementing a high order controller both in hardware and software is a challenging task and leads to numerical problems. Even though there are some methods to reduce the order of the controller, they do not guarantee that the reduced controller will achieve the requirements of stability and performance. Structural constraints can be applied to standard robust control synthesis and design fixed order (as low as possible order for controller) control. Structural constraints applied to H_∞ loop shaping result in robust fixed order H_∞ loop shaping controller. These constraints have nonsmooth and nonconvex behaviour, which can be solved by steepest descent nonsmooth optimization method.

4.1.4. Robust Fixed Order H_∞ Loop Shaping Controller

In order to apply robust fixed order H_∞ loop shaping, three steps will be followed:

- Select tuneable fixed order state space model for controller
- Select the desired open loop shape transfer function
- Apply nonsmooth fixed order H_∞ loop shaping formula to optimize the controller. Flowchart of whole process for designing controller is shown in Figure 4. 3.

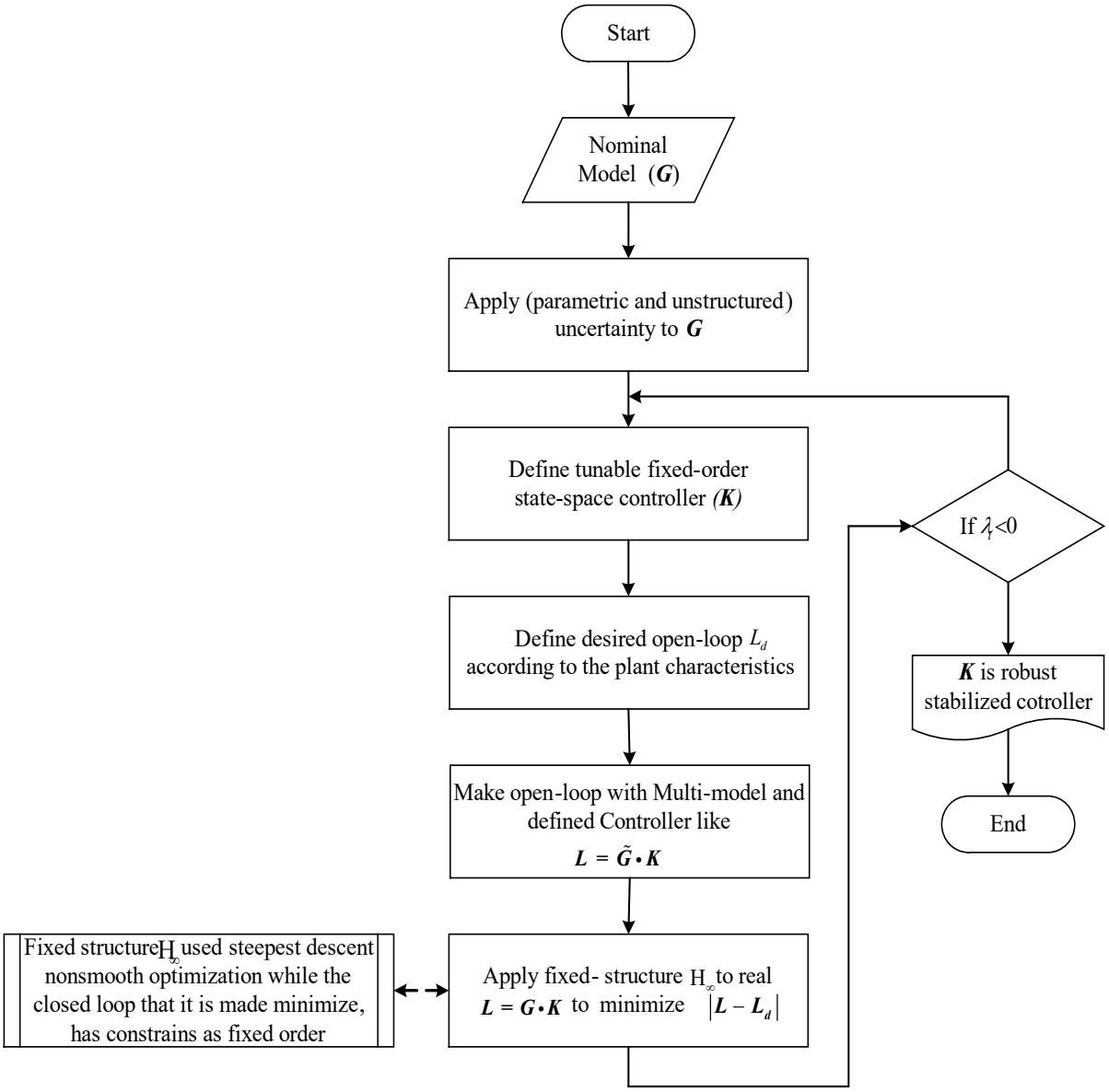

Figure 4. 3. Nonsmooth robust fixed order control procedure

4.1.5. Tuneable Fixed Order State Space Model

Tuneable generalized LTI models represent systems having both fixed and tuneable (or parametric) coefficients, which are used for modelling a control system that contains:

- Fixed components, such as plant dynamics and sensor dynamics,
- Tenable components, such as filters and compensators.

In this research, tunable generalized LTI models for tuning fixed control structures are used. 'Model object' for creating tuneable fixed order state space models is used. Tuneable fixed

order state space model lets the user parametrize a state space model of a given order for parameter studies. In order of making the control robust in face of uncertainty and variety of study parameters, robust structure control criteria are applied for tuneable state space model. It means that tuneable fixed order state space model with robust criteria (such as robust stability and robust performance) are considered together. In this research, H_∞ loop shaping controller is a robust controller with target loop, which makes constraints on the closed loop gains.

4.1.6. H_∞ Loop Shaping

The objectives of H_∞ controller synthesis include ensuring the stability of systems in the face of uncertainties in the system referred to as robust stability. The term 'loop shaping' refers to adjustment of frequency response of the whole system within certain bounds so as to ensure sufficiently robust performance and robust stability.

In loop shaping method of H_∞ controller synthesis closed loop objectives are specified in terms of requirements on open loop singular values. H norm is defined as the supremum of the largest singular value over all frequencies. Desired open loop shape L_d is achieved by designing a controller which provides sufficiently high open loop gain at low frequency (where the modelling error is low) and robust stability is ensured by having a controller which provides sufficiently low open loop gain at high frequency (where modelling error is high). Desired open loop shape L_d and its reciprocal are filtered the error signal e and the white noise source n_w. Figure 4. 4 shows how loop shaping is applied for closed loop that contains robust tuneable fixed order state space model. A generic choice for L_d is ω_c/s where ω_c is the desired open loop bandwidth for any system.

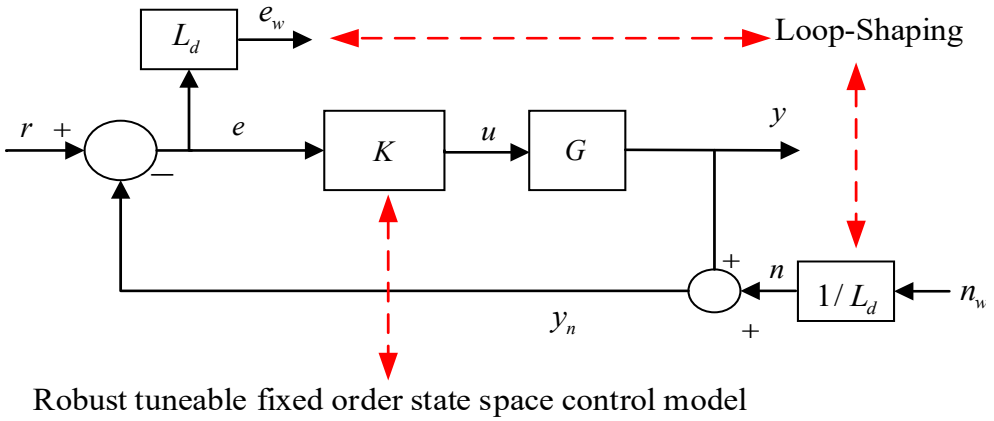

Figure 4. 4. Control structure

4.1.7. Nonsmooth Robust Fixed Order Controller

H_∞ synthesis problems are considered as convex optimization while H_∞ synthesis problems with 'additional structural constraints' represent a nonsmooth and nonconvex optimization. These constraints include:

- Static,
- Fixed order H_∞ output feedback control,
- Structured, sparse or decentralized synthesis,
- Simultaneous stabilization problems,
- Multiple performance channels.

In this research H_∞ synthesis problems solve these problems with a nonsmooth optimization method exploiting the structure of the H_∞ norm. In nominal H_∞ synthesis, feedback controllers are computed via:

- Semi Definite Programming (SDP),
- Algebraic Riccati equations.

When structural constraints on the controller are added, the H_∞ synthesis problem is no longer convex. The customary H_∞ synthesis is solved by LMI while by these constraints are not convex; therefore Bilinear Matrix Inequalities, BMIs, which are genuinely nonconvex, are used to solve. It is applied in some optimization codes for BMI, but it appears that the BMI has numerical difficulties even for problems of moderate size due to the presence of Lyapunov variables, whose number grows quadratically with the number of states. Regarding this problem, it does not use the bounded real lemma and thereby it avoids Lyapunov variables. The cost functions are nonsmooth and require special optimization techniques. The H_∞ norm via the Hamiltonian bisection algorithm is evaluated and exploited further to compute subgradients, which are then used to compute descent steps. Notice, however, that the method is not a pure frequency domain method. In fact, it allows both frequency domain and state space domain parameterizations of the unknown controller. This method under 'Hinfstruct' formula in MATLAB is usable and is described by detail as follows. [96] , [97] .

4.1.7.1. The H_∞ Synthesis Problem

Problem 1: Given a linear time invariant (LTI) system

$$\begin{bmatrix} \dot{x} \\ z \\ y \end{bmatrix} = \begin{bmatrix} A & B_1 & B_2 \\ C_1 & D_{11} & D_{12} \\ C_2 & D_{21} & D_{22} \end{bmatrix} \begin{bmatrix} x \\ w \\ u \end{bmatrix} \tag{4.8}$$

Where $x \in R^n$ is the state, $u \in R^{m2}$ is the control input, $y \in R^{p2}$ is the measured output, $w \in R^{m1}$ is the external input and $z \in R^{p1}$ is the controlled output. The goal is to design a controller K defining:

$$\begin{bmatrix} \dot{x}_k \\ u \end{bmatrix} = K \begin{bmatrix} x_k \\ y \end{bmatrix} = \begin{bmatrix} A_k & B_k \\ C_k & D_k \end{bmatrix} \begin{bmatrix} x_k \\ y \end{bmatrix} \tag{4.9}$$

Let $u = K(s)y$ be a dynamic output feedback control law for the open loop plant (4.8), and let $T_{w\to z}(K)$ denote the closed loop transfer function of the performance channel mapping w into z are given by

$$\begin{bmatrix} \dot{x} \\ z \end{bmatrix} = \begin{bmatrix} A+B_2KC_2 & B_1+B_2KD_{12} \\ C_1+D_{12}KC_2 & D_{11}+D_{12}KD_{21} \end{bmatrix} \begin{bmatrix} x \\ w \end{bmatrix} \tag{4.10}$$

Our aim is to compute K such that the following design requirements are met:

- Internal stability: K stabilizes the original plant (4.10) in closed loop
- Performance: Among all stabilizing controllers, K minimizes performance function $\|T_{w\to z}(K)\|_\infty$

We assume that the controller K has the following frequency domain representation:

$$K(s) = C_K(sI - A_K)^{-1}B_K + D_K, \quad A_K \in R^{k\times k} \tag{4.11}$$

Where k is the order of the controller, and where the case $k = 0$ of a static controller $K(s) = D_K$ is included. Often practical considerations dictate additional challenging structural constraints.

Indeed, for a given system (4.8), suppose we want to find an order $k \le n$ dynamic controller of the form (4.9). Formally, the synthesis problem may then be represented as [96] :

$$\begin{aligned} &\underset{subjectto}{\text{minimize}} \ \|T_{w\to z}(K)\|_\infty \\ &\quad K stabilizes \\ &\quad K_{ind} \in K \end{aligned} \tag{4.12}$$

Where $K_{ind} \in K$ represents a structural constraint on the controller (4.9) like fixed order controller. The H_∞ synthesis problem involves finding an output feedback control matrix K that minimizes the H_∞ norm of a certain transfer function, subject to the constraint that K is stabilizing. This is a challenging problem and even finding a stabilizing K can be difficult. Indeed, if the entries of K are restricted to lie in prescribed intervals, then finding a stabilizing K is a Nondeterministic Polynomial (NP) time hardness hard problem [96] .

4.1.7.2. Multidisk H∞ Synthesis

In this work, optimization of composite function of multi modal is considered which is described as

$$f(K)=\max_{i=1,2,\ldots,N}\left\|T_{w^i\to z^i}(K)\right\|_\infty \tag{4.13}$$

Where $T_{w^i\to z^i}(K)$ are performance specifications of the closed loop multi model system.

- Each $T_{w^i\to z^i}(K)$ is a smooth operator defined on the open domain D of stabilizing feedback controllers K.
- The composite function $f(K)=\max_{i=1,2,\ldots,N}\left\|T_{w^i\to z^i}(K)\right\|_\infty$, are neither smooth nor convex, but their structure can be exploited algorithmically.

This work is suited for local optimization of functions of the form f, and more generally, for semi-infinite nonconvex maximum eigenvalue functions with a related structure. Notice that the max H_∞ function $f(K)$ may be written as

$$f(K)=\max_{i=1,2,\ldots N}\left\|T_{w^i\to z^i}(K)\right\|_\infty=\max_{\omega\in R}\bar{\sigma}(T(K,j\omega))=\max_{\omega\in R}\lambda_1(T(K,j\omega)T(K,j\omega)^H)^{1/2} \tag{4.14}$$

where $\sigma(M)$ and $\lambda_1(M\,M^H)$ denote the maximum singular value respectively the maximum eigenvalue, and where $T(K, j\omega)$ has a block structure with N blocks regrouping the different performance channels:

$$T(K,j\omega)=diag(T_{w^1\to z^1}(K,j\omega),\ldots,T_{w^N\to z^N}(K,j\omega)) \tag{4.15}$$

In particular, $T(K, j\omega)T(K, j\omega)^H$ is then block diagonal with N blocks, so that f may be interpreted as an infinite maximum of maximum eigenvalue functions. This structure will be exploited for the nonsmooth analysis of f. We mention that this particular structure of the objective f already occurs in the simpler H_∞ synthesis discussed in [97] .

Multi model $P^i(s)$ represents a family of $P(s)$ and is described in state space form as

$$\boldsymbol{P}^i(s):\begin{bmatrix}\dot{x}^i\\ z^i\\ y^i\end{bmatrix}=\begin{bmatrix}A^i & B^i{}_1 & B^i{}_2\\ C^i{}_1 & D^i{}_{11} & D^i{}_{12}\\ C^i{}_2 & D^i{}_{21} & D^i{}_{22}\end{bmatrix}\begin{bmatrix}x^i\\ w^i\\ u^i\end{bmatrix},\quad i=1,...,N \tag{4.16}$$

The goal is to design a controller $K\,u^i = K(s)y^i$ for the plant family in (4.16).

$$\begin{bmatrix}\dot{x}_k\\ u^i\end{bmatrix}=K\begin{bmatrix}x_k\\ y^i\end{bmatrix}=\begin{bmatrix}A_k & B_k\\ C_k & D_k\end{bmatrix}\begin{bmatrix}x_k\\ y^i\end{bmatrix} \tag{4.17}$$

4.1.7.3. Subdifferential of the H_∞ Norm

In this section, the subdifferential of the H_∞ norm derives *s* for the Clarke subdifferential of several nonconvex composite functions $f(x)=\|G(x)\|_\infty$, where *G* is a smooth operator defined on some R^n with values in the space of stable matrix transfer functions H_∞.

Consider the H_∞ norm of a nonzero transfer matrix function *G(s)*:

$$\|G\|_\infty=\sup_{\omega\in R}\bar{\sigma}(G(j\omega)) \tag{4.18}$$

where *G* is stable and $\bar{\sigma}(x)$ is the maximum singular value of *X*. $\|G\|_\infty=\bar{\sigma}(G(j\omega))$ is attained at some frequency ω that the case $\omega = \infty$ is allowed.

G is a smooth operator, mapping R^n onto the space H_∞ of stable transfer functions *G*. Then the composite function *f*, $f(x)=\|G(x)\|_\infty$ is Clarke subdifferentiable at *x* with

$$\partial f(x)=G'(x)^*\left[\partial\|.\|_\infty G(x))\right] \tag{4.19}$$

Where $\partial\|.\|_\infty$ is the subdifferential of the H_∞ norm obtained above, and $G'(x)^\star$ is the adjoint of $G'(x)$, mapping the dual of H_∞ into R^n. In the sequel, we will compute this adjoint $G'(x)^\star$ for special classes of closed loop transfer functions defined as:

$$\partial\|.\|_\infty\circ G(x)=\phi(H)=\|G\|_\infty^{-1}\,\mathrm{Re}\sum_{\nu=1}^{P}TrG(j\omega_\nu)^H Q_\nu Y_\nu Q_\nu^H H(j\omega_\nu) \tag{4.20}$$

Where $Y_\nu\geq 0$, $\sum Tr\,(Y_\nu)=1$

4.1.7.4. Clarke Subdifferentionals in Closed Loop

Considering a stabilizing controller *K(s)* and a plant

$$\boldsymbol{G}(s) := \begin{bmatrix} G_{11}(s) & G_{12}(s) \\ G_{21}(s) & G_{22}(s) \end{bmatrix} \tag{4.21}$$

the closed loop transfer function is

$$T_{w\to z}(K) := G_{11} + G_{12}K(I - KG_{22})^{-1}G_{21} \tag{4.22}$$

Where the state space data of G_{11}, G_{12}, G_{21} and G_{22} are given in (4.21) and the dependence on *s* is omitted for brevity. Our aim is to compute the subdifferential $\partial f(K)$ of $f := \|\cdot\|_\infty \circ T_{w\to z}$ at *K*. The derivative $T_{w\to z}(K)$ of $T_{w\to z}$ at *K* is

$$T'_{w\to z}(K)\delta K := G_{12}(I - KG_{22})^{-1}\delta K(I - G_{22}K)^{-1}G_{21} \tag{4.23}$$

Where δK is an element of the same matrix space as *K*.

$\phi = \phi_Y$ is a subgradient of $\|\cdot\|_\infty$ at $T_{w\to z}(K)$ that is a finite number of frequencies $\omega_1,\ldots,\omega_q$ of the form

$$\begin{aligned} \boldsymbol{\Phi}_Y &= \|T_{w\to z}(K)\|_\infty^{-1} \sum_{\nu=1}^{q} \mathrm{Re}((I - G_{22}(j\omega_\nu)K)^{-1}G_{21}(j\omega_\nu) \\ &T_{w\to z}(K, j\omega_\nu)^H Q Y_\nu Q^H G_{12}(j\omega_\nu)(I - KG_{22}(j\omega_\nu))^{-1})^T \end{aligned} \tag{4.24}$$

Whereas $Y = (Y_1,..,\ Y_q)$, $Y_\nu \geq 0$ and $\sum_{\nu=1}^{q} Tr(Y_\nu) = 1$

4.1.7.5. Subdiffrentials of the Max H_∞ Mapping

The Clarke subdifferential of the combination function, finite maximum $f(K) = \max_{i\in I(K)} \left\| T_{w^i\to z^i}(K) \right\|_\infty$ by considering the following condition

$$I(K) = \{i \in \{1,\ldots,N\} : \left\| T_{w^i\to z^i}(K) \right\| = f(K)\} \tag{4.25}$$

The set of active indices at a given *K*. More over for each $i \in I(K)$, we consider the set of active frequencies

$$\Omega^i(K) = \{\omega \in [0,+\infty] : \bar{\sigma}(T_{w^i\to z^i}(K, j\omega)) = f(K)\} \tag{4.26}$$

It is assumed through that $\Omega^i(K)$ is a finite set, indexed as

$$\Omega^i(K)=\{\omega_\nu^i:\nu=1,...,P^i\},i\in I(K) \tag{4.27}$$

The set of all active frequencies is denoted as $\Omega(K)$

$$\partial f(K)=\mathrm{co}\{\partial(\|.\|_\infty\circ T_{w^i\to z^i})(K)\quad i\in I(K)\} \tag{4.28}$$

$$\begin{aligned}\Phi_{Y,\Gamma}=&\|T_{W^i\to z^i}(K,j\omega_\nu^i)\|_\infty^{-1}\sum_{i\in I(K)}\sum_{\nu=1}^{q_i}\mathrm{Re}\{(I-G_{22}^i(K,j\omega_\nu^i))^{-1}G_{21}^i(K,j\omega_\nu^i)\\ &T_{w^i\to z^i}(K,j\omega_\nu^i)^H Q_\nu^i\Gamma_i Y_\nu^i(Q_\nu^i)^H G_{12}^i(K,j\omega_\nu^i)(I-KG_{22}^i(K,j\omega_\nu^i))^{-1}\}^T\end{aligned} \tag{4.29}$$

From the definition of the Γ_i and the Y_ν^i

$$Tr\sum_{i\in I(K)}\sum_{\nu=1,...,p^i}\Gamma_i Y_\nu^i=\sum_{i\in I(K)}\Gamma_i Tr\sum_{\nu=1,...,p^i}Y_\nu^i=1$$

4.1.7.6. Dynamic Controllers

Assume that the controller is dynamic as in (4.11). The subgradient set is again via formula (4.24) by performing the substitutions for multi model:

$$\begin{aligned}&\boldsymbol{K}\to\begin{bmatrix}A_K & B_K\\ C_K & D_K\end{bmatrix},\ \boldsymbol{A}\to\begin{bmatrix}A^i & 0\\ 0 & 0\end{bmatrix},\ \boldsymbol{B}_1\to\begin{bmatrix}B_1^i\\ 0\end{bmatrix},\ \boldsymbol{C}_1\to\begin{bmatrix}C_1^i & 0\end{bmatrix}\\ &\boldsymbol{B}_2\to\begin{bmatrix}0 & B_2^i\\ I_K & 0\end{bmatrix},\ \boldsymbol{C}_2\to\begin{bmatrix}0 & I_K\\ C_2^i & 0\end{bmatrix},\ \boldsymbol{D}_{12}\to\begin{bmatrix}0 & D_{12}^i\end{bmatrix},\ \boldsymbol{D}_{21}\to\begin{bmatrix}0\\ D_{21}^i\end{bmatrix}\end{aligned} \tag{4.30}$$

The following Clarke partial sub gradients with respect to the controller variables A_k, B_k, C_k and D_k:

$$\begin{aligned}\Phi_{Y,A_K}=&\|T_{w^i\to z^i}(K,j\omega_\nu^i)\|_\infty^{-1}\sum_{i\in I(K)}\sum_{\nu=1}^{q}\mathrm{Re}\{(j\omega_\nu^i I-A_K)_{-1}B_K G_{21}^i(K,j\omega_\nu^i)\\ &T_{w^i\to z^i}(K,j\omega_\nu^i)^H Q_\nu^i\Gamma_i Y_\nu^i(Q_\nu^i)^H G_{12}^i(K,j\omega_\nu^i)C_K(j\omega_\nu^i I-A_K)^{-1})^T\end{aligned} \tag{4.31}$$

$$\begin{aligned}\Phi_{Y,B_K}=&\|T_{w^i\to z^i}(K,j\omega_\nu^i)\|_\infty^{-1}\sum_{i\in I(K)}\sum_{\nu=1}^{q_i}\mathrm{Re}\{G_{21}^i(K,j\omega_\nu^i)T_{w^i\to z^i}(K,j\omega_\nu^i)^H\\ &Q_\nu^i\Gamma_i Y_\nu^i(Q_\nu^i)^H G_{12}^i(K,j\omega_\nu^i)C_K(j\omega_\nu^i I-A_K)^{-1}\}^T\end{aligned} \tag{4.32}$$

$$\Phi_{Y,C_K} = \left\| T_{w^i \to z^i}(K, j\omega_\nu^i) \right\|_\infty^{-1} \sum_{i \in I(K)} \sum_{\nu=1}^{q_i} \mathrm{Re}\{(j\omega_\nu^i I - A_K)^{-1} B_K G_{21}^i(K, j\omega_\nu^i) \\ T_{w^i \to z^i}(K, j\omega_\nu^i)^H Q_\nu^i \Gamma_i Y_\nu^i (Q_\nu^i)^H G_{12}^i(K, j\omega_\nu^i)\}^T \tag{4.33}$$

$$\Phi_{Y,D_K} = \left\| T_{w^i \to z^i}(K, j\omega_\nu^i) \right\|_\infty^{-1} \sum_{i \in I(K)} \sum_{\nu=1}^{q} \mathrm{Re}\{G_{21}^i(K, j\omega_\nu^i) T_{w^i \to z^i}(K, j\omega_\nu^i)^H \\ Q_\nu^i \Gamma_i Y_\nu^i (Q_\nu^i)^H G_{12}^i(K, j\omega_\nu^i)\}^T \tag{4.34}$$

With the notations

$$G_{21}^i(s) = (I - P_{22}^i(s)K(s))^{-1} P_{21}^i(s) \\ G_{12}^i(s) = P_{12}^i(s)(I - K(s)P_{22}^i(s))^{-1} \tag{4.35}$$

The entire Clarke subdifferential is described by the set of subgradients in $M_{K+m_2,K+P_2}$

$$\Phi_Y = \begin{bmatrix} \Phi_{Y,A_K} & \Phi_{Y,B_K} \\ \Phi_{Y,C_K} & \Phi_{Y,D_K} \end{bmatrix} \tag{4.36}$$

Whereas before *Y= (Y1,.., Yq),* $Y_\nu \geq 0$ and $\sum_{\nu=1}^{q} Tr(Y_\nu) = 1$

4.1.7.7. Steepest Descent Method

The standard form of a continuous optimization problem is

$$\begin{array}{ll} \text{minimize} & f(x) \\ \text{subjectto} & i\text{nequality} \\ & \text{constraints} \end{array}$$

Solving the optimization program first order descent algorithm for composite functions of the H_∞ norm is devised while steepest descent method fails to converge due to the nonsmoothness of H_∞ norm. $\|T_{w\to z}(K)\|_\infty$ is a nonsmooth objective function which is subject to two sources of nonsmoothness. The nonsmoothness of the maximum eigenvalue function and the nonsmoothness introduced by the operator sup which in the case of $\|.\|_\infty$ is even infinite.

$$f(K, \omega) = \bar{\sigma}(T(K, j\omega)) = \max_{i=1,\ldots,N} \bar{\sigma}(T_{w^i \to z^i}(K, j\omega)) \tag{4.37}$$

Minimization of *f* may be interpreted as a semi-infinite minimization problem involving the infinite family *f (., ω)*. At a given *K*, recall that *Ω(K)* is the set of active frequencies at *K*. Clearly *f(K, ω)≤ f(K)* for all *ωϵ R* and *f(K, ω)=f(K)* for all *ωϵ Ω(K)* at *K* is defined as the set of subgradients (4.31) -(4.34).

Optimality function for any set $\Omega_e(K)$ and for some δ>0 is

$$\theta_e(K) := \inf_{H\in R^{m2}\times R^{p2}} \sup_{\omega\in\Omega_e(K)} \sup_{Y_\omega\in y_w(K)} -f(K)+f(K,\omega)+\langle \Phi_{Y,\omega}, H\rangle + \frac{1}{2}\delta\|H\|_F^{\,2} \tag{4.38}$$

θ_e is the optimally function and the first order model for the original problem augmented by a second order $\frac{1}{2}\delta\|H\|_F^{\,2}$.

For computing $\theta_e(K)$ via SDP equation (4.38) is considered as

$$\theta_e(K) := \sup_{\sum_{w\in\Omega_e(K)} \Gamma_w=1,\Gamma_w>0} \sup_{Y_w\in y_w(K)} \sum_{w\in\Omega_e(K)} G_w(f(K,w) - f(K)) - \frac{1}{2d}\left\| \sum_{w\in W_e(K)} \Gamma_w \Phi_{Y,w} \right\|_F^2 \tag{4.39}$$

$$H(K) = -\frac{1}{\delta} \sum_{\omega\in\Omega_e(K)} \Gamma_\omega \Phi_{Y,\omega} \tag{4.40}$$

The change of variable $Z_\omega=\Gamma_\omega Y_\omega$ we readily get

$$Z_\omega = \underset{i\in I_\omega(K)}{diag}\, Z_\omega^i \text{ with } Tr(Z_\omega)=\Gamma_\omega, Z_\omega = Z_\omega^H \geq 0 \tag{4.41}$$

$$\Phi_{Z,\omega} = f(K,\omega)^{-1} \sum_{i\in I_\omega(K)} \mathrm{Re}\left\{ G_{21}^i(K,j\omega) T_{w^i\to z^i}(K,j\omega)^H Q_\omega^i Z_\omega^i (Q_\omega^i)^H G_{12}^i(K,j\omega) \right\}^T \tag{4.42}$$

$$\theta_e(K) := \sup_{\sum_{\omega\in\Omega_e(K)} TrZ_\omega=1, Z_\omega\geq 0} \sum_{\omega\in\Omega_e(K)} TrZ_\omega (f(K,\omega)-f(K)) - \frac{1}{2\delta}\left\| \sum_{\omega\in\Omega_e(K)} \Phi_{Z,\omega} \right\|_F^2 \tag{4.43}$$

Since $f(K,\omega)\leq f(K)$ for all ω then $\theta_e(K)<0$. Using formula (4.39) shows $\theta_e(K)=0$ when $\Gamma_\omega=0$ for all $\omega\epsilon\, \Omega_e(K)\setminus \Omega(K)$. But then $\theta_e(K)=0$ comes down to

$$0 = \sup_{Y_\omega\in y_w(K)} -\frac{1}{2\delta}\left\| \sum_{\omega\in\Omega(K)} \Gamma_\omega \Phi_{Y,\omega} \right\|_F^2 \tag{4.44}$$

For certain $\Gamma_\omega\geq 0$, $\omega\epsilon\, \Omega(K)$, summing up to one, independently of the extension $\Omega_e(K)$ of $\Omega(K)$. By the defining of $\Phi_{Y,\omega}$ equality (4.44) is equivalent to

$$\sum_{\omega\in\Omega(K)} \Gamma_\omega f(K)^{-1} \sum_{i\in I_\omega(K)} \mathrm{Re}\left\{ G_{21}^i(K,j\omega) T_{w^i\to z^i}(K,j\omega)^H Q_\omega^i Z_\omega^i (Q_\omega^i)^H G_{12}^i(K,j\omega) \right\}^T = 0 \tag{4.45}$$

When $\theta_e(K)<0$ then $H(K)$ in (4. 4) is qualified descent direction of f at K in the sense that

$$f'(K,H(K)) \leq \theta_e(K) - \frac{\delta}{2}\|H(K)\|^2 < 0 \tag{4.46}$$

Where $f'(K; H)$ denotes the Clarke directional derivative of f at K in direction H. It used the fact that for $\omega \epsilon\, \Omega(K)$ the terms $-f(K)+f(K, \omega)$ vanish.

The above analysis follows the nonsmooth descent algorithm for the minimization of $f(K)$ where, $0<\alpha<1$, $0<\beta<1$ and $\delta>0$ are fixed parameters.

A nonsmooth algorithm for structured H_∞ synthesis [96] , [97] :

1. Initialization. Find a controller K, which stabilizes the original plant G.
2. Generate frequencies. Given the current K, compute $f(K)$ and obtain active frequency $\Omega(K)$. Select a finite enriched set of frequencies $\Omega_e(K)$ containing $\Omega(K)$.
3. Descent direction. Compute $\theta_e(K)$ and solution (τ, K) of SDP. If $\theta_e(K)=0$, stop, because $0 \epsilon\, \partial f(K)$. Otherwise compute descent direction (K).
4. Line search. Find largest $t=\beta k$ such that $f(K+ tH(K)) \leq f(K)+t_\alpha \theta_e(K)$ and such that $K+tH(K)$ remains stabilising.
5. Step. Replacing K by $K+tH(K)$, increase iteration counter by one, and go back to step 2.

It is important how to choose the frequency set $\Omega_e(K)$ in step 2 of the algorithm in order to achieve convergence of the method. Furthermore, multidisk H_∞ synthesis requires repeated computations of H_∞ norms that is done quite efficiently using the bisection algorithm. As a byproduct, this algorithm returns estimates of the primary and secondary peak frequencies $\omega \in \{\omega_1(K), \ldots, \omega_p(K)\}$. In the numerical experiments, it has been observed that it is generally beneficial to consider an extended set of frequencies including the primary and secondary peak set $\Omega_e(K) \supseteq \Omega(K)$. For more details, [96] , [97] . gives accurate information about nonsmooth optimization for H_∞ and multidisk H_∞ synthesis.

CHAPTER 5 .EFFECT OF UNCERTAINTY ON POWER PLANT TRANSFER FUNCTION

5.1. Introduction

The uncertainties of plants may take various forms. But in order to establish an effective theory for analysis and design, the form of plant set description must be limited. It is especially important to ensure that the uncertainty description can be widely applied. To achieve a high performance, the key in control design is how to make use of information about the uncertainty as much as possible. This information can only be described as the boundary of the uncertainty set. Moreover, how to set up a bounding model for the uncertainty 'Δ'. Obviously, the gain of Δ is a useful information.

In this chapter, different sources of uncertainty that can affect on power system stability is introduced and categorized. The influence of different kind of uncertainty on the open loop transfer function denominator of the linearized two area, four machine power system benchmark model is studied independently. Effect of all uncertainty sources will be considered in design of controller that is shown.

5.2. Two Area, Four Machine System

The two area, four machine system was created to exhibit the different types of oscillations that occur in both large and small interconnected power systems. Detailed model descriptions are given in Appendix A. Figure 5. 1 shows the two area, four machine system. All synchronous machines are modeled with static excitation system. The export power P_{tie} from Area 1 to Area 2 through the tie line is 400 MW and chosen as nominal operating point. Power systems have some uncertainties naturally. This type of uncertainties as unstructured (frequency dependent) and structured will be studied for this grid as follows.

Time delay is considered in controller structure to compensate distance and computation between measurements and actuators with controller. These influences will be presented by parametric uncertain time delay in propagated and fixed types. Scalar real parameters are used for this type of uncertainty, which are described in one dimension.

Dynamic response of loads, high penetration of renewable energy sources, variant generation, consumption and grid topology will be presented by frequency dependent uncertainty in this study. Full complex perturbation matrix Δ usually with dimensions compatible with of the nominal model is used for this type of uncertainty.

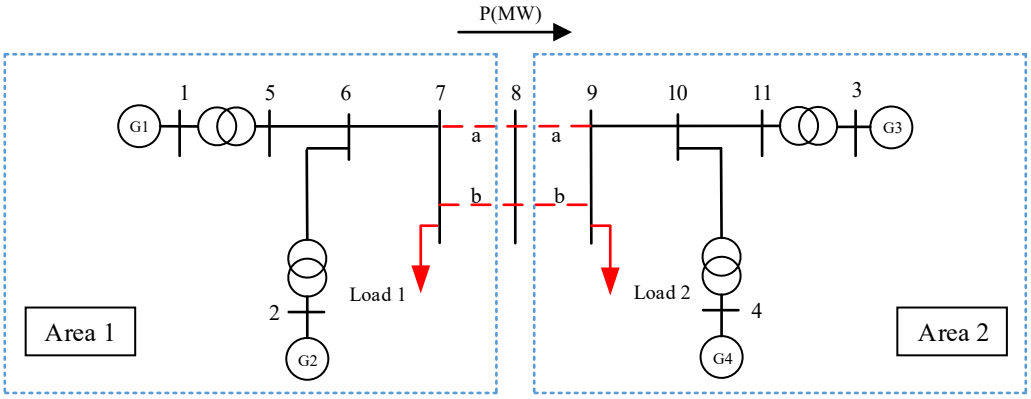

Figure 5. 1. Two area, four machine test system

5.3. Time Delay as Structured Uncertainty

Many control design algorithms cannot handle time delays directly. A common technique is to replace delays with all pass filters that approximate the delays. To approximate time delays in continuous time LTI models, the Padé command to compute a Padé approximation is applicable. The Padé approximation is valid only at low frequencies and provides better frequency domain approximation than time domain approximation.

The impact of time delays evoked by remote signal transmission and computation in the large interconnected power systems for wide area measurement has to be considered. $T(s) = e^{-Ts}$ is Laplace domain function, which is described as Padé approximation in the linearized power system model, which is given by [98] :

$$e^{-sT} \approx \sum_{i=0}^{2n} (-1)^i \frac{(Ts)^i}{i!} = \frac{\sum_{i=0}^{n-1} p_i (Ts)^i}{\sum_{i=0}^{n} q_i (Ts)^i} \tag{5.1}$$

Where $p_0, p_1, \ldots, p_{n-1}$ and $q_0, q_1, \ldots, q_n$ are constant and n is the order of Padé approximation of the continuous time.

The closed loop feedback control system with time delays is shown in Figure 5. 2. The time delay is considered in two parts:

- T_{in} is the time used for measurement processing, synchronization and transmission from PMUs to the controller;
- T_{out} is the time used for control signal calculations and transmission from the controller to control sites.

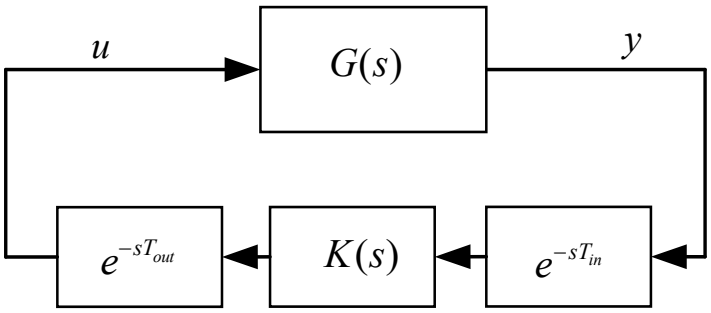

Figure 5. 2. Controller design with time delay

In the Laplace domain, time delays are expressed in the exponential form (e^{-sT}). It can be replaced by a first order Padé approximation [98] :

$$e^{-sT_d} \approx \frac{-\frac{1}{2}sT_d+1}{\frac{1}{2}sT_d+1} \tag{5.2}$$

The state expression for the delay is:

$$\dot{x} = -\frac{2}{T_d}x + \frac{4}{T_d}u \tag{5.3}$$

$$y = x - u \tag{5.4}$$

Time delay as a parametric uncertain amount is considered as a real scalar perturbation, δ_t and $-1 \le \delta_t \le 1$, which is written:

$$T_d = a + b\delta_t \ , \qquad \delta_t \in [-1,1] \tag{5.5}$$

$T_{in}=0.125(1+0.6\delta_t)$ covers an uncertain time delay from 75 ms to 200 ms.

$T_{out}=0.1\ (1+0.5\delta_t)$ covers an uncertain time delay from 50 ms to 150 ms.

The total time delay is in the range of [125 –350] ms.

Figure 5. 3 gives a delay free system without the controller connected with a time delay block.

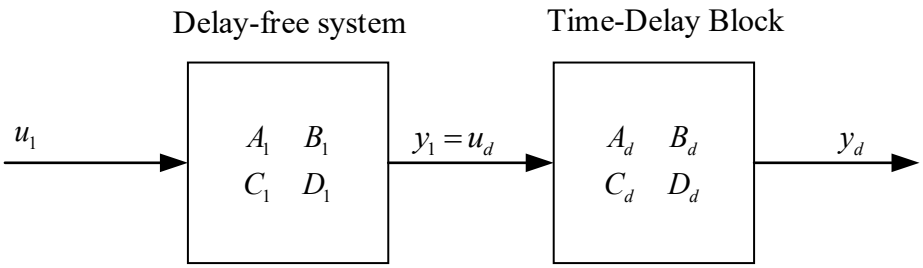

Figure 5. 3. Delay free system connected with time delay block

The state spaces of these two systems are represented mathematically as:

$$\dot{x}_1 = A_1 x_1 + B_1 u_1 \tag{5.6}$$

$$y_1 = C_1 x_1 + D_1 u_1 \tag{5.7}$$

$$\dot{x}_d = A_d x_d + B_d u_d \tag{5.8}$$

$$y_d = C_d x_d + D_d u_d \tag{5.9}$$

Since $u_d = y_1$ we have

$$\begin{bmatrix} \dot{x}_1 \\ \dot{x}_d \end{bmatrix} = \begin{bmatrix} A_1 & 0 \\ B_d C_1 & A_d \end{bmatrix} \begin{bmatrix} x_1 \\ x_d \end{bmatrix} + \begin{bmatrix} B_1 \\ B_d D_1 \end{bmatrix} u_1 \tag{5.10}$$

$$yd = \begin{bmatrix} D_d C_1 & C_d \end{bmatrix} \begin{bmatrix} x_1 \\ x_d \end{bmatrix} + D_d D_1 u_1 \tag{5.11}$$

The $\boldsymbol{A}$, $\boldsymbol{B}$, $\boldsymbol{C}$ and $\boldsymbol{D}$ matrices for the connected system are,

$$\boldsymbol{A} = \begin{bmatrix} A_1 & 0 \\ B_d C_1 & A_d \end{bmatrix}, \boldsymbol{B} = \begin{bmatrix} B_1 \\ B_d D_1 \end{bmatrix}, \boldsymbol{C} = \begin{bmatrix} D_d C_1 & C_d \end{bmatrix}, \boldsymbol{D} = D_d D_1 \tag{5.12}$$

Time delay does not have any considerable effect on magnitude on frequency domain but it is noticeable effect on phase diagram that as shown in Figure 5. 4.

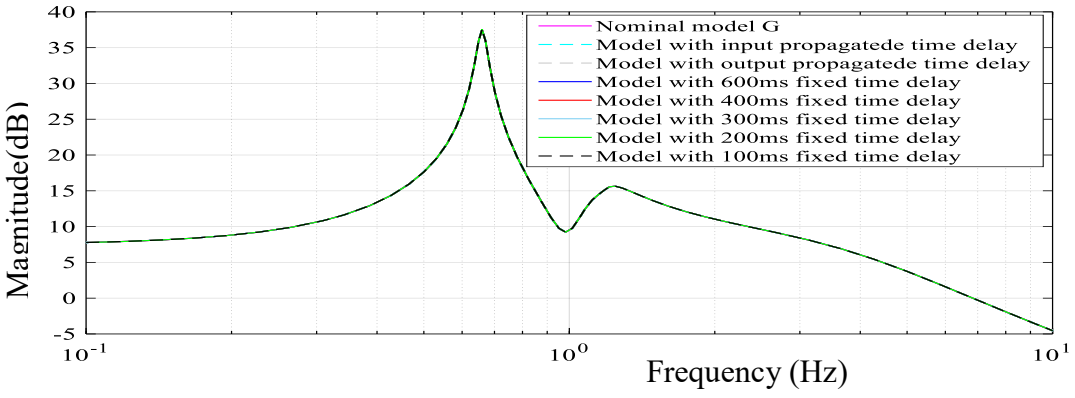

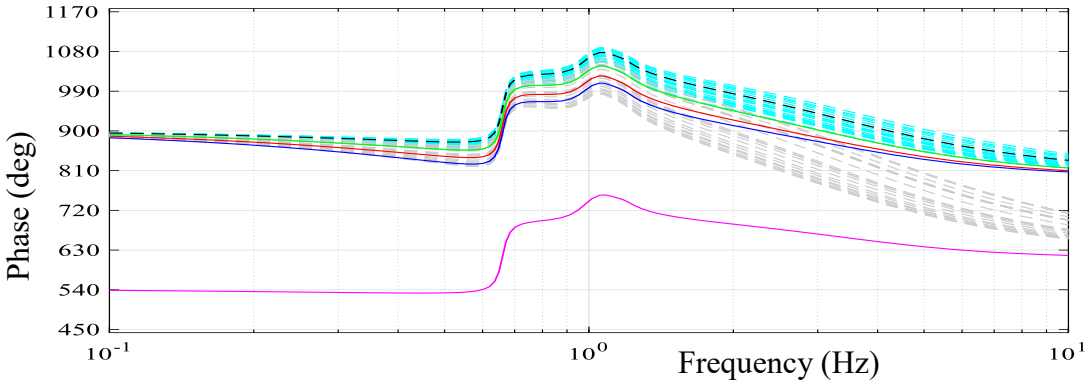

Figure 5. 4. Magnitude and phase of frequency response to time delay

The impact of time delay is concealable on designing WADC due to its effect on wide area measurement and control system destabilizing the system in some cases [99] . Time delays in WADC arise from

- Measurements processing,
- Transmission,
- Synchronization,
- Control signals calculation and transmission.

The value of time delay is an uncertain amount and becomes a significant limitation in the design and operation of wide area damping control systems. A WADC should be robust not only for different operating conditions but also for this uncertain time delay.

Data latency is the biggest part of time delay in a wide area damping control system. Data latency is the time it takes from measuring the synchrophasor at the PMU to deliver the control input to the application

Time delays are caused by the following factors:

- Transducer delays
- Window size of the DFT
- Processing time of PMU
- Data size of the PMU output
- Multiplexing and transitions
- Communication links involved

Data processing and synchronizations delay includes two parts:

- *Fixed delay*

- Delay due to processing, DFT, multiplexing and data processing and synchronizations
- Independent of communication medium used
- Estimated to be around 75 ms [100] .

- *Propagation delay*

- Function of the communication link and physical separation
- Ranges from 20 ms in case of fiber optic cables to 200 ms in case of low earth orbiting satellites

The total time delays takes for different communication links, from data measured by PMUs to control locations [100] , are:

- Fiber optic cable ~ 100-150 ms
- Microwave links ~ 100-150 ms
- Power Line Cable (PLC) ~ 150-350 ms
- Telephone lines ~ 200-300 ms
- Satellite link ~ 500-700 ms

5.4. Unstructured Uncertainty

Power systems constantly experience changes in operating conditions due to variations in generation (renewable and conventional generations) load patterns and types (dynamic and static), as well as changes in transmission networks (topology changes). Even under nominal operating conditions, there is still some uncertainty present due to only an approximate knowledge of the power system parameters, neglected high frequency dynamics, or invalid assumptions made in the model formulation process. There is a discrepancy between the nominal plant and real system in the special frequency band (in this study inter-area frequency). Therefore, for unstructured uncertainty its gain bound must be described by a function of frequency. Concretely, we carry out identification experiments under different conditions to get a number of models $\tilde{G} = G_i(j\omega)$ (i = 1, 2, ⋯). Then, by calculating the gains of all $G_i(j\omega) - G(j\omega)$ and drawing curves, we can find a bounding function $w_{unc}(j\omega)$ satisfying

$$\left|\tilde{G}(j\omega) - G(j\omega)\right| \le \left|\Delta(j\omega).w_{unc}(j\omega)\right| \quad \forall \omega, i$$

$\tilde{G}$ is multi model (perturbed model) which contains linearized models with different uncertainties.

5.4.1. Perturbed Model with Unstructured Uncertainties

Nominal plant transfer function is *G,* and perturbed plant transfer function $\tilde{G}$ is considered as

$$\tilde{G}(j\omega) = (G(j\omega)) \cdot (I + \Delta(j\omega) \cdot w_{unc}(j\omega)) \tag{5.13}$$

which is represented by Figure 5. 5.

- *G* is a nominal model of the system that is linearized around a given operating point.
- *Δ* is a full complex perturbation matrix usually with dimension compatible with that of the nominal model used for this type of uncertainty where at each frequency *Δ(jω)* satisfying $\sigma(\Delta(j\omega)) \leq 1$ is allowed.
- w_{unc} is an uncertain weighting function to describe the set of plants (linearized models with different uncertainties) by a single (lumped) complex perturbation matrix.
- $\tilde{G}$ is a multi model (perturbed model) transfer function of identification experiments under different conditions.

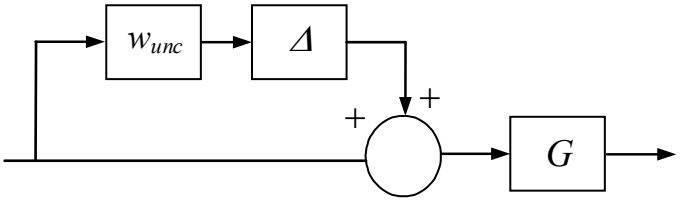

Figure 5. 5. Model with multiplicative uncertainty

w_{unc} is a fixed stable transfer function. The idea behind this uncertainty model is that $\Delta \cdot w_{unc}$ is the normalized plant perturbation away from 1:

$$\frac{G}{\tilde{G}} - 1 = \Delta \cdot w_{unc} \tag{5.14}$$

Hence if $||\Delta||_\infty < 1$, then

$$\left| \frac{G(j\omega)}{\tilde{G}(j\omega)} - 1 \right| \leq |w_{unc}(j\omega)| \tag{5.15}$$

w_{unc} is extracted of multi model, which is shown in Figure 5. 6 [92] , [93] , [94] .

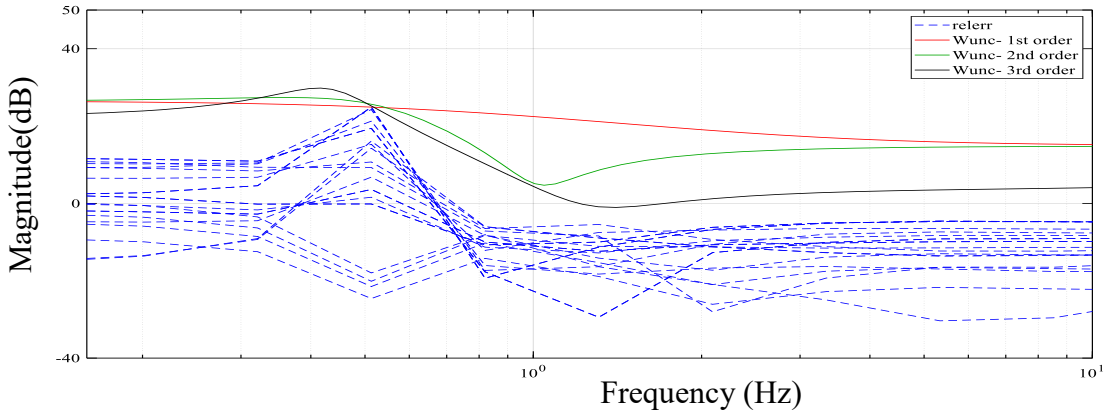

Figure 5. 6. Transfer function of extracted w_{unc} of multi model, ($relerr = \left| \frac{G(j\omega)}{\tilde{G}(j\omega)} - 1 \right|$)

w_{unc} has possibility to be selected in different orders. Higher order of w_{unc} contains more accurate features of uncertain model.

5.4.2. Load Model Uncertainty

The mathematical representation of load modelling depends on the measured voltage and/or frequency at a bus, and the active and reactive power consumed by the load. Due to the high diversity and distribution of power system loads, several alternatives have been proposed throughout the time for their representation, depending on their main purpose. The load models are traditionally classified into two broad categories: static and dynamic models. A static load model is not dependent on time, and therefore it describes the relation of the active and reactive power at any time with the voltage and/or frequency at the same instant of time. On the other hand, a dynamic load model expresses this relation at any instant of time, as a function of the voltage and/or frequency time history, including normally the present moment [51] .

In chapter 2 different types of loads have been described by detail. In the following by use of Bode diagram, it is shown how changing load parameters and types can impact on behaviour of the system.

5.4.2.1.Static Load

In case of static exponential load model, load components are shown in Table 2. 4 with different exponents for active and reactive power. Identification experiments under the behaviour of the test power system with same parameters (amount of active and reactive load powers are constant) and different load components (n_p and n_q, exponential values are changed) are given a number of models ($\tilde{G} = G_i(j\omega)$) which are shown in Figure 5. 7.

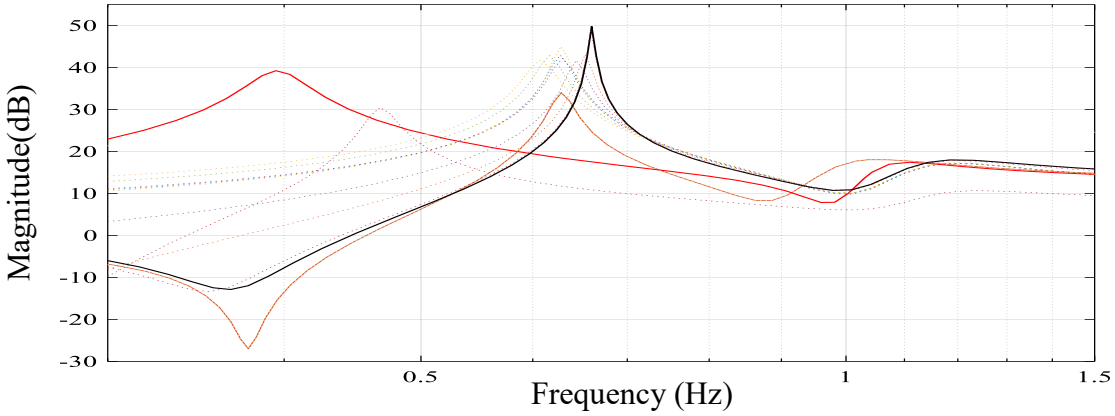

Figure 5. 7. Inter-area and local modes of perturbed model with different load components

As it can be seen in Figure 5. 7 the range of inter-area frequency [0.1, 1] Hz, as the interest of WADC design, changes in magnitude and range of frequency dramatically.

5.4.2.2. Dynamic Load Models

Physical dynamic load model is used in this research as described by detail in chapter 2. A simplified induction motor model is simulated as dynamic load. Even though the structure of synchronous generator and induction machines is different, a system wide aggregation of state variables is possible. This aggregation is useful in interpreting certain modes arising from the interaction of both types of machines. These aggregation concepts are illustrated below with the test power system composed of 4 synchronous generators and 2 aggregated IM loads as shown in Figure 5. 1.

The effect of dynamic and static loads on the damping and frequency of the oscillatory modes is analysed by eigenvalue analysis. Eigenvalue analysis is compared in Table 5. 1 for three cases:

- Composite load with 100 % static load in both sides. (Change of Load 1 and 2 in Figure 5. 1)
- Composite load with 50 % dynamic and static ones in one side. (Change of Load 1 in Figure 5. 1)
- Composite load with 50 % dynamic and static ones in both sides. (Change of Load 1 and 2 in Figure 5. 1)

According to eigenvalue analysis, damping ratio of inter-area and local frequencies is generally worse by presence of dynamic loads. Any induction machine collective creates a local mode with high damping ratio (ζ) which is shown in Table 5. 1.

Table 5. 1. Eigenvalue analysis

Mode type	**Eigenvalue** $\sigma \pm j\omega$	ζ **(%)** $-\sigma/\sqrt{\sigma^2+\omega^2}$	**Frequency (Hz)** $\omega/2\pi$
Power grid with 100% static load			
Inter-area	$0.05 \pm j3.86$	-1.27	0.61
Local	$-0.668 \pm j7.05$	9.43	1.12
Local	$-0.81 \pm j7.18$	11.2	1.15
Power grid with 50% dynamic and static load in one side			
Inter-area	$0.14 \pm j4.08$	-3.39	0.64
Local	$-0.58 \pm j7.15$	8.1	1.14
Local	$-0.72 \pm j7.25$	9.94	1.16
Local-IM	$-12.1 \pm j2.94$	97.1	1.98
Power grid with 50% dynamic and static load in both sides			
Inter-area	$0.02 \pm j4.08$	-0.05	0.60
Local	$-0.48 \pm j7.16$	6.72	1.14
Local	$-0.82 \pm j7.23$	11.3	1.16
Local-IM	$-7.81 \pm j4.47$	86.8	1.43
Local-IM	$-12.1 \pm j2.94$	97.1	1.94

Dynamic loads cause changing amount and number of critical oscillatory frequencies as shown in Figure 5. 8. Rather additional local modes which are created by induction machines with high damping ratio don't have critical effect.

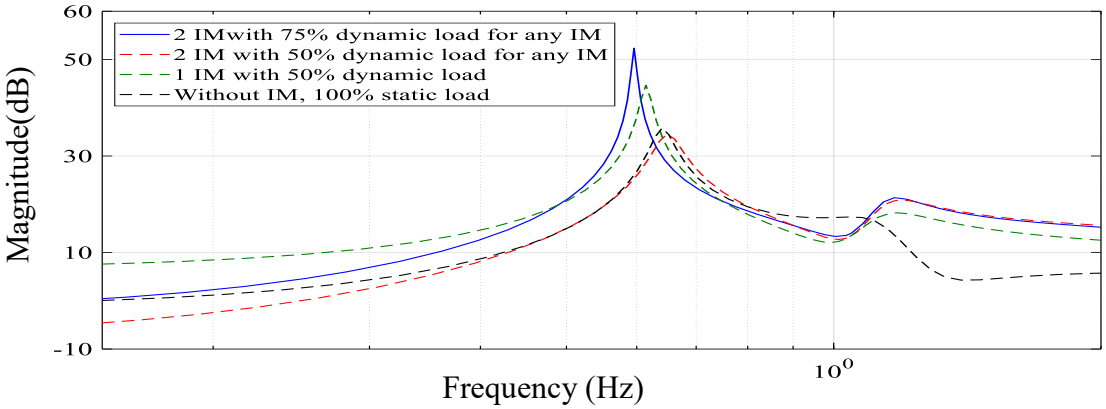

Figure 5. 8. Effect of dynamic load on inter-area and local modes

To study the effect of uncertainties in load model parameters on inter-area oscillations and on fault clearing time in time domain simulations PCM has been used [51] . In general, the

parameterized model fails to describe the plant because the plant (with dynamic loads in different size and number of induction motors) will always have dynamics that are not represented in model which is described by parametrized model with static loads.

In this research uncertainty of load model is considered as unstructured uncertainty, not parametric uncertainty. Variant percentage of static and dynamic load with respect to different operating conditions is investigated. Dynamic load is considered as induction motors. Different percentage of dynamic load is defined by 3 sizes of motor:

1) Large Motor (LM): This is the aggregate of large inertia motors used in the industries.

2) Medium industrial Motor (MM): This represents three phase motors driving constant torque loads, such as commercial air conditioning and refrigerator compressors with low inertia.

3) Trip Motors (TM): This model aggregates smaller motors as e.g. used in residential air conditioning.

The structural or inner dynamics of three phase induction motors depend largely on inertia and open circuit time constants. Smaller induction machines operate at relatively large slips, large induction motors and generators are designed more efficiently with higher X/R ratios. They have higher open circuit time constants and operate at relatively lower slips.

Identification experiments under models with variant percentage of static and dynamic load with respect to different operating conditions and different motor size and numbers are considered as perturbed plant transfer functions $\tilde{G} = G_i(j\omega))$ which are shown in Figure 5. 9.

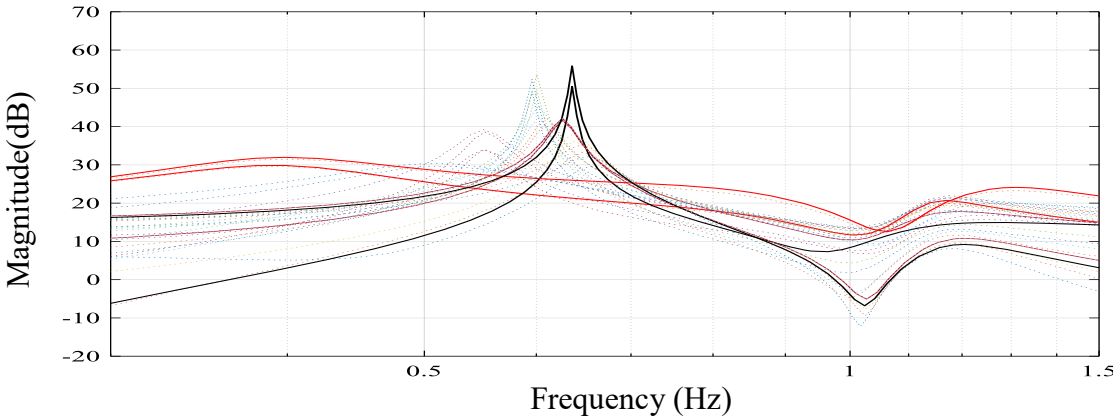

Figure 5. 9. Inter-area oscillation frequencies of perturbed model with load uncertainties

As it can be seen in Figure 5. 9 inter-area range of frequency [0.1, 1] Hz as the interest of wide area damping controller design has been affected with uncertain load type.

5.4.2.3. Operating Condition and Topology Uncertainty

A power system grid experiences different operating conditions due to variety of load and generation during days, nights, weeks, seasons and years. Also grid topology can change. These typical changes are shown with red colour in Figure 5. 1 for two area, four machine grid. Identification experiments under models with different operating conditions due to change of two loads connected to Bus 7 and Bus 9 (which are shown in change like indicated in Table 2. 5 are considered. Furthermore, identification experiments are considered changing topology models, like removed transmission line 7-8 a, b and 8-9 a, b. It should be regarded that removed line is not causing island grids, because of remaining line in parallel.

Table 2. 5. Different operating points for two area system

Operating point No.	**Load of Area 1 (MW)**	**Load of Area 2 (MW)**	**Tie-Line Power (1-2) (MW)**
1	920	1814	480
2	976	1767	400
3	1076	1675	300
4	1176	1577	200
5	1276	1482	100
6	1465	1282	-100

Models with different operating conditions and different topologies are considered as perturbed plant transfer functions ($\tilde{G} = G_i(j\omega)$); the frequency diagram is shown in Figure 5. 10.

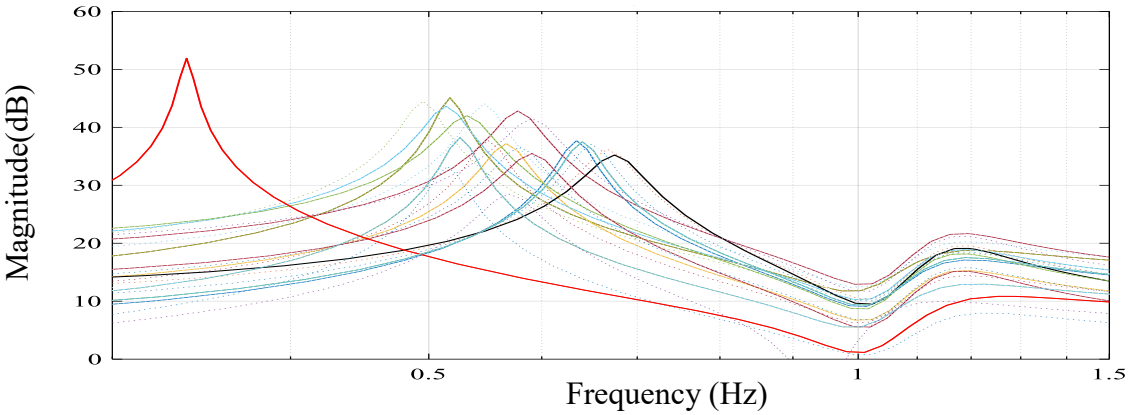

Figure 5. 10. Inter-area oscillation frequencies of perturbed model with operating condition and topology uncertainties

Figure 5. 10 clearly shows that inter-area range of frequency [0.1, 1] Hz as the interest of WADC design has been influenced with operating condition and topology uncertainties.

5.4.2.4.VSC based Source Uncertainty

Wind and solar power sources are uncertain renewable energy sources, they are modelled with VSC. Power generation of uncertain renewable sources has basic characteristics of uncertainty, such as intermittence, randomness, and fluctuations. Identification experiments under models with variant amount and number of wind power and photovoltaic source are considered as perturbed plant transfer functions $\tilde{G} = G_i(j\omega)$ which are shown in Figure 5. 11.

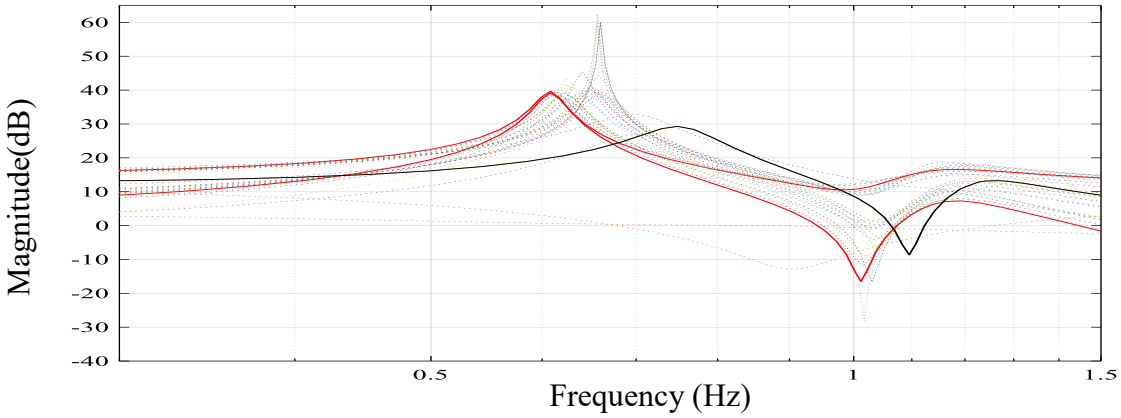

Figure 5. 11. Inter-area oscillation frequencies of perturbed model with VSC based uncertainties

5.4.2.5 w_{unc} Transfer fuction for Two Area, Four Machine Power

The influence of different unstructured uncertainty on the open loop transfer function denominator of the linearized two area, four machine power system benchmark model has been studied independently. Identification experiments with consideration of all uncertainty sources is $\tilde{G}$. By calculating the $G_i(j\omega) - G(j\omega)$ and drawing curves, a bounding function $w_{unc}\ (j\omega)$ is gained.

$w_{unc}\ (j\omega)$ will be considered in design of controller in chapter 6.

CHAPTER 6. IMPLEMENTATION OF CONTROL SCHEME

6.1. Introduction

Robust nonsmooth fixed order controller as described in chapter 4 will be applied as WADC in different architectures for power test grids. Designing the controller for two area, four machine grid as a small test grid as shown in Figure 5. 1, will be done step by step and will be described in detail.

6.2. Controller Design Procedure

Steps of designing a fixed order WADC will be described by detail as follows:

a. Selection of controller architecture.
b. Linearization of the system around nominal point.
c. Selection of appropriate wide area signal and control position.
d. Applying uncertainty for nominal model *G*.
e. Design of fixed order controller.

6.2.1. Controller Architecture

The first step in designing a WADC is to choose a control architecture. Centralized and decentralized architectures are used for designing WADC in this dissertation. Centralized and decentralized architectures will be implemented to evaluate and compare the efficient and reasonable performance of controllers.

Centralized WADCs (CWADCs) utilize input signals providing sufficient observability of the mode and acting on generators, which are most efficient in damping of the oscillation. Wide area control, however, requires some communication links to gather the inputs and to send out the control signals. The centralized controller is a unique controller with MIMO and its schema is shown in Figure 6. 1.

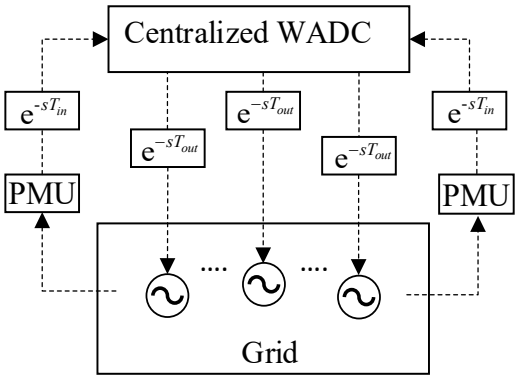

Figure 6. 1. Centralized WADC structure

In most cases, Decentralized WADC (DWADC) is based on local measurements and, therefore, easier to implement. However, these types of decentralized schemas may not be effective to damp inter-area oscillations. DWADC in this approach utilizes input signals providing sufficient observability of the mode and acting on generators, which are most efficient in damping of the oscillation. DWADCs are designed for any areas, it means for any area which has a generator that is effective on damping inter-area mode, a DWADC is installed. Input signals for any controller can come from another area or the same area which depends on inter-area mode. Wide area control, however, requires some communication links to gather the inputs and to send out the control signals [102] . The decentralized controller scheme is thus proposed and shown in Figure 6. 2.

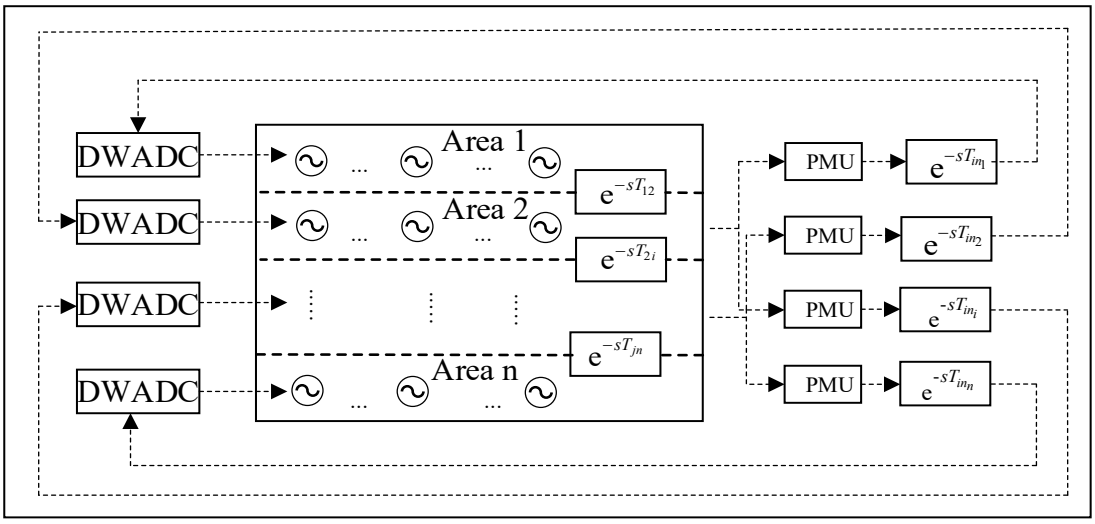

Figure 6. 2. DWADC structure

6.2.2. Model Definition

The full order nonlinear power system model is linearized around a nominal operating point. A linear time invariant model of the interconnected power system for designing controller is considered as *G(s)*, which is shown in equation (4.8).

As described in controller architecture, centralized controller is a unique controller which is designed for whole of the system; this means that only one space state model with MIMO describes the system characteristic. Decentralized controller's number is equal to number of subsystems (areas) of system and can have multi or single input and output. Any area has space state model with effective input and output for its controller, which will be shown in following.

The same interconnected power system with *n* areas (subsystems) is described by the following state space equations for designing decentralized controller:

$$\dot{\boldsymbol{x}}_i(t) = \boldsymbol{A}_i\boldsymbol{x}_i(t) + \boldsymbol{B}_i\boldsymbol{u}_i(t) + \boldsymbol{B}_{w_i}\boldsymbol{w}_i(t) \tag{6.1}$$

$$\boldsymbol{Z}_i(t) = \boldsymbol{C}_{z_i}\boldsymbol{x}_i(t) + \boldsymbol{D}_{zu_i}\boldsymbol{u}_i(t) + \boldsymbol{D}_{zw_i}\boldsymbol{w}_i(t) \tag{6.2}$$

$$\boldsymbol{y}_i(t) = \boldsymbol{C}_i\boldsymbol{x}_i(t) + \boldsymbol{D}_{w_i}\boldsymbol{w}_i(t) \tag{6.3}$$

Index *i* represents *i*th subsystem, $1 \le i \le n$

G(s) considers matrix of power system transfer function consisting of *n* interconnected subsystems.

$$\boldsymbol{G}(s) = \begin{bmatrix} g_{11} & \cdots & g_{1n} \\ \vdots & \ddots & \vdots \\ g_{n1} & \cdots & g_{nn} \end{bmatrix} \tag{6.4}$$

The signals selected as plant input signals of one area to specific generators have not much influence on the other generators in other areas. Therefore, controlling electrical quantity and modes of one area by the generators of other areas is not necessary and so it is possible to neglect interaction that is represented by the off diagonal terms of matrix ***G***. Then the electrical interaction between subsystems with each other are considered as $g_{ij}(s)$ (that $i \neq j$) in equation (6.4) which is interpreted as unstructured uncertainties and ignored from transfer function matrix of power system ***G(s)*** and is exposed as :

$$\boldsymbol{G}_d(s) \overset{\Delta}{=} diag\{g_{ii}\} \begin{bmatrix} g_{11} & & \\ & \ddots & \\ & & g_{nn} \end{bmatrix} \tag{6.5}$$

6.2.3. Wide Area Signal Selection

Geometric observability and controllability which is explained in (3.25), (3.26) are used to evaluate the strength of different measurements with different physical significances and the performance of controllers at different locations with respect to the inter-area mode. The candidate input signals are

- Real powers of tie lines, $P_{i\text{-}j}$ denotes the real power of transmission line connecting bus i and j
- Generator rotor speeds, ω_k
- Bus voltage angle difference $\theta_{i\text{-}j}$, denoting the voltage angle difference between bus i and j
- Center Of Inertia (COI), difference between two areas $\delta_{a1\text{-}a2}$, which is defined as:

$$COI = \delta_{a1-a2} = \frac{\sum_{i=1}^{2} \delta_i H_i}{\sum_{i=1}^{2} H_i} - \frac{\sum_{i=3}^{4} \delta_i H_i}{\sum_{i=3}^{4} H_i} \tag{6.6}$$

where δ_i and H_i are rotor angle and inertia constant of generator i. The results are normalized so that their values are in the range [0 1].

Table 6. 1 shows the joint controllability/observability measures for all candidate signals and control locations of the test grid.

Table 6. 1. Joint controllability/observability measures (two area system)

	$P_{6\text{-}7}$	$P_{7\text{-}8}$	$P_{8\text{-}9}$	$P_{9\text{-}10}$	ω_1	ω_2	ω_3	ω_4	$\theta_{7\text{-}9}$	$\delta_{\alpha1\text{-}\alpha2}$
G_1	0.04	0.23	0.2	0.077	9e-4	5e-4	14e-4	12e-4	0.26	0.69
G_2	0.05	0.28	0.27	0.09	11e-4	7e-4	17e-4	15e-4	0.32	0.84
G_3	0.047	0.24	0.23	0.08	9e-4	6e-4	14e-4	13e-4	0.27	0.72
G_4	0.06	0.31	0.29	0.10	12e-4	7e-4	18e-4	16e-4	0.35	0.92

The rows of the table correspond to generators G1,…, G4 and the columns correspond to measurements.

From the calculation results shown in Table 6. 1, we have the following conclusions:

1) The most efficient generators for damping the inter-area mode are G4 and G2.

2) The most efficient stabilizing signal is $\delta_{a1\text{-}a2}$, the difference of COI between two areas.

3) Real tie line powers are also suitable stabilizing signals because they have high joint controllability/observability measure.

4) None of single generator rotor speed is good choice for input signals of controller to damp the inter-area mode.

According to the above observation, we may choose G2 and G4 as our control locations and real power of tie line from Bus 7 to Bus 8 as our stabilizing signal. What should be noticed here is that we don't choose the difference of COI between two areas as input signal even though it has the highest measures of controllability/observability with respect to the inter-area mode. We have several reasons to do so. First, generator states such as rotor angle are hard to obtain while system output like tie line power are easily obtained by PMUs. This explains why output feedback control is more practical than state feedback in wide area control system design for power grids. Second, to calculate COI, all generator rotor angles are needed. This increases the cost for measurement devices and communication channels compared to the only measurement of tie line power. At last, even if we could obtain rotor angles easily and economically, they still need to be synchronized so that the time delay may be larger than for the measurement of tie line power.

6.2.4. Applying Uncertainty for Nominal Model G

The uncertainty for power system grid is described by detail in chapter 5.
Time delay as structured uncertainty and pertubed multi model by considering :

- Static load
- Dynamic load
- Different operating point
- Different topology
- Renewable power source

as unstructured uncertainty are considered.

In this part, defined Δ and w_{unc} are applied to nominal model G and make $\tilde{G}$ as an uncertain multi model transfer function which controller is applied to it.

6.2.5. Fixed Order Loop Shapping Controller

6.2.5.1. Centeralized Controller

A generic choice for L_d is ω_c/s where ω_c is the desired open loop bandwidth for any area. L_d is large enough in low frequencies and small in high frequencies. The zero dB crossover frequency ω_c dictates how fast the system responds and is limited by factors such as stability, delays, actuator bandwidth, and modelling errors. The desired open loop bandwidth for designing WADC to damp inter-area oscillation is gained around two times of inter-area mode frequency in radian per second (ω_c=10 rad/s). The overall design is to find *K(s)* as fixed order loop shaping H_∞ controller for the linear time invariant uncertain system $\tilde{G} = G \cdot (I + \Delta \cdot w_{unc})$. Norm *T* (transfer function from *(r, n)*, to *(y, e))* as shown in Figure 6. 3 for controller, is smaller than a specified positive number, .i.e.

$$\|\mathbf{T}\|_\infty < \gamma \tag{6.7}$$

$$\boldsymbol{T} = (\boldsymbol{K}(s) \cdot \tilde{\boldsymbol{G}}(s)) \cdot (\boldsymbol{I} + \boldsymbol{K}(s) \cdot \tilde{\boldsymbol{G}}(s))^{-1} \tag{6.8}$$

$$\boldsymbol{L(s)} = \boldsymbol{K}(s) \times \tilde{\boldsymbol{G}}(s) \tag{6.9}$$

with *L(s)* as open loop function as depicted as black solid line in Figure 6. 4.

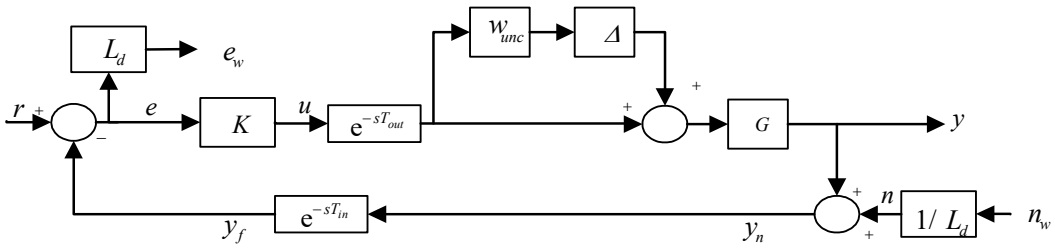

Figure 6. 3. Centralized control structure

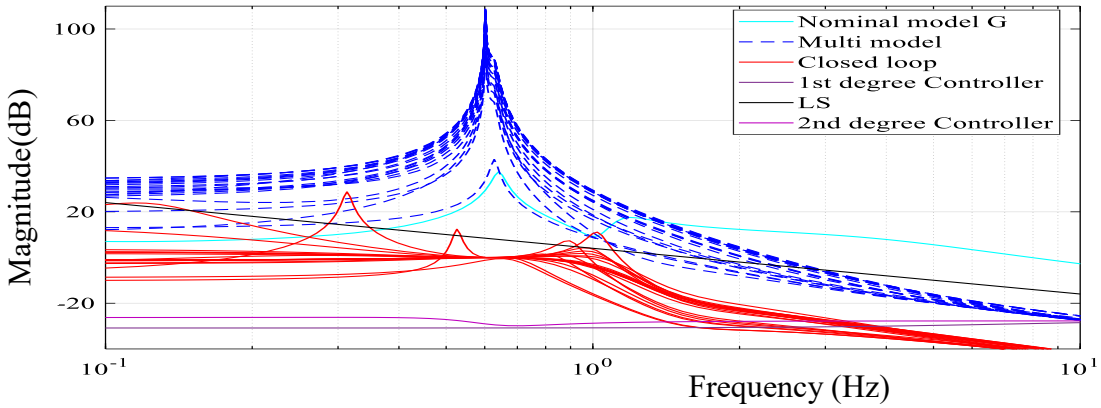

Figure 6. 4. Effect of fixed order of controller on uncertain model

6.2.5.2. Decenteralized Controller

It is assumed that $\tilde{\boldsymbol{G}}(s)$ is a square plant, which is to be controlled using a diagonal controller

$$\mathbf{G}_d(s) \overset{\Delta}{=} diag\{g_{ii}\} \begin{bmatrix} g_{11} & & \\ & \ddots & \\ & & g_{nn} \end{bmatrix} \boldsymbol{K}(s) = \begin{bmatrix} K_1(s) & & \\ & \ddots & \\ & & K_n(s) \end{bmatrix} \tag{6.10}$$

$$U_i(s) = -K_i(s)Y_i(s) \tag{6.11}$$

Where $U_i(s)$ and $Y_i(s)$ indicate the Laplace transforms of, respectively, $u_i(t)$ and $y_i(t)$ and, $K_i(s)$ is the Transfer Function Matrix (TFM) of the i^{th} controller area i^{th} designed. The design of the i^{th} controller is to be based on the nominal local model of the i^{th} subsystem (g_{ii}),

Each controller $K_i(s)$ is to be designed such that

(i) The local nominal closed loop of any subsystem (area) $g_{ii}(s)$ is robustly stable,

(ii) The criteria of nominal subsystem are satisfied,

(iii) The actual overall system $\boldsymbol{G}$ is robustly stable and performs for all uncertainties.

Desired closed loop L_{d_i} performance for any area is liked for centralized controller.

The TFM of the actual overall system, is obtained from (6.6) as $\boldsymbol{G}(s)$. Thus, since the controller design is to be based on the models (6.1)-(6.3), the overall design TFM is given as:

$$\boldsymbol{G}(s) = bdiag\,[\, g_{11}(s)\,,\, g_{22}(s)\,,\, \ldots\,,\, g_{nn}(s)\,] \tag{6.12}$$

The problem of designing decentralized controllers [103] is the multiplicative error matrix, $\boldsymbol{E}(s)$, between the true TFM, $\boldsymbol{G}(s)$, and the design TFM, $\boldsymbol{G}_d(s)$, which satisfies

$$\boldsymbol{G}(s) = \boldsymbol{G}_d(s)(\boldsymbol{I} + \boldsymbol{E}(s)) \tag{6.13}$$

It should be mentioned for designing centralized controller $\Delta \cdot w_{unc}$ is considered as uncertainty while for decentralized controller also error, between the true TFM, $\boldsymbol{G}(s)$, and the design TFM, $\boldsymbol{G}_d(s)$ is included. $\boldsymbol{E}(s)$ contains the real parametric uncertainty (time delay) with norm bounded dynamical uncertainty interaction effect of subsystems on each other. To achieve stability of the overall system with all loops closed, it is required that the interactions do not cause instability.

Each local controller is to be designed to stabilize the local nominal models with equations (6.1) -(6.3) and to achieve desired performance for the same model. The overall closed loop system guarantees robustness and stability by ‘‘frequency dependent upper bound on the norm of

E(jω)'' method. Due to this method [103] , the actual overall closed loop system, (6.1)-(6.3) under controls (6.11), is stable as long as:

$$\bar{\sigma}(T(j\omega)) < \frac{1}{\bar{\sigma}(E(j\omega))} \tag{6.14}$$

Figure 6. 5 is shows structure of decentralized controller by considering loop shaping and robust tuneable fixed order state space model.

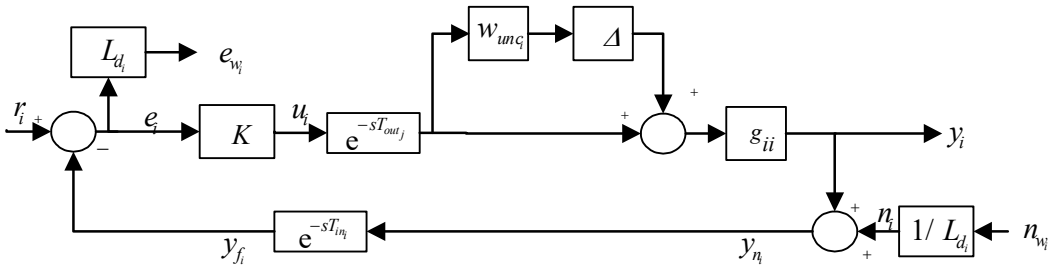

Figure 6. 5. Decentralized control structure

CHAPTER 7. CONVENTIONAL GENERATION CASE STUDY

7.1. Introduction

In this chapter, damping controller is designed for grids, which have conventional power generation sources. Robust fixed order nonsmooth WADC is designed in two centralized and decentralized architectures for two area, four machine test system and New England 39 bus, 10 machine system. Detailed model descriptions and all parameters including network data and dynamic data for the generators, excitation systems, PSSs are given in Appendix A and Appendix B. Robustness and performance of controllers are tested by applying fault and changes in operating point, load type and grid topology.

7.2.Centralized Robust Controller for Two Area, Four Machine System

7.2.1. Controller Model, Inputs and Outputs

Figure 7. 1 shows the two area, four machine system. All synchronous machines are modelled with static excitation system. The export power P_{tie} from Area 1 to Area 2 through the tie line is 400 MW and chosen as nominal operating point.

Small signal analysis of linearized model is applied for two area, four machine system. The inter-area mode that caused to design WADC is shown in Table 7. 1.

Table 7. 1. Eigenvalue, damping ratio and frequency of the test system

Eigenvalue (1/s) $\sigma \pm j\omega$	**Damping Ratio (%)** $-\sigma / \sqrt{\sigma^2+\omega^2}$	**Frequency (Hz)** $\omega / 2\pi$
$0.0597 \pm j3.94$	-1.5	0.66

The objective of the WADC is aimed at achieving acceptable damping for this mode.

According to modal analysis and geometric observability/controllability for inter-area mode that was mentioned in chapter 6, G2 and G4 have the best controllability are chosen as the control locations and real power of tie line from Bus 7 to Bus 8 has the best observability and was selected as stabilizing signal for controller. According to more controllable generators and more observable measurements, centralized control system is designed like Figure 7. 1.

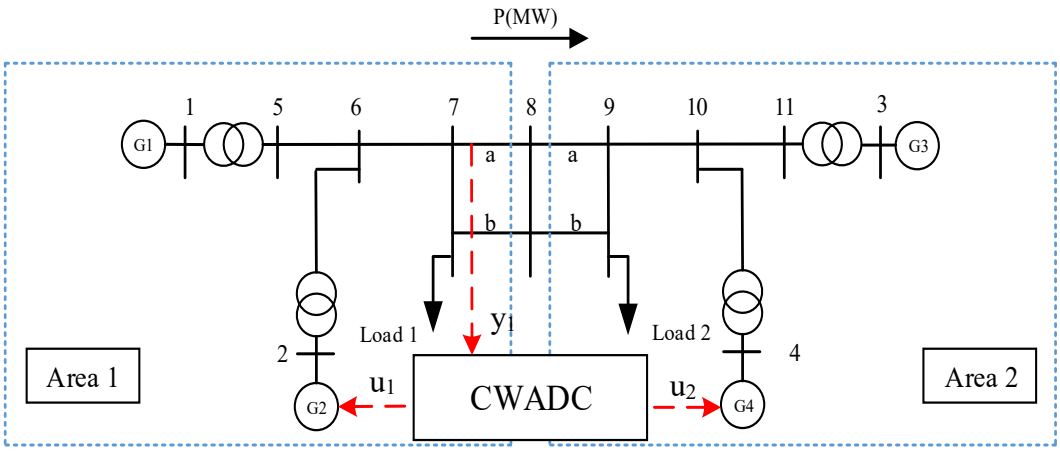

Figure 7. 1. CWADC for two area, four machine system

7.2.2. Model and Controller Order

Model reduction is considerable emphasis on reduced order models obtained by residualizing the less controllable and observable states of a balanced realization for special goal. Model order reduction aims to lower the computational complexity, for example, in simulations of large scale dynamical systems and control systems. By a reduction of the model's associated state space dimension or degrees of freedom, an approximation to the original model is computed which is commonly referred to as a reduced order model. Also for the research based on measurement, it is not always possible to identify every mode, because they might not be observable or prohibited by numerical issues with identification and limitations of identification algorithm. The original linear two area, four machine system model is 48^{th} order. Not all states of the model are dominant. In fact, no more than a few states can contain the characteristics of this small system. Therefore, model reduction can be used to reduce the original high order model to reduced order model. The frequency responses of the full order model and reduced order model are shown in Figure 7. 2. It can be seen that for the bandwidth of interest, the reduced order model is reliable for robust controller design, in particular around the dominant mode.

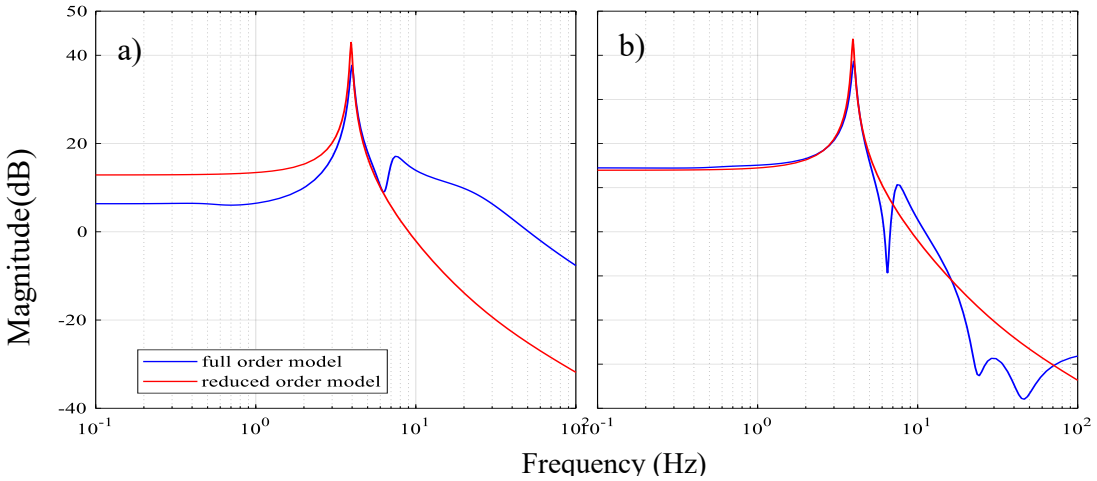

Figure 7. 2. Frequency response comparison of full and reduced order model (two area, four machine system) a) from u_1 (input) to y_1 (output) and b) from u_2 to y_1

Centralized fixed order controller is applied for full and reduced order models and is evaluated by short circuit fault in time domain.

Figure 7. 3 is a time domain response comparison of models and controllers of different orders.

- Full order nominal model 48th and fixed 3rd order controller.
- 4th order model (reduced one) with fixed 1st order controller.

Time responses are compared for short circuit's fault, applied to Bus 8 for 100 ms.

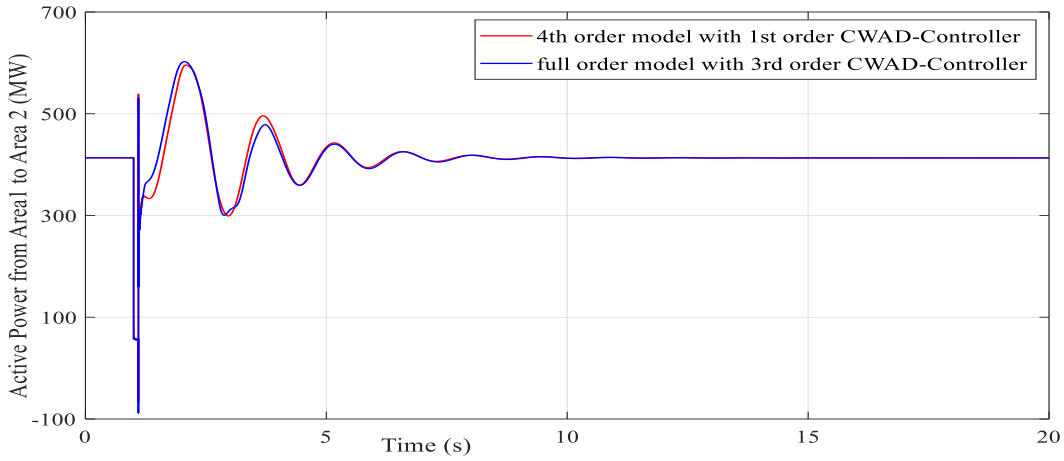

Figure 7. 3. Comparison of model and controller order time response

Order of controller is selected by try and error from the lowest order. Robust controller performance and stability is tested with eigenvalue analysis, robustness criteria. According to Figure 7. 3, the 1st order controller for 4th order model shows almost the same behavior as the full order model. Therefore, the 1st order controller was chosen in this study.

7.3. Closed Loop Verification and Nonlinear Time Domain Simulation and Centralized Controller Robustness

The resulting fixed order centralized controller is first verified by small signal analysis. The damping ratio of the inter-area mode is improved to 17.4% under closed loop conditions. Then, time response of linear closed loop system is used to verify the performance of the controller. Figure 7. 3 verifies the performance and stability of controller for nominal model.

To test the robustness of the test system, different uncertainties like

- Three phase short circuit
- Changing operating point
- Tripping transmission line
- Removing transmission line

were applied by fixed or propagated time delays applied to system.

- *Three phase short circuit fault*

Figure 7. 4 shows CWADC improving the damping greatly in comparison with conventional PSS for three phase short circuit which is applied at Bus 9 and is cleared after 100 ms, for different operating point from nominal model. Designed CWADC considers propagated time delay.

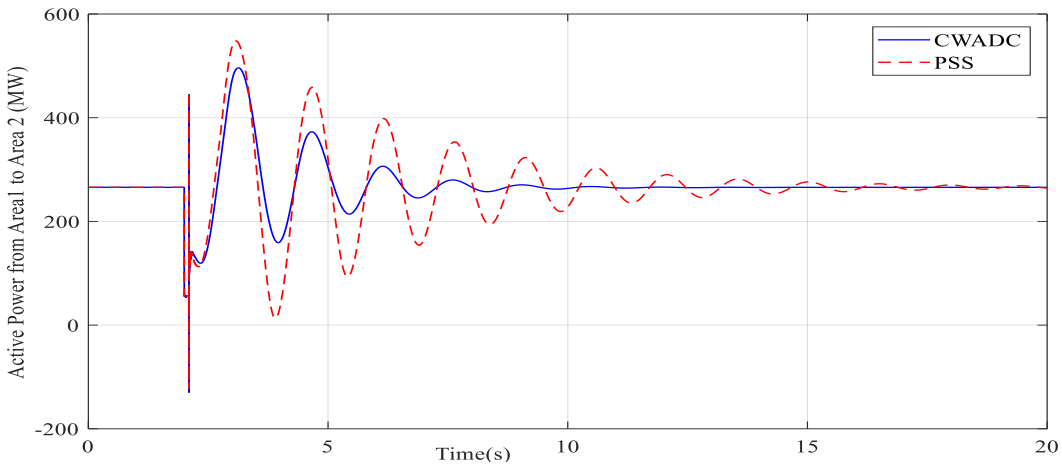

Figure 7. 4. Tie line power response to a three phase fault at Bus 9

Totally 30% of loads are considered as dynamic type in this case. A three phase short circuit fault was applied on Bus 9, and the fault was cleared after 100 ms. Figure 7. 5 shows that with only PSS, the system is unstable and the proposed controller stabilizes the system.

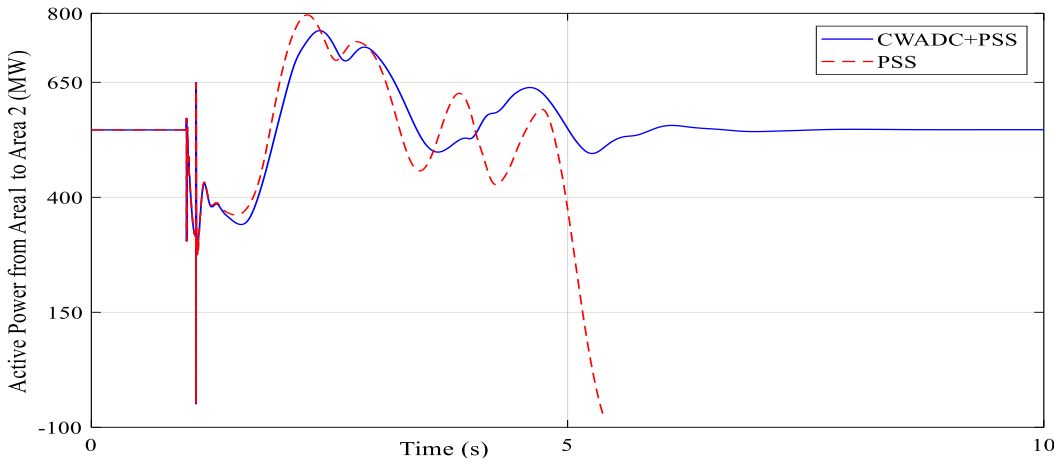

Figure 7. 5. Tie line power response to a three phase fault at Bus 9

- *Changing operating point*

In this case operating point is changed in two steps which is shown in Figure 7. 6; in the last step the direction of power flow is changed. Designed CWADC considers propagated time delay.

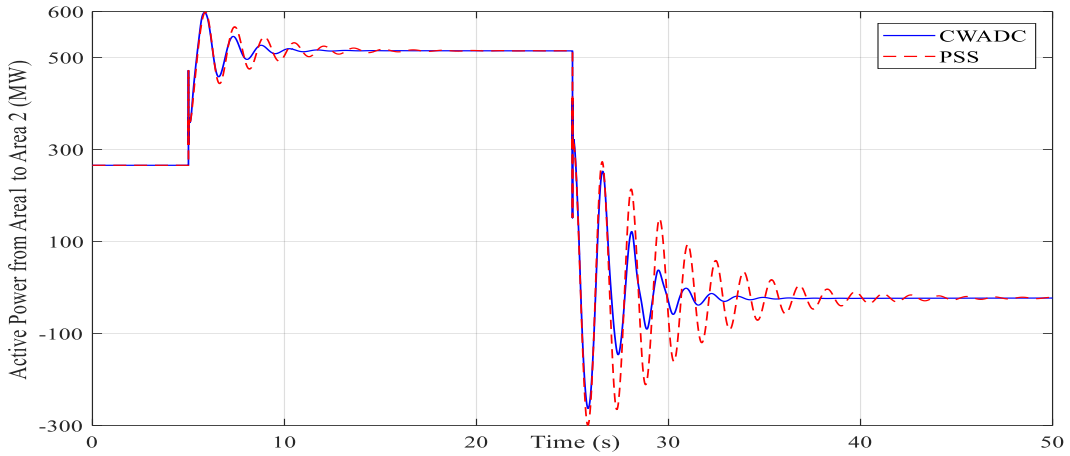

Figure 7. 6. Tie line power response to changing operating point

- *Changing grid topology*

In this case, grid topology is changed by considering line removing and line tripping. In parallel, to show the robust stability and performance, three phase short circuit and changing operating point are also applied.

Figure 7. 7 shows removing a line in the first phase of simulation which causes a new operating point. For showing the robustness of CWADC to this change (removing line) also load amounts in three steps are changed by considering propagated time delay. It should be mentioned that PSS also can handle these varieties but cannot damp oscillation as fast as CWADC can do.

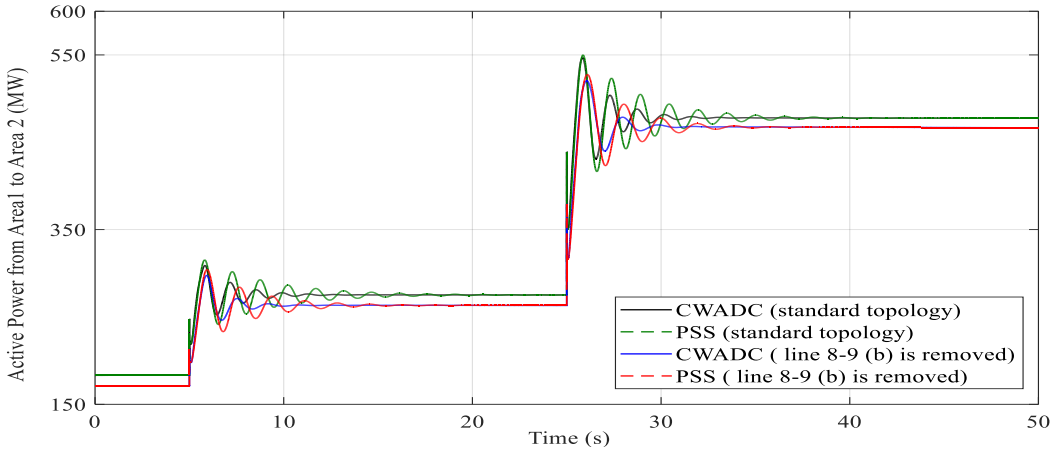

Figure 7. 7. Tie line power response to changing topology as well as changing operating point

Figure 7. 8 shows tripping of line 8-9 at 2 sec which causes a new operating point. For showing the robustness of CWADC in other disturbances, three phase short circuit is applied by considering 400 ms time delay.

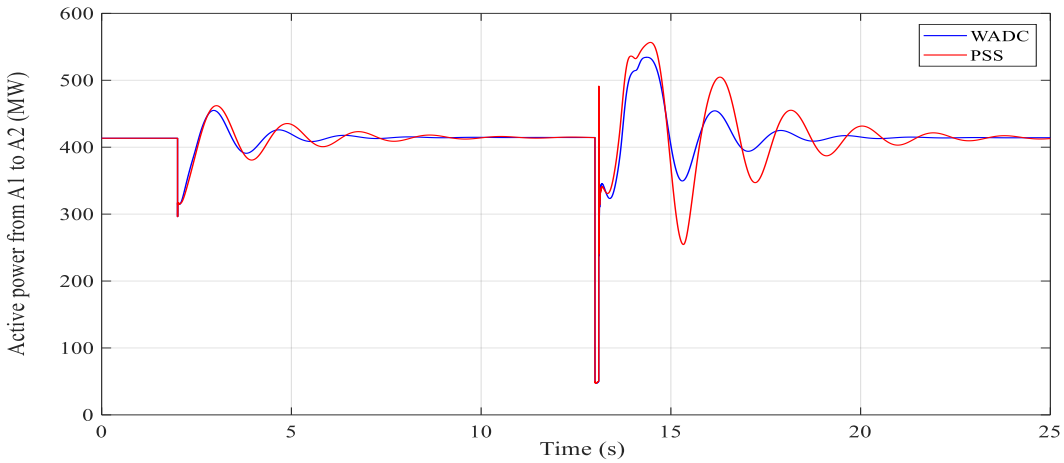

Figure 7. 8. Tie line power response to changed topology as well as three phase short circuit

- *Effects of time delays*

Figure 7. 9 shows the effect of different time delay amounts, which are evaluated by applying three phase short circuit. CWADC can handle time delay around 500 ms. As it is shown, more than 500 ms cannot be handled well. In chapter 6 the range of time delay is already described.

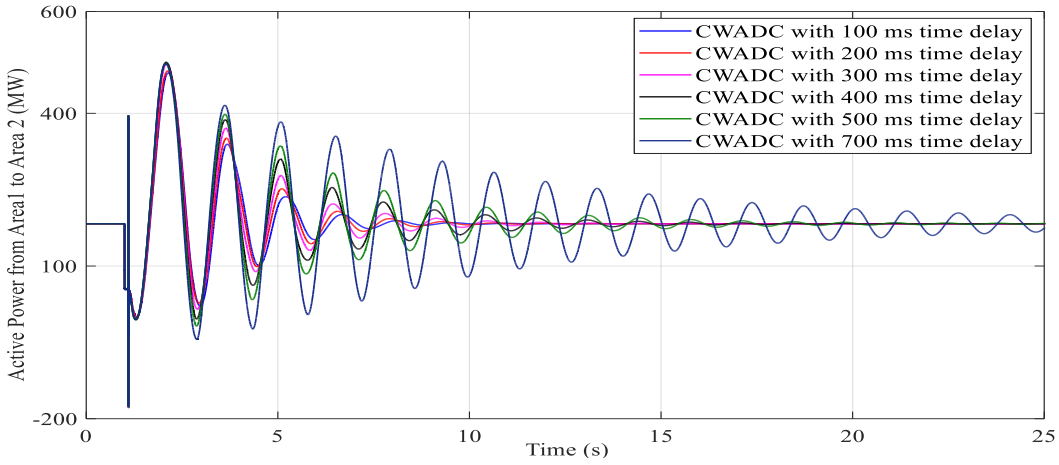

Figure 7. 9. Active tie line power with controllers that can handle time delays

7.4. Decentralized Robust Controller for Two Area, Four Machine System

As it is mentioned in chapter 6, decentralized controller is designed for any power area separately. According to more controllable generators and more observable measurements, which was discussed for centralized controller design, decentralized control system is designed like shown in Figure 7. 10.

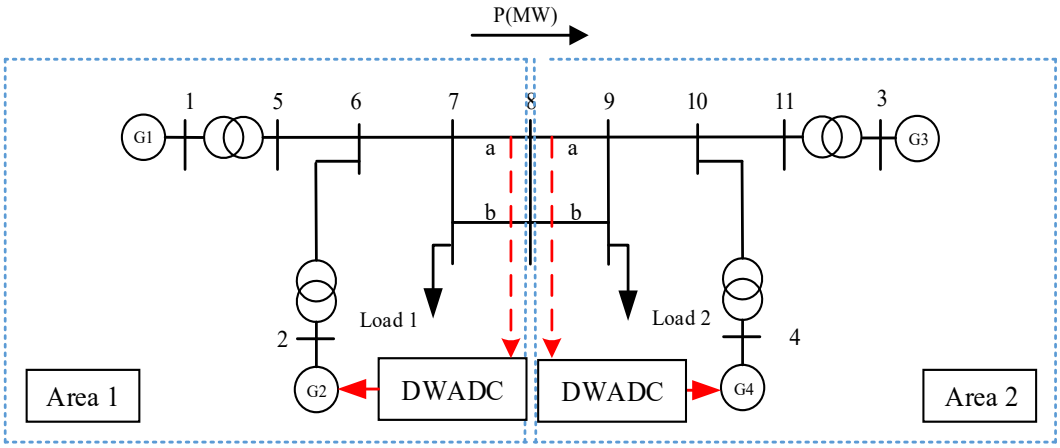

Figure 7. 10 DWADC for two area, four machine system

- *Model and controller order*

Decentralized fixed order controller is applied for full and reduced order models and it is evaluated by short circuit fault in time domain.

Figure 7. 11 is a time domain response comparison of models and controllers of different orders for DWADC.

- Full order 48th nominal model and fixed 3rd order controller,
- 4th order model (reduced one) with fixed 1st order controller.

Time responses are compared for short circuit's fault, applied to Bus 8 for 200 ms.

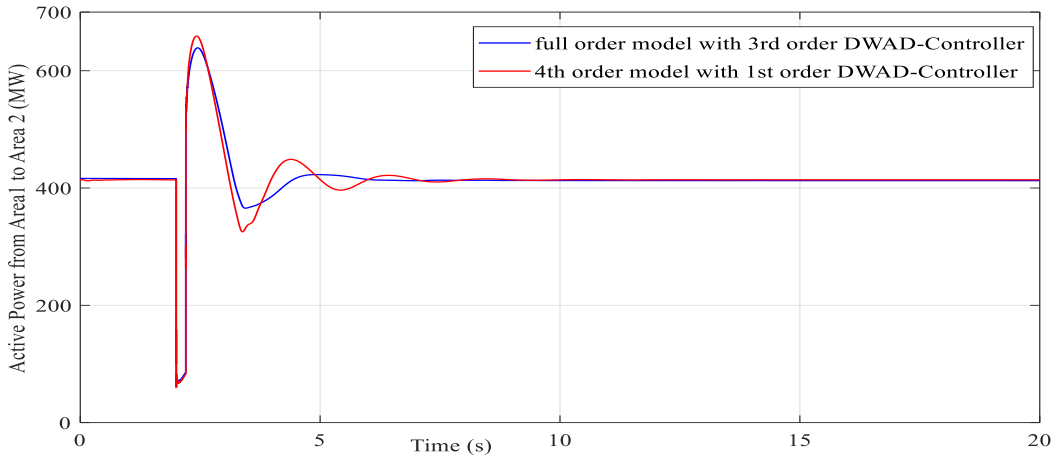

Figure 7. 11. Comparison of model and controller order time response

7.5. Closed Loop Verification and Nonlinear Time Domain Simulation and Decentralized Controller Robustness

The resulting fixed order controller is first verified by small signal analysis. The damping ratio of the inter-area mode is improved to 23.6% under closed loop conditions. Figure 7. 11 verifies the performance and stability of controller for nominal model.

To test the robustness of the decentralized controller, different uncertainties that were mentioned in part 7.3 for evaluation of centralized controller are applied.

- *Three phase short circuit fault*

Figure 7. 12 shows that DWADC improves the damping greatly in comparison with conventional PSS for three phase short circuit which is applied to Bus 7 and is cleared after 200 ms for different operating form of nominal model. Designed DWADC considers propagated time delay in parallel.

- *Changing operating point*

In this case operating point is changed in two steps as shown in Figure 7. 13. DWADC with 200 ms fixed time delay could handle changing operating points and damp the oscillation better than PSS.

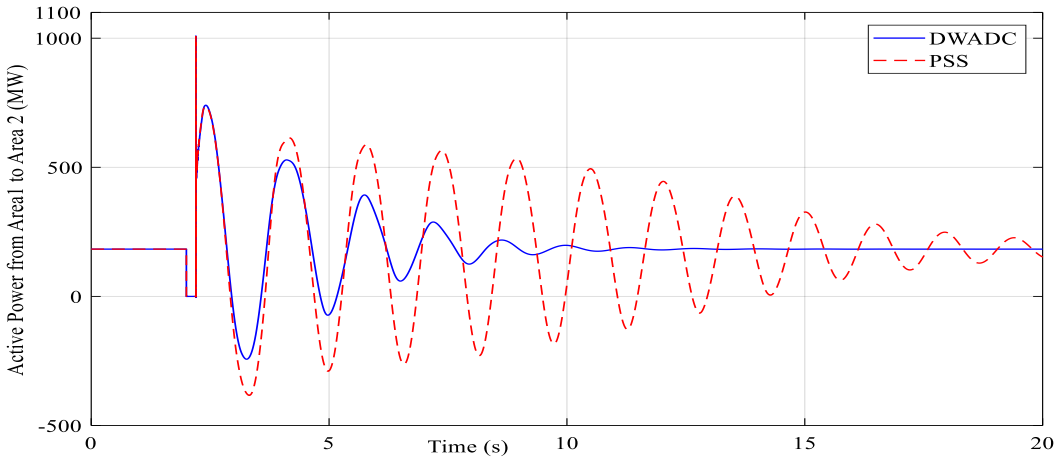

Figure 7. 12. Tie line power response to a three phase fault at Bus 7

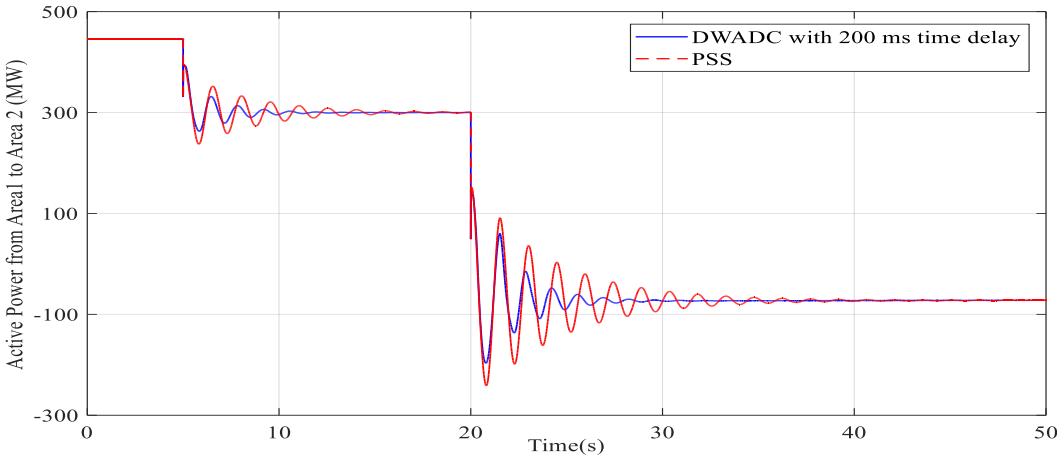

Figure 7. 13. Tie line power response to changing operating point

- *Change of grid topology*

In this case, grid topology is changed by considering line removal. In parallel, to show the robust stability and performance, three phase short circuit with different operating points from nominal are also applied. Figure 7. 14 shows removing line in the first step of simulation, which causes a new operating point. For showing the robustness of DWADC to this changing (removing line) also a three phase short circuit was applied by considering fixed 300 ms time delay.

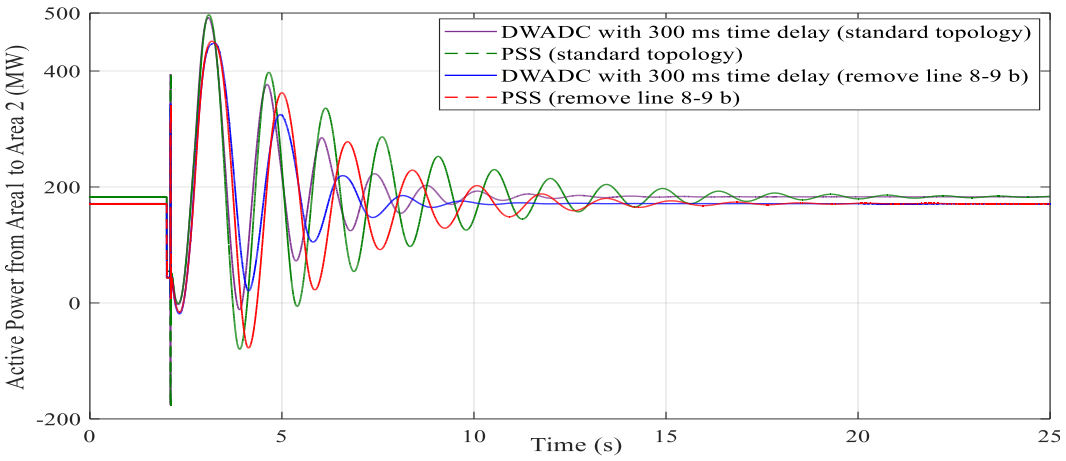

Figure 7. 14. Tie line power response to changing topology as well as three phase short circuit

7.6. Eigenvalue Analysis and Controllers Performance

Figure 7. 15 compares the performance of conventional PSS, CWADC and DWADC together in time domain in face of a severe disturbance (short circuit for 200 ms at Bus 8). As it is shown DWADC has the best performance of damping oscillation because evaluation of stability and performance criteria were done one time for any area separately and one time overally. CWAD is the second best with evaluation of performance done one time overally. At last, PSS because of its local and traditional control features that was already mentioned, cannot damp inter–area oscillation properly.

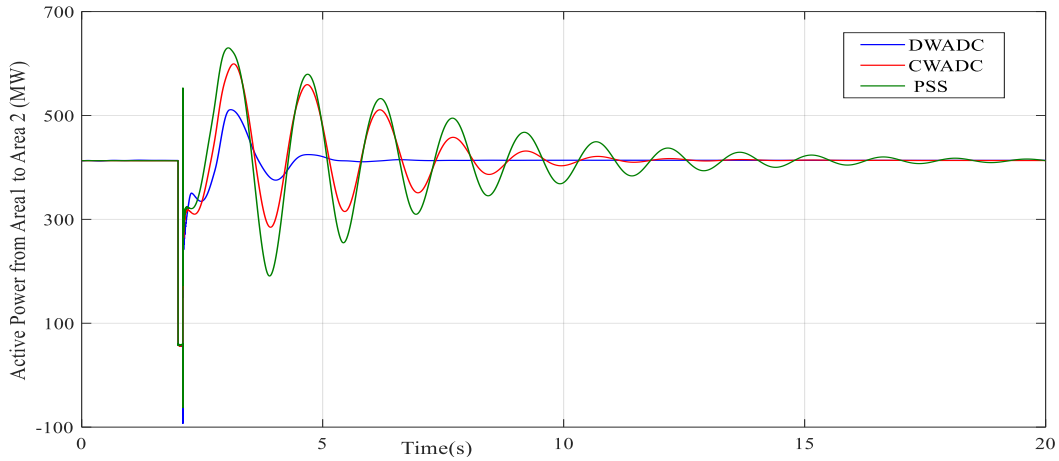

Figure 7. 15. Time domain response comparison of DWADC, CWADC, PSS

- *Eigenvalue analysis*

Eigenvalue study has been done to examine the performance of the damping controller in terms

of improving the damping ratio ξ of the inter-area modes. The results are summarized in Table 7. 2. It can be seen that the damping ratio at different load conditions is improved.

Table 7. 2. Eigenvalue analysis

Transmitted power from Area 1 to Area 2 (MW)		500	400	300	200	100	-100
Without damping	ξ (%)	-1.35	-1.5	-1.87	-2.19	-2.49	-2.91
	f(Hz)	0.654	0.660	0.67	0.67	0.68	0.69
With PSS	ξ (%)	8	7	7.3	6.7	6.2	6
	f(Hz)	0.6	0.67	0.67	0.680	0.685	0.692
CWADC	ξ (%)	17.7	17.4	16.8	16.3	15.9	14.9
	f(Hz)	0.641	0.646	0.654	0.663	0.668	0.675
DWADC	ξ (%)	22.1	23.6	25.5	25.5	23.8	25
	f(Hz)	0.502	0.509	0.518	0.528	0.528	0.518

7.7. Centralized Robust Controller for New England 39 Bus, 10 Machine System

In this section, a CWADC is designed for New England 39 bus, 10 machine system, which is shown in Figure 7. 16. Detailed model descriptions and all parameters including network data and dynamic data for the synchronous generators, excitation systems, PSSs are given in Appendix B. All synchronous machines (except G1, which is an equivalent unit) are modelled with static excitation system.

7.7.1. Controller model, input and outputs

The whole procedure of designing the WADC is like steps of designing the controller for two area, four machine system.

New England 39 bus, 10 machine model is linearized around the nominal operating point, which is shown in Appendix B. Table 7. 3 shows the result of eigenvalue analysis: mode shapes, the frequencies and the damping ratios, which represent the inter-area modes at the nominal operating point.

Table 7. 3. Eigenvalue analysis of New England system

Mode Index	**Mode Type**	**Mode Shape**	**Frequency (Hz)**	**Damping Ratio %**
1	Inter-area	G1 with all others	0.596	-4.12
2	Inter-area	G (4,5,6,7), G (8,9,10)	0.89	-4.01
3	Inter-area	G1 with all others	0.96	1.88

There are 3 inter-area modes in this model. According to modal analysis and geometric observability/controllability for inter-area mode that was mentioned in chapter 6, G3, G5 and G9 have the best controllability and are chosen as the control locations. Real power of tie line from Bus 14 to Bus 15, from Bus 15 to Bus 16 and from Bus 1 to Bus 39 have the best observability and are selected as stabilizing signals for controller which is shown in Table 7. 4. According to more controllable generators and more observable measurements, centralized control system is designed like shown in Figure 7. 16.

Table 7. 4. Observability and controllability of New England system

Mode Frequency (Hz)	Maximum Controllability	Maximum Observability
0.596	G9, G5, G3	$P_{1\text{-}39}$, $P_{16\text{-}17}$
0.89	G9, G5	$P_{16\text{-}17}$
0.96	G9, G5, G3	$P_{14\text{-}15}$, $P_{3\text{-}4}$

7.7.2. Model and Controller Order

The original linear New England 39 bus, 10 machine model is 127^{th} order. Not all states of the model are dominant. In fact, no more than a few states can contain the characteristics of this system. Therefore, model reduction can be used to reduce the original high order model to reduced order model. The frequency responses of the full order model and reduced order model are shown in

Figure 7. 17. It can be seen that for the interesting bandwidth, the reduced order model is reliable for robust controller design because of good coverage around the relevant oscillation modes.

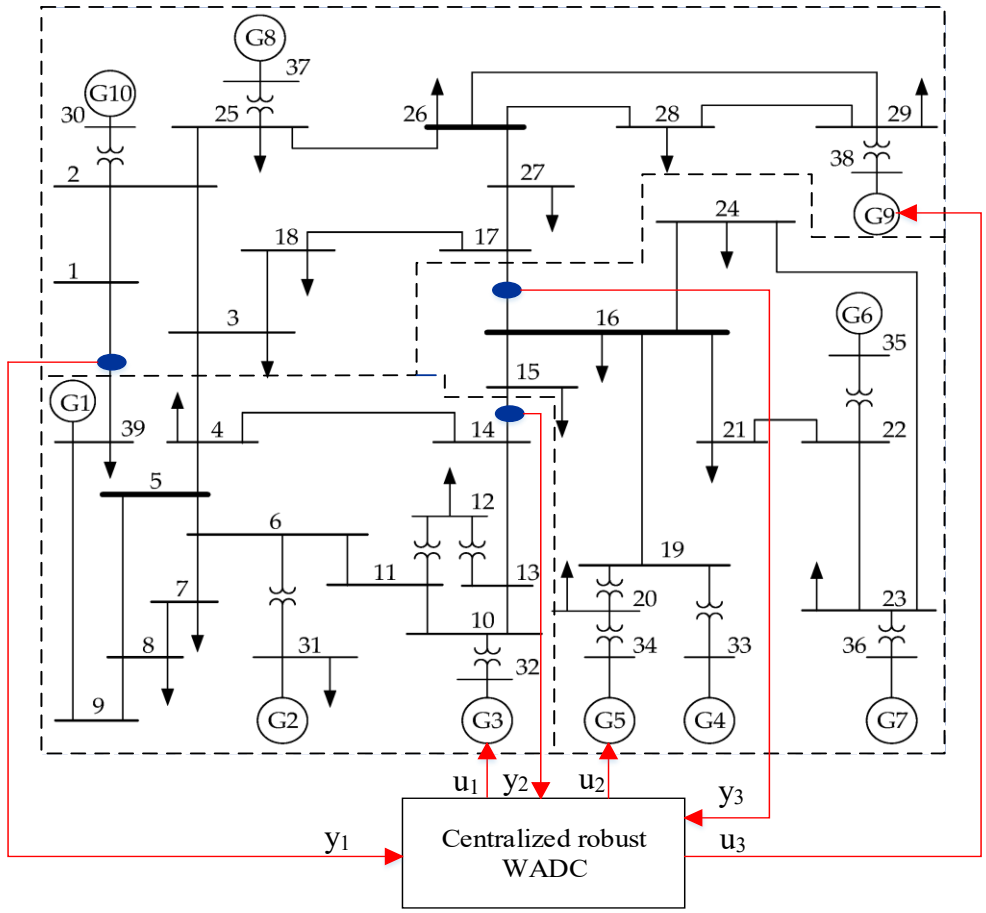

Figure 7. 16. CWADC for New England system

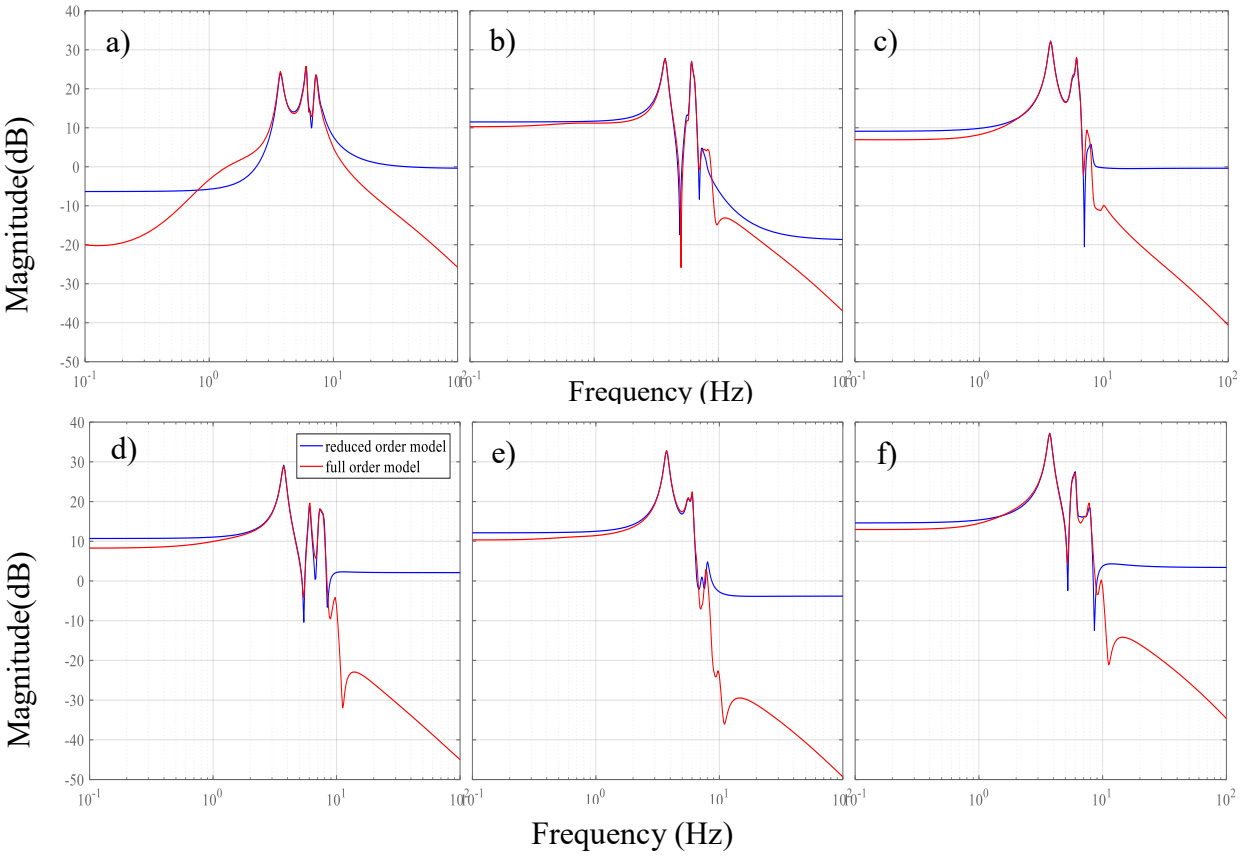

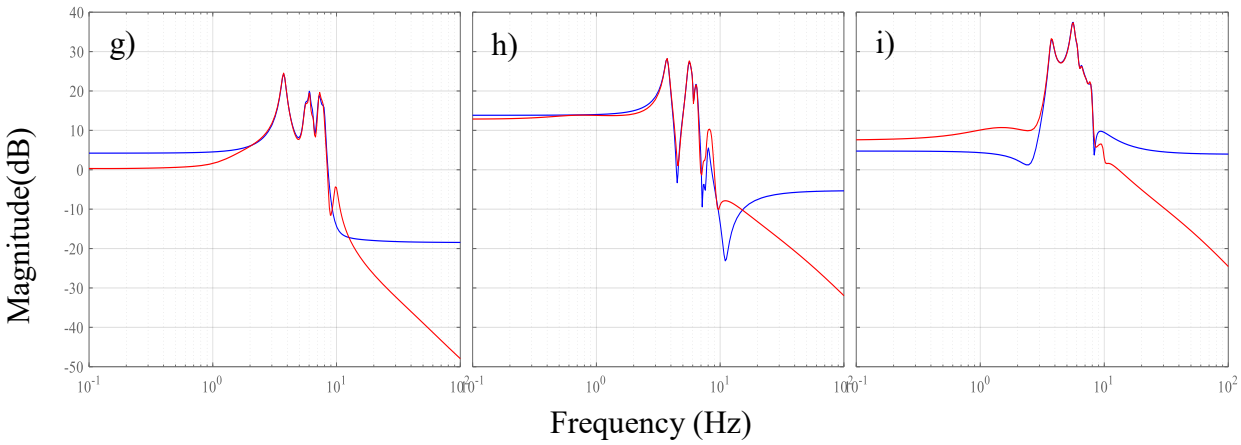

Figure 7. 17. Frequency response comparison of full and reduced order model (New England 39 bus) a) from u_1 (input) to y_1 (output), b) from u_2 to y_1, c) from u_3 to y_1, d) from u_1 to y_2, e) from u_2 to y_2, f) from u_3 to y_2, g) from u_1 to y_3, h) from u_2 to y_3, h) from u_3 to y_3

Different order of centralized fixed order controller is applied for reduced order models and it evaluated by short circuit fault in time domain.

Figure 7. 18 is a time domain response comparison of different orders of controllers.

- Reduced 14th order nominal model and fixed 6th order controller.
- Reduced 14th order nominal model and fixed 1st order controller with PSS,

Time responses are compared for short circuit's fault, applied at Bus 14 for 100 ms.

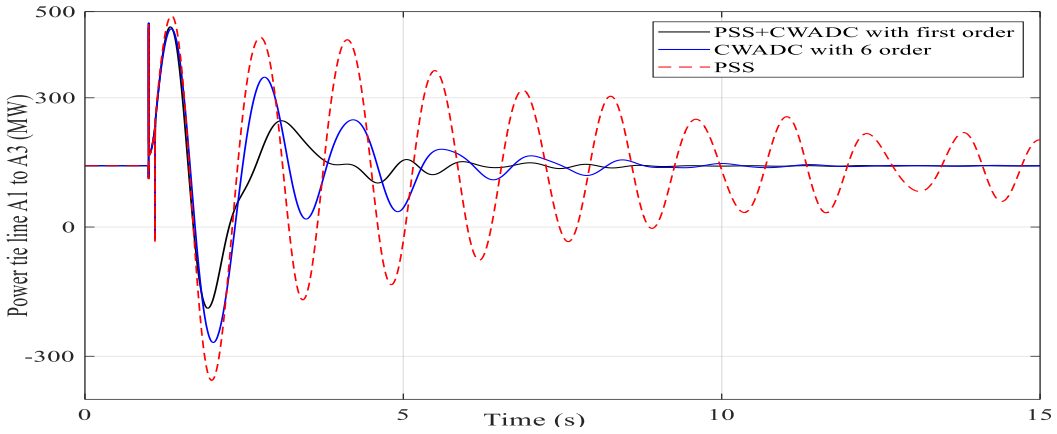

Figure 7. 18. Comparison of controller order time response

7.8. Closed Loop Verification, Nonlinear Time Domain Simulation and Centralized Controller Robustness

In this part, the result of fixed order centralized controller is verified by small signal analysis. The damping ratio of the inter-area modes is improved from -4.12 to 12.34%, from -4.01 to 21 % and from 1.88 to 18.3% under closed loop conditions. Then, time response of linear closed

loop system is used to verify the performance of the controller. Figure 7. 19 verifies the performance and stability of controller for nominal model.

To test the robustness of New England 39 bus, 10 machine system, like to two area, four machine system, different uncertainties are applied to model as follows:

- *Three phase short circuit fault*

A three phase short circuit is applied at Bus 16 and cleared after 100 ms. The time domain response is shown in Figure 7. 19. It proves that CWADC improves the damping greatly in comparison with conventional PSS. Fixed 200 ms time delay is considered in this case.

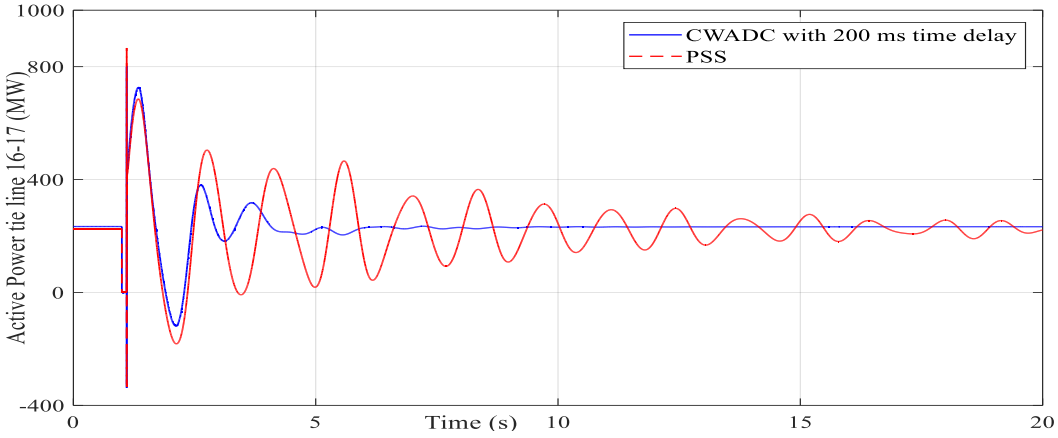

Figure 7. 19. Active power on tie line 16-17

In the next case, 50% of static loads change to dynamic ones, which causes change of system dynamic. A three phase short circuit fault was applied on Bus 14, and is cleared after 100 ms. Figure 7. 20 shows the active power flow on the line 16-17 with only PSS, and together with the proposed controller. It is evident that with only PSS, the system is unstable and the proposed controller stabilizes the system. CWADC considers propagated time delay.

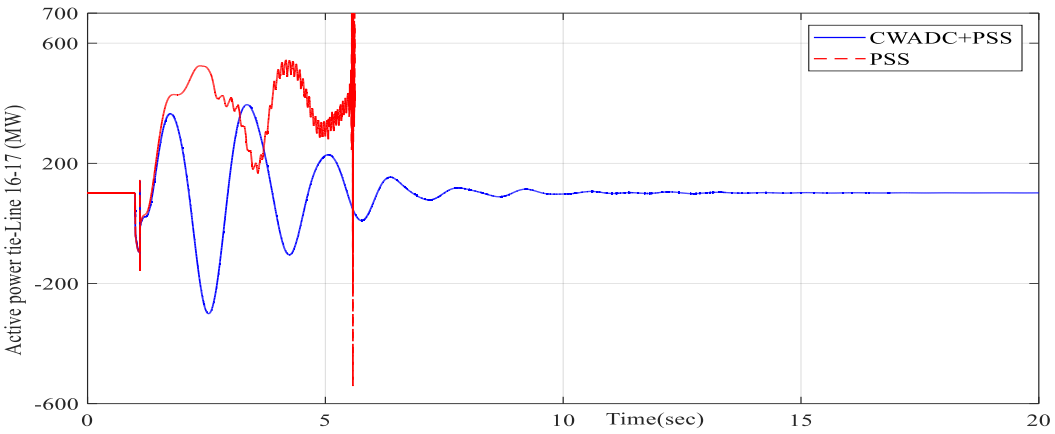

Figure 7. 20. Active power on tie line 16-17

- *Changing operating point*

In this case operating point is changed in two steps as shown in Figure 7. 21. Designed CWADC by considering fixed 300 ms time delay can handle changing operating points and damp the oscillation better than PSS.

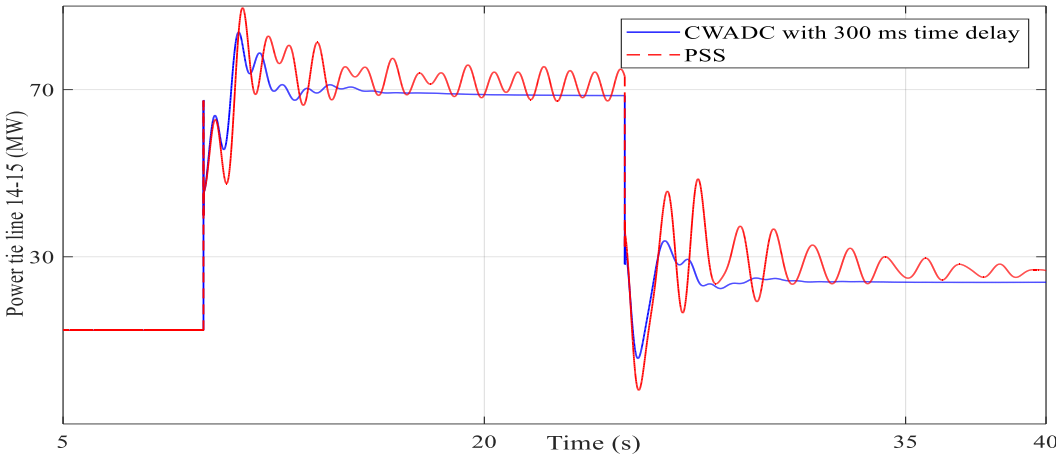

Figure 7. 21. Active power on tie line 14-15

30% of the total load is considered as dynamic type in this case where the effectiveness of the proposed controller is also tested for load parameter changes. First, the controller is designed by omitting the effect of load uncertainties. Then, the controller is again designed by considering the load model uncertainties. The proportion of the tripped motor load is changed, which triggers the inter-area oscillations. The performance of these two controllers for a change in tripped motor load proportion is shown in Figure 7. 22.

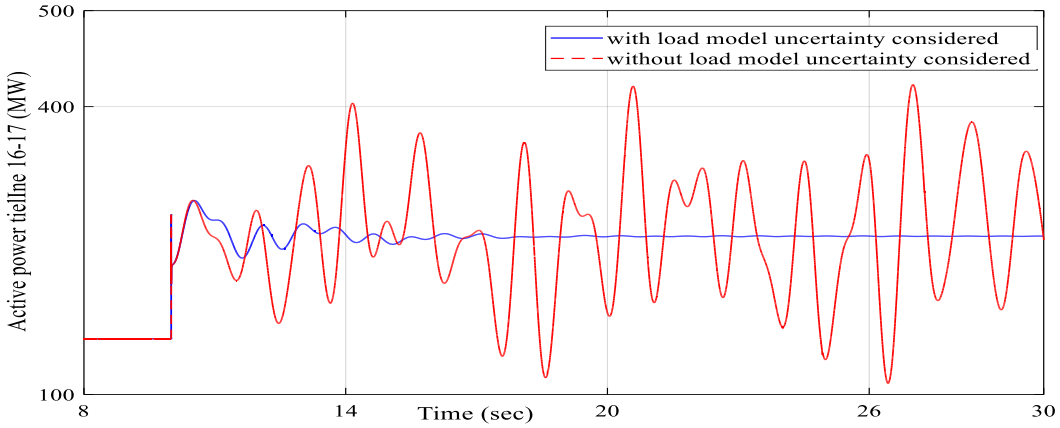

Figure 7. 22. Active power on tie line 16-17

- *Change of grid topology*

Figure 7. 23 shows removal of line from the begin of simulation, which causes a new operating point. For showing the robustness of CWADC to this change (removing line), also a three phase

short circuit is applied by considering propagated time delay. It should be mentioned that PSS also can handle these varieties but cannot damp oscillation as fast as CWADC can do.

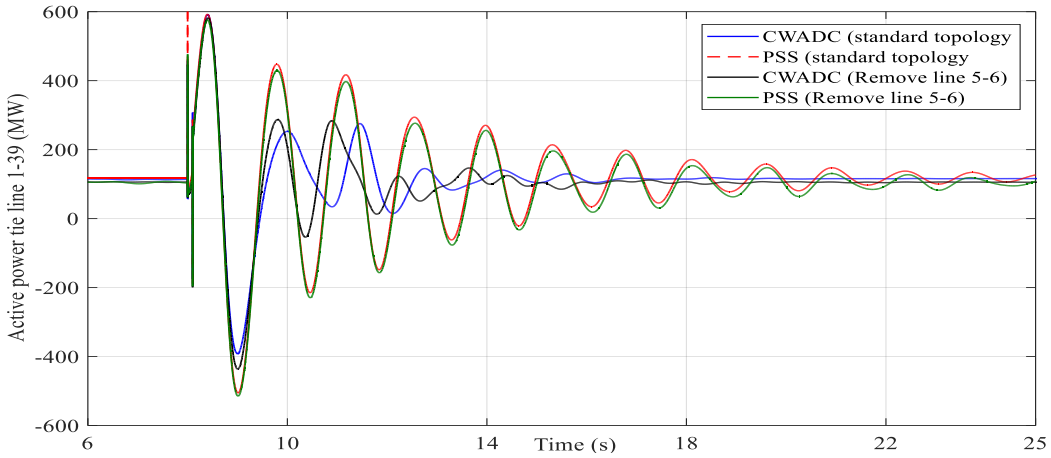

Figure 7. 23. Tie line power response to changed topology as well as three phase short circuit

7.9. Time Domain Response of Decentralized Robust Controller for New England 39 bus, 10 machine System

New England 39 bus, 10 machine system has three areas and in any area exists a controllable generator. It means for any area, one decentralized controller is necessary to design. According to more controllable generators and more observable measurements, which was discussed for centralized controller design, decentralized controllers input and output signals are like shown in Figure 7. 24. According to observability for inter-area modes, the measured signals for decentralized controllers are the tie line power through the lines 14–15 or 16–17 that are used as inputs to the robust centralized controller as shown in Figure 7. 24. G3, G5 and G9 have more controllability like before, which are considered as targets of controllers.

To test the robustness of the decentralized controller, different uncertainties that were mentioned in part 7.3 for evaluation of centralized controller are applied.

- *Changing operating point*

In this case operating point is changed in three steps as shown in Figure 7. 25. Designed DWADC with propagated time delay can handle changing operating points and damp the oscillation better than PSS.

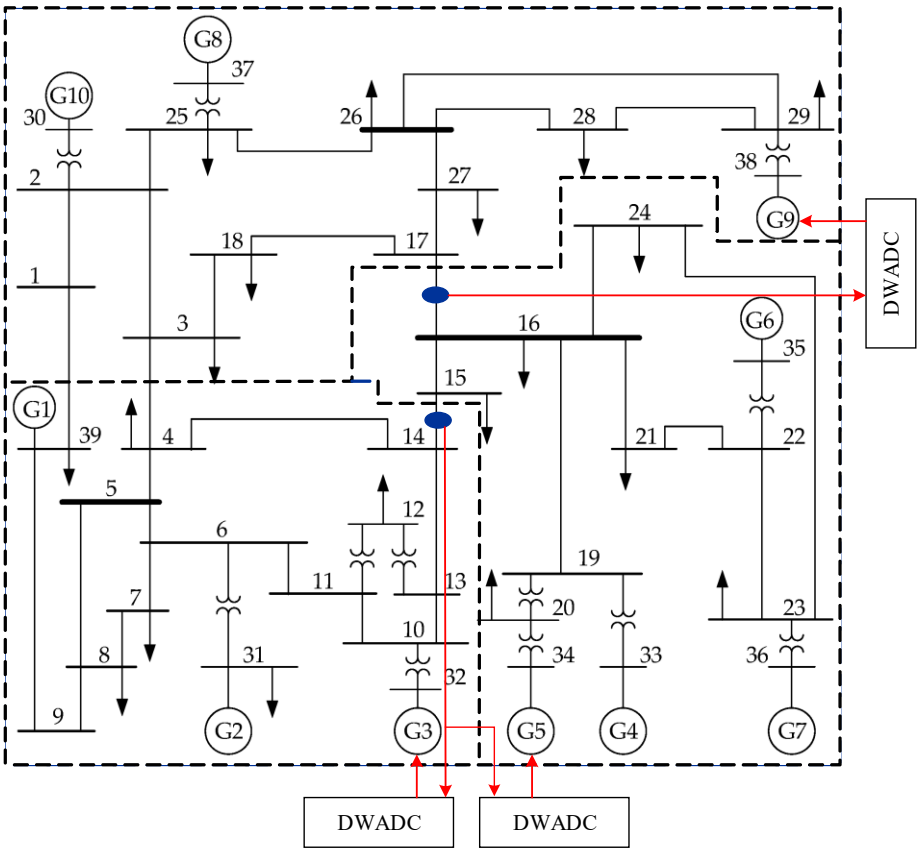

Figure 7. 24. DWADC for New England system

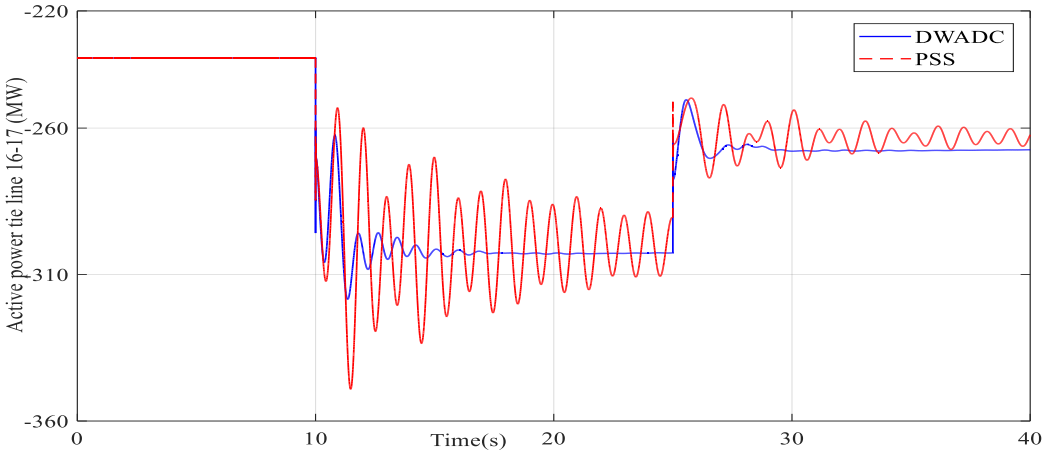

Figure 7. 25. Active power on tie line 16-17

- *Change of grid topology*

Figure 7. 26 shows removal of a line from the begin of simulation which causes a new operating point. For showing the robustness of DWADC to this change (removal of line) also a three phase short circuit is applied by considering propagated time delay. It should be mentioned that PSS also can handle the varieties but cannot damp oscillation as fast as DWADC can do.

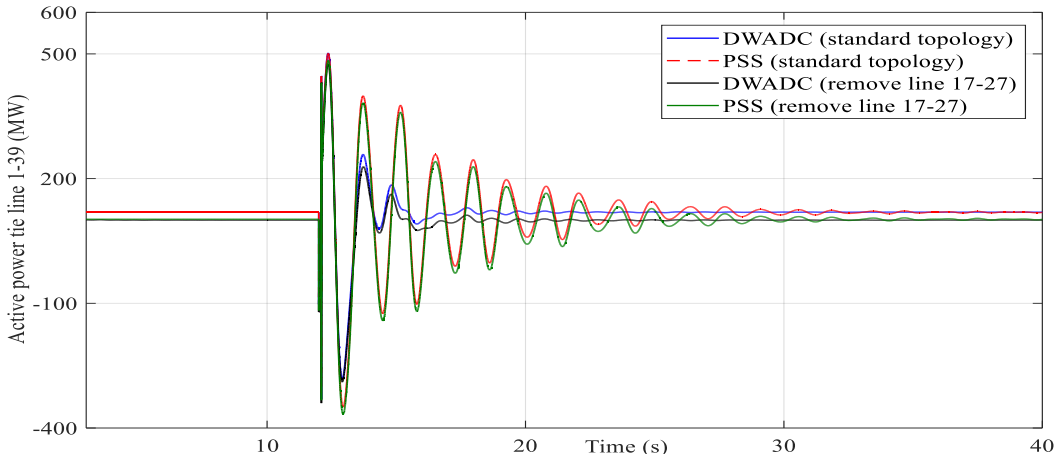

Figure 7. 26. Tie line power response to changing topology as well as three phase short circuit

7.10. Evaluation of Controllers Performance

Figure 7. 27 compares the performance of conventional PSS, CWADC and DWADC together in time domain in face of a severe disturbance (short circuit for 100 ms at Bus 17). As it is shown DWADC has the best performance of damping oscillation; evaluation of stability and performance were done one time for any area and one time overally. CWAD has the second place with evaluation of performance done one time overally, and PSS because of lack of observability cannot damp oscillation properly and is placed at last order.

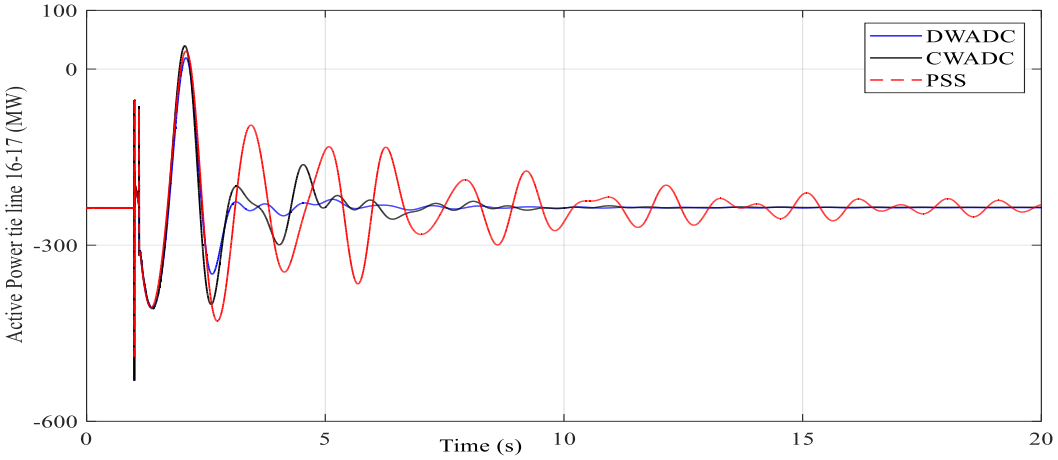

Figure 7. 27. Time domain response comparison of DWADC, CWADC, PSS

CHAPTER 8 .CONVERTER BASED CASE STUDIES

8.1. Introduction

Over the last decades, the installation of renewable power generation systems has been increasing exponentially. Renewable based Generation (RG) plants have the well known merits and when they interface the grid through power converters, they can produce negative impacts on the electrical grid, due to their different behavior from traditional generation plants. The regulation capability of the grid decreases as much as the share of the RG increases. To cope with this problem, power conversion systems belonging to RG plants are requested to be more grid friendly, responsive to the electrical network conditions, as well as grid supportive. In this way, they can contribute to the electrical network stability as other generation does, instead of behaving as simply grid feeding systems focused on injecting as much power as possible. In other side power systems with relatively small share of converter based generation have a large benefit from the coordinated control of them. The simulation studies show a significant improvement of the dynamic power system performance after disturbances, both in small benchmark systems and in a large model.

8.2. Centeralized Power Oscillation Damping Control with HVDC Link

8.2.1. Controller Model, Inputs and Outputs

The process of designing a VSC-HVDC link based WADC for addressing inter-area power oscillations in a system is the main concern in this section. Power oscillations can be damped effectively through modulation of both active and reactive power of a VSC based HVDC link. The challenge, however, is how to coordinate the control action properly at the two ends of the link with using a centralized control. For emphasizing the impact that WADC has on the damping performance, the two area, four machine power system shown in Figure 8. 1 is used. The system accommodates a VSC-HVDC link connecting Buses 7 and 9 and operating in parallel with the two long AC transmission corridors and performing power transmissions of different amount.

Small signal analysis of linearized model is applied for two area, four machine system with the 220 km long HVDC cable link which has a rated power of 100 MW and a DC voltage rating of

±230 kV and which was chosen as nominal operating point. The existing inter-area mode to design WADC is shown in Table 8. 1.

Table 8. 1. Eigenvalue, damping ratio and frequency of the test system

Eigenvalue (1/s) $\sigma \pm j\omega$	**Damping Ratio (%)** $-\sigma/\sqrt{\sigma^2+\omega^2}$	**Frequency (Hz)** $\omega/2\pi$
$0.0412 \pm j\ 3.84$	-1.07	0.61

According to modal analysis and geometric observability/controllability for inter-area mode that was mentioned in chapter 6, G2 and G4 belonging to conventional generators and HVDC line as VSC based equipment have the best controllability and are chosen as the control locations. Real power on tie line from Bus 7 to Bus 8 has the best observability and was selected as stabilizing signal for the controller. According to most controllable generators and most observable measurements, centralized control system is designed like shown in Figure 8. 1.

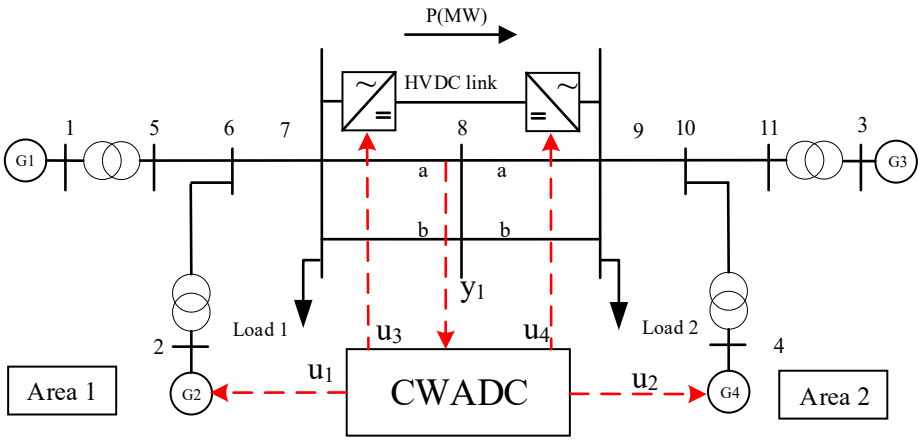

Figure 8. 1. System with a VSC-HVDC link

8.2.2. Model and Controller Order

Model reduction is considerable like chapter 7 emphasizes on reduced order models obtained by residualizing the less controllable and observable states of a balanced realization. The frequency responses of the full order model and reduced order model are shown in Figure 8. 2. It can be seen that for the interesting bandwidth, the reduced order model is reliable for robust controller design.

Centralized fixed order controllers with different output signals are applied for reduced order model, which is described as follow.

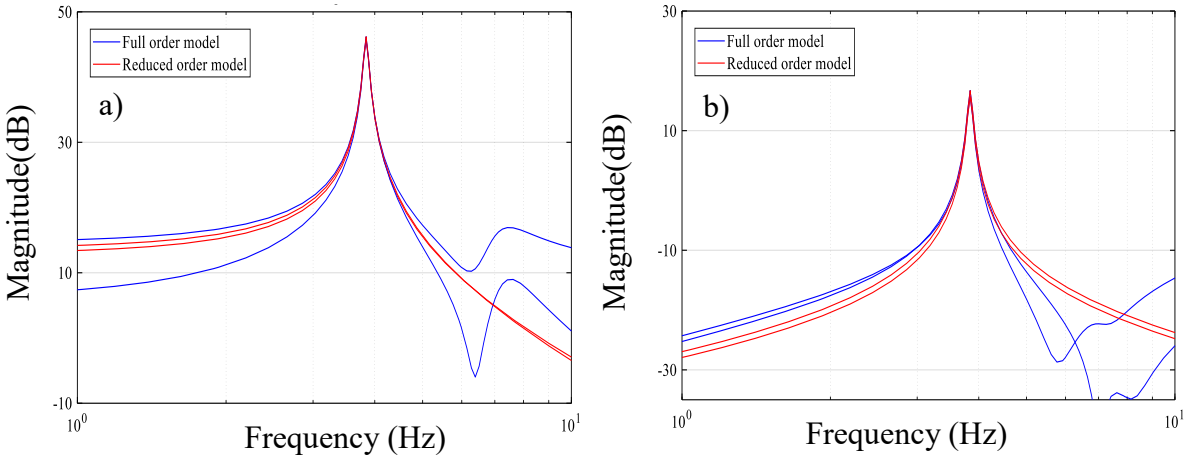

Figure 8. 2. Frequency response comparison of full and reduced order model a) from u_1 (input) to y_1 (output) and b) from u_2 to y_1

The robust VSC-HVDC CWADC can be considered in two structures:

- VSC-HVDC CWADC output signals consider synchronous generator as well as HVDC line (only for sender side), which is shown in Figure 8. 3.

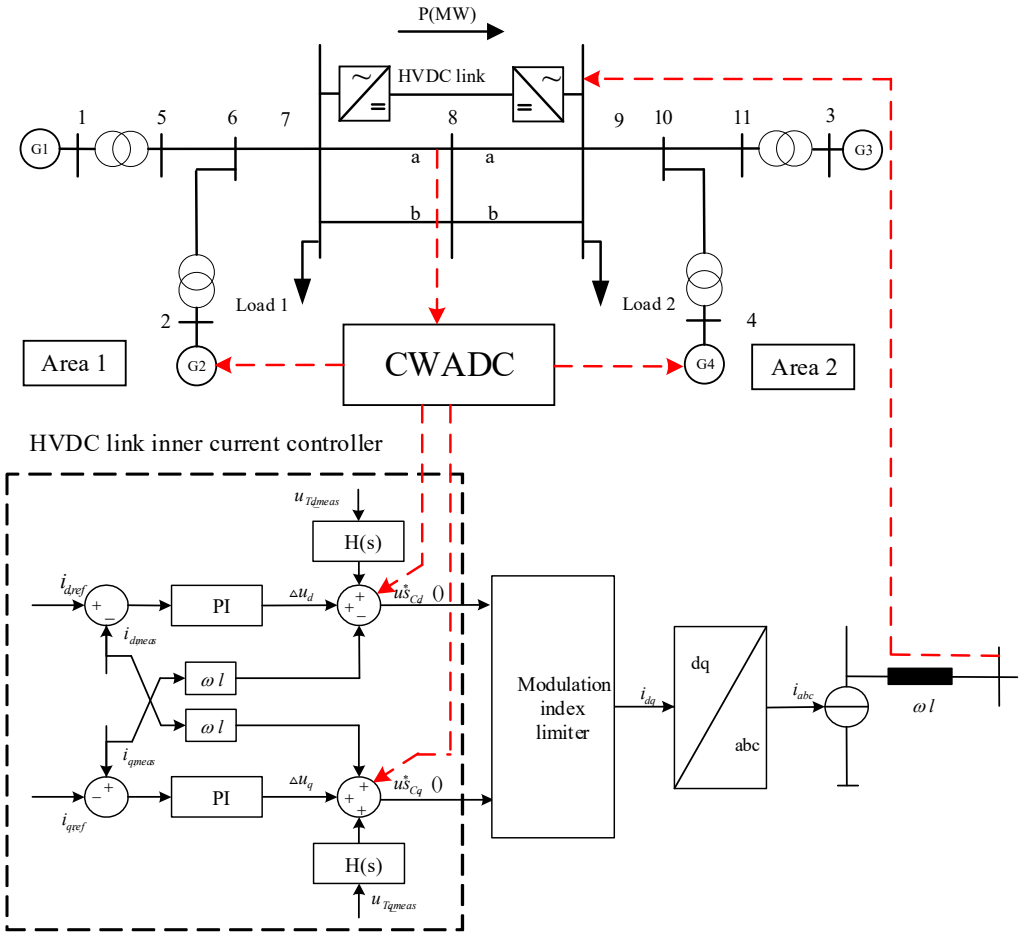

Figure 8. 3. VSC-HVDC WADC's outputs are applied to G2, G4 and HVDC line

- VSC-HVDC CWADC output signals consider only HVDC line, which is shown in Figure 8. 4.

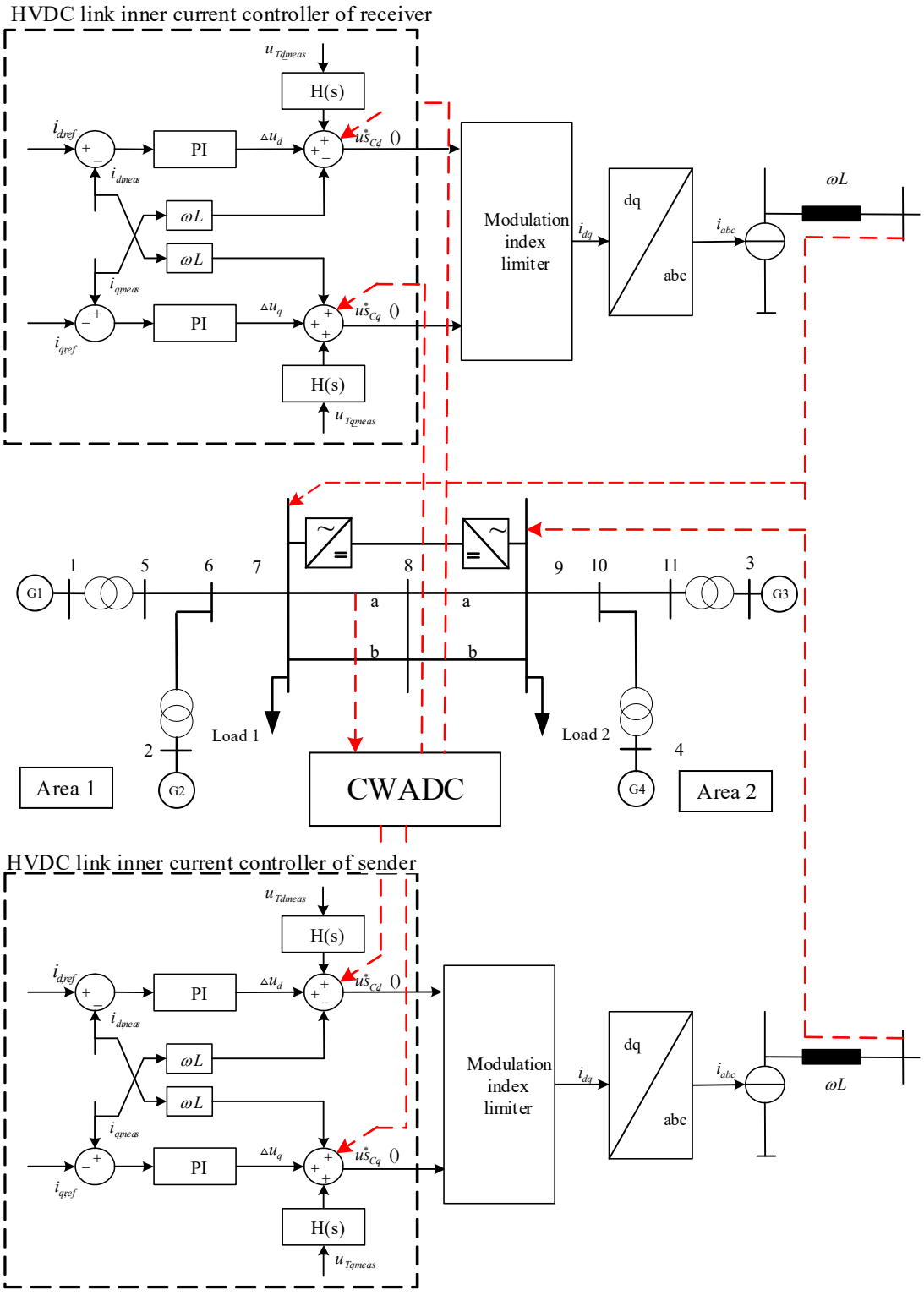

Figure 8. 4. VSC-HVDC WADC's outputs are applied to HVDC line only

In this case, it is better to apply the controller for both sides (sender and receiver of the HVDC).

Fixed order VSC-HVDC CWADC is applied for reduced order model with two possibilities; with consideration of HVDC line with and without synchronous generators; it is evaluated by short circuit fault in time domain.

Figure 8. 5 is a time domain response comparison of different controller structures:

- Reduced 5th order model and fixed 2nd order VSC-HVDC CWADC with synchronous generators effect.
- Reduced 5th order model and fixed 2nd order VSC-HVDC CWADC without synchronous generators effect.

Time responses are compared for short circuit's fault, applied to Bus 8 for 100 ms.

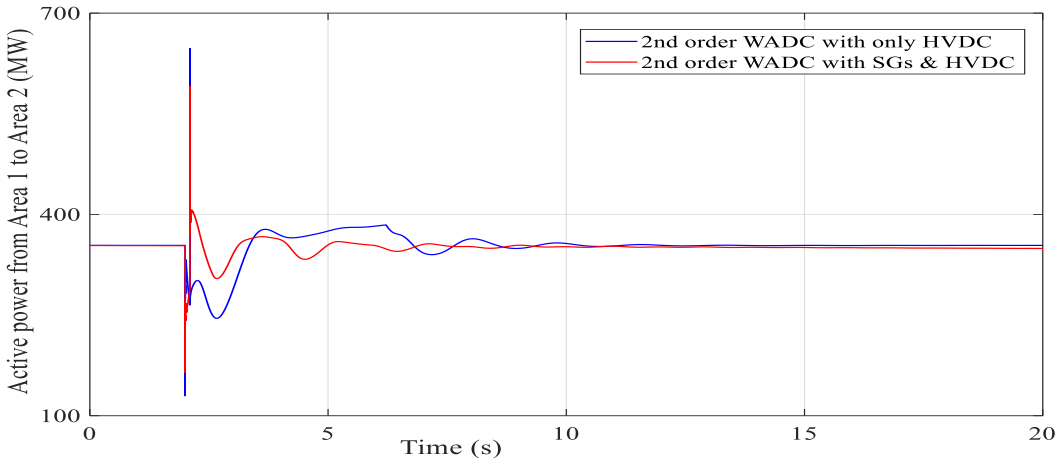

Figure 8. 5. Comparison of damping of oscillation HVDC WADC with and without contribution of synchronous generators

The coordinated control of HVDC is significant and has good contribution with synchronous generators to suppress oscillation of inter-area modes.

8.2.3. Time Domain Simulation and Centralized Controller Robustness

Effects of VSC-HVDC transmission line on inter area oscillation is studied with two area, four machine system. Oscillation of synchronous generators in Area 1 against synchronous generators in Area 2 produces inter-area frequency. 2nd order WADC with contribution of only HVDC is selected to suppress oscillation. It has to be mentioned that HVDC can work in two directions. It means sending and receiving VSCs are not fixed. Different amount of active power, which is transferred through HVDC line and VSC-HVDC line in both sides as frequency dependent uncertainty and time delay in structure of WADC as parametric uncertainty are considered.

Different operating points are considered with different amount of active power transmission through HVDC to test the robustness of the test system. In parallel, three phase short circuit at Bus 7 or 8 or 9 is applied to different operating points and it is cleared after 100 ms. The controller has been designed based on multi model, which is mentioned before (in 5.4.1). Also propagated time delay is considered in control structure. The simulation results are shown in Figure 8. 6.

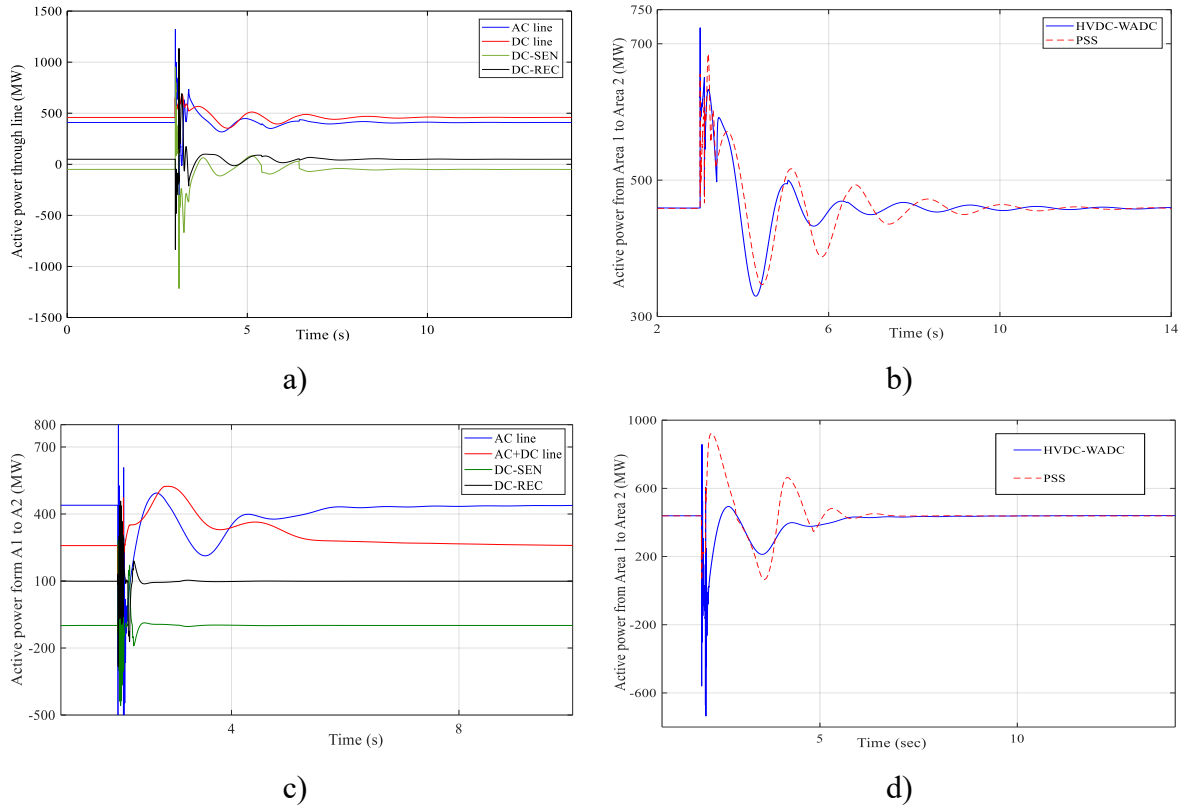

Figure 8. 6. Tie line power at different load conditions and fault locations

In Figure 8. 6. a), b) the direction of HVDC power is considered from Area 2 to Area 1. 50 MW active power is transferred via HVDC line. Part a) shows active power P in AC, DC, AC+DC line. In part b) results by considering WADC and PSS are compared. It should be mentioned that three phase short circuit was applied at Bus 7. It is clear that WADC supresses oscillation faster than PSS.

In Figure 8. 6. c), d) the direction of HVDC is considered from Area 1 to Area 2. 200 MW active power is transferred via HVDC line. Part c) shows active power P in AC, DC, AC+DC. In part d) results by considering WADC and PSS are compared. Three phase short circuit was applied at Bus 8. It is shown that WADC time response has rather smaller over damping in comparison with PSS time response.

8.3.Integration of Renewable Energy Sources in the WADC

Recent trends of legislative changes and environmental concerns around the globe are likely to increase penetration of renewable energy resources into power systems in the form of Distributed Generation (DG) units. The integration and high penetration of renewable energy resources into a distribution system could introduce a number of key issues, including oscillatory stability, which is also traditionally referred to as small signal stability. Oscillatory instability may be caused by dynamic characteristics of DGs and improper tuning of the controllers. It is one of the limiting criteria for synchronous operation of DGs. For example, dynamics of a transmission network are governed by large synchronous generators while the dynamics of emerging distribution networks will be affected by different types of generators such as synchronous, induction, static generators and their controllers. Generators in a transmission system are usually equipped with PSS for small signal stability while generators in emerging distribution systems (wind and solar generators) usually do not have such stabilizing functionality. Owing to the closeness of the generators and their controllers, dynamic interaction in a distribution system is a more complex issue. As a result, not only EM modes but also some control modes become prominent issue for small signal stability. Hence assessment and enhancement of small signal stability becomes an important task for accommodating higher penetration of renewable energy based distributed generation for secure operation of the electricity distribution system.

In conventional power systems, damping of low frequency oscillations is supported by either PSSs installed at synchronous generators or supplementary control loops of voltage control. With increased penetration of renewable energy resources, there are also efforts to utilize DG for oscillation damping. It has been reported that additional controllers at DFIG can also support damping of inter-area oscillations. Similarly, a PV generator may be controlled for stability enhancement. In this research, supplementary control loops of voltage control with contribution of conventional generators as well as Renewable Energy (RE) is applied.[104]

In [105] , [106] the methodology presented considers only the system's generators to derive the WADC signals. Therefore, all the necessary modifications of the aforementioned methodology are discussed in detail here, in order to also include renewable sources into the WADC design. Furthermore, the ultimate goal is to illustrate that the correct coordination of generators and renewable sources, through the WADC, improves the damping performance of the entire system instead of decreasing it, even under a high penetration of renewables. Figure 8. 7 depicts the general view of the proposed scheme for the development of coordinated signals

for generators and renewable sources. By obtaining the appropriate wide area measurements from the renewable sources, the methodology of [105] ,[106] can now be modified accordingly in order to become applicable for the renewables as well.

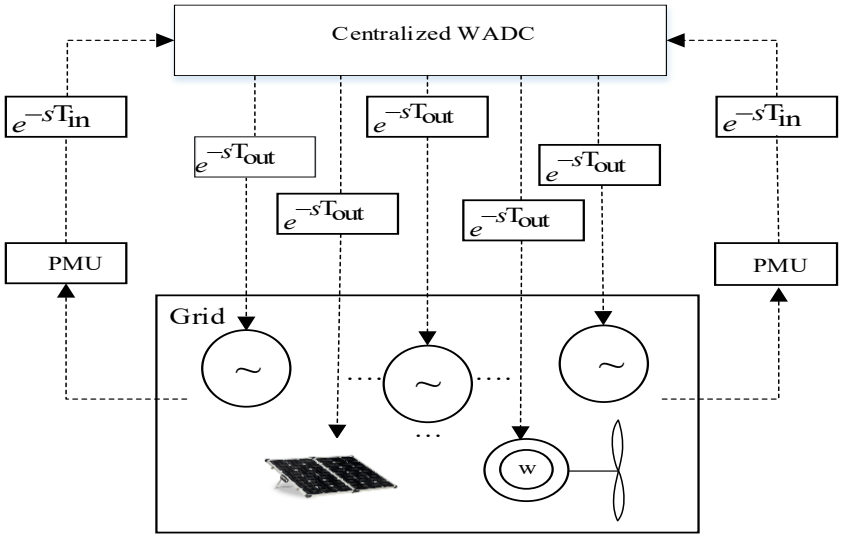

Figure 8. 7. Centralized WADC structure

8.4. Robust CWADC Design with Integration of Wind Power

In this study, the 2 area, 4 machine power system has been modified to assess the impact of a DFIG based wind power plant on inter-area oscillations. A single equivalent model (aggregated model) was used to represent all individual units within the power plant in order to avoid increased computation time. A 1.5 MW DFIG based Wind Generator (WG) (phasor model) in MATLAB/SIMULINK toolbox was utilized. The impact of wind farm is considered in two scenarios: the penetration by aggregated wind power plant (in range of 50 to 400 MW) and replacement of synchronous generator by wind power plant (700 MW total).

8.4.1. Controller Model, Input and Outputs

The process of designing a WAD Controller design with integration of wind power for addressing inter-area power oscillations in a system is the main concern in this section. For emphasizing the impact that wide area damping controller has on the damping performance of the power system, the two area, four machine test power system network with penetration of WG at Bus 7 and 9 or replacing of G1 or G3 with WG as shown in Figure 8. 1 is used. Table 8. 2 shows the eigenvalue analysis.

Penetration and replacing of WG make a new inter-area mode because of interaction between synchronous generators and DC voltage regulator loop of WGs. This extra inter-area mode

which is highlighted with grey colour in Table 8. 2 is damped perfectly because of its electrical nature. In case of wind power penetration, inertia of whole grid does not change and regarding frequency of inter-area and local modes, variation is not significant and is predictable. By replacing one synchronous generator by WGs, total grid inertia decreases which effects on frequency of inter-area and local modes as it is shown in Table 8. 2 and makes the grid more unstable.

Table 8. 2. Eigenvalue analysis

Mode type	**Eigenvalue (1/s)** $\sigma \pm j\omega$	**Damping Ratio (%)** $-\sigma / \sqrt{\sigma^2+\omega^2}$	**Frequency (Hz)** $\omega / 2\pi$
Power grid without WG			
Inter-area	$0.05 \pm j3.86$	-1.27	0.61
Local	$-0.668 \pm j7.05$	9.43	1.12
Local	$-0.81 \pm j7.18$	11.2	1.15
Power grid with penetrating 200MW WG			
Inter-area	$0.034 \pm j3.98$	-0.87	0.63
Inter-area (WG)	$-4.79 \pm j0.20$	99.37	0.52
Local	$-0.9 \pm j6.97$	12.83	1.10
Local	$-.76 \pm j7.16$	10.64	1.14
Power grid with replacing synchronous generator by WG			
Inter-area	$0.12 \pm j4.66$	-2.35	0.74
Inter-area (WG)	$-22.93 \pm j2.23$	99.7	0.35
Local	$-1.19 \pm j709$	15.5	1.21
Local	$-0.85 \pm j762$	10.4	1.29

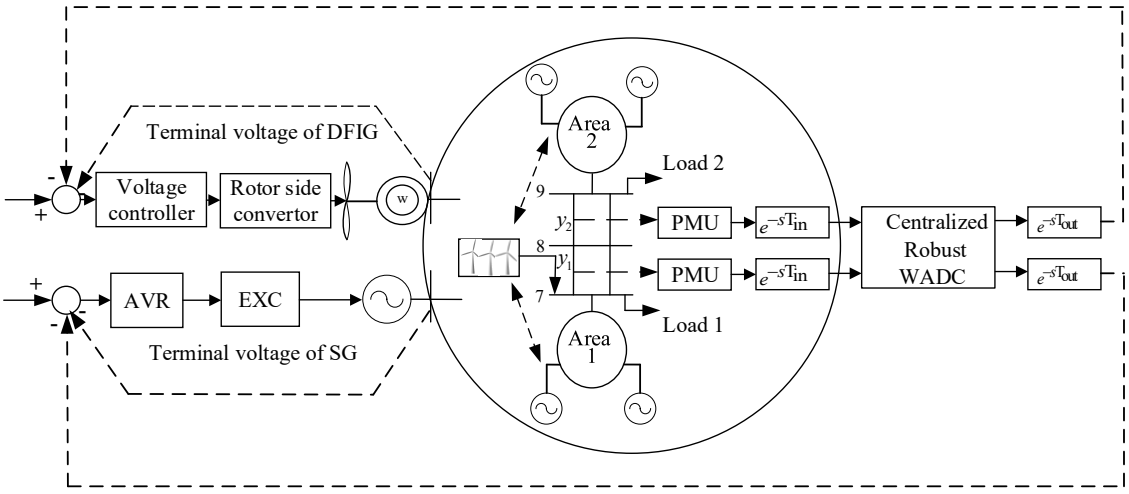

Figure 8. 8. Proposed WADC for 2 areas 4 machine system and wind power integrated

According to modal analysis and geometric observability/controllability for inter-area mode that was mentioned in chapter 6, G2 and G4 belonging to conventional generators and WG as renewable source have the best controllability and are chosen as the control locations. Real power of tie line from Bus 7 to Bus 8 has the best observability and is selected as stabilizing signal for controller.

In [105] , the centralized controller for 2 areas and 4 machine system has 1 input and two outputs. In present approach, reserved input and output are considered because of possible interruption and fail of input/output channels. The measured signals y_1, y_2 are the tie line power through the left lines 7–8 and 8–9, which are used as inputs to the robust CWADC as shown in Figure 8. 8., depicting the overall survey of the proposed scheme for the development of coordinated signals for synchronous generators and WGs. By obtaining the appropriate wide area measurements, the methodology of [105] can now be modified accordingly in order to become applicable for the renewables as well.

8.4.2. Model and Controller Order

Model reduction is considerable like chapter 7 emphasizes on reduced order models obtained by residualizing the less controllable and observable states of a balanced realization. The controller design technique can use the full order system for designing a robust loop shaping controller since the order of the controller is fixed without sacrificing the computational time required. This eliminates the need for using an approximate reduced order model rather than the actual model. The proposed approach can also use reduced order systems:

- 3rd order controller applied to full 51st order model;
- 1st order controller applied to reduced 6th order model.

Time responses are compared in Figure 8. 9 for a three phase short circuit fault, which is applied to Bus 8 for 100 ms. According to Figure 8. 9, the 1st order controller for 3rd order model shows almost the same behaviour as the full order model. Therefore, the 1st order controller was chosen in this study. It should be mentioned that the performance of the designed fixed order robust H_∞ controllers is considered without PSS.

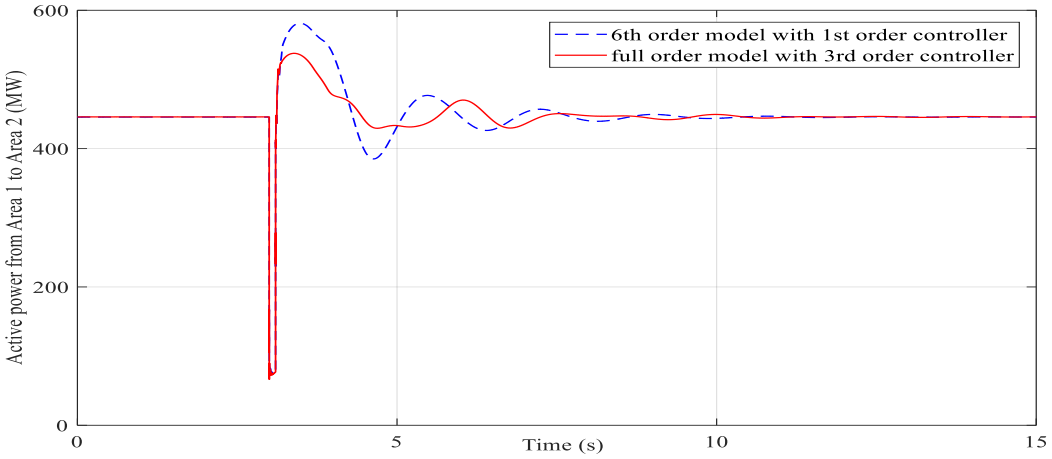

Figure 8. 9. Time domain response comparison of models and controllers of different orders

8.4.3. Nonlinear Time Domain Simulation and Centralized Controller Robustness

A robust 1st order WADC with two inputs and three outputs without PSS was designed. This controller can handle different uncertainties like different percentage of WG penetration, synchronous generator replacing, different topologies and operating points. The wind power uncertainties are considered for two scenarios:

- *Scenario 1: Penetration by WGs*

In this scenario, in the first case one aggregated WG with 200 MW capacity penetrates the grid. A three phase short circuit was applied to Bus 8 for 100 ms. Figure 8. 10 shows the effect of input/output signal interruption in the proposed controller. Interruption of the control signal to WG as expected would have no significant effect, but also interruption of the signal to one of conventional generators would be sustained which is considered in this case. The proposed controller can damp oscillations while input or/and output signals are interrupted. It can be seen that the effect is acceptable.

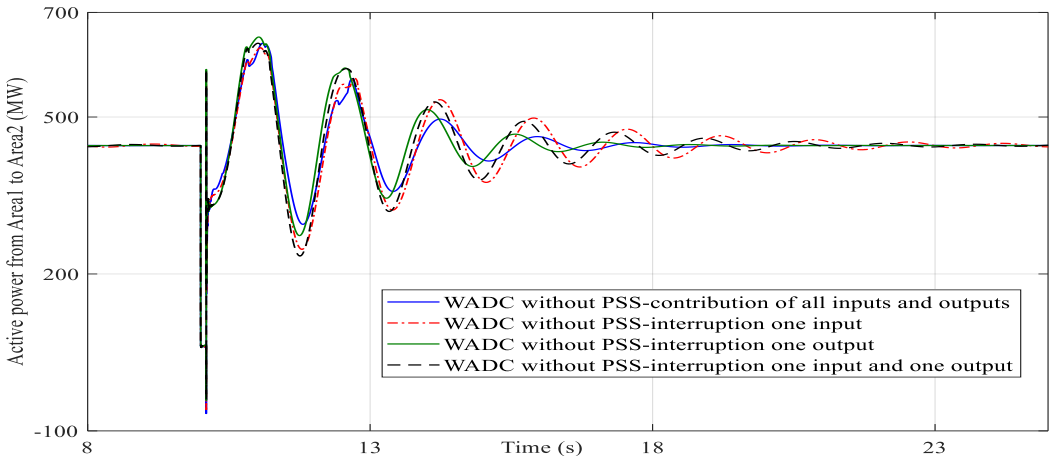

Figure 8. 10. Time domain response by considering input/output interruption

In the second case, a 90 MW aggregated WG penetrates the test grid. The operating point changes to 300 MW active power transfer from Area 1 to Area 2. Controller performance is tested with removing one line 7-8. Figure 8. 11 shows robust stability and performance of the proposed controller in this case while PSS cannot handle.

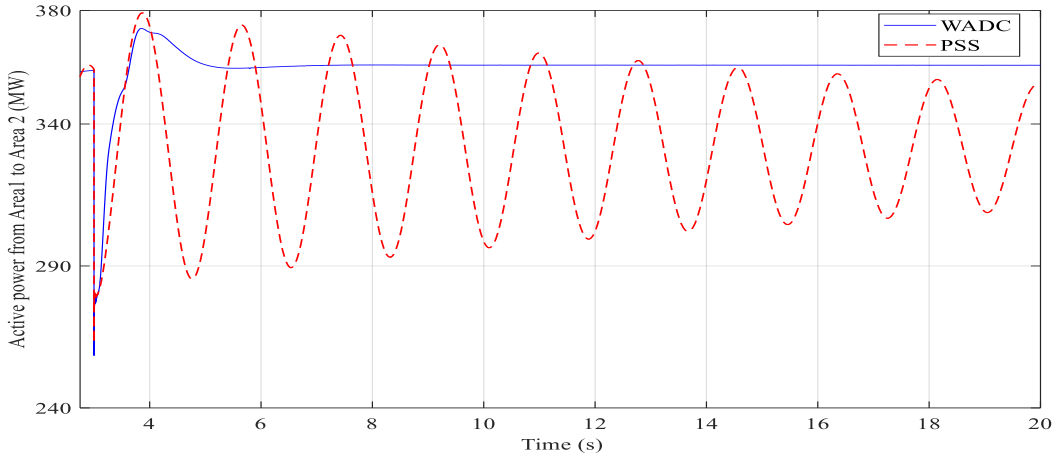

Figure 8. 11. Active power flow transmitted from Area 1 to Area 2

- *Scenario 2: replacing of synchronous generator by WG*

In this scenario, in first case one aggregated WG with 700 MW active power capacity replaces G1. A three phase short circuit was applied to Bus 8 for 100 ms. Figure 8. 12 shows the active power flow from Area 1 to Area 2 with only PSS, and with the proposed fixed order WADC without PSS.

It is evident that with conventional PSS, the system is not well damped and the proposed controller stabilizes the system almost perfectly.

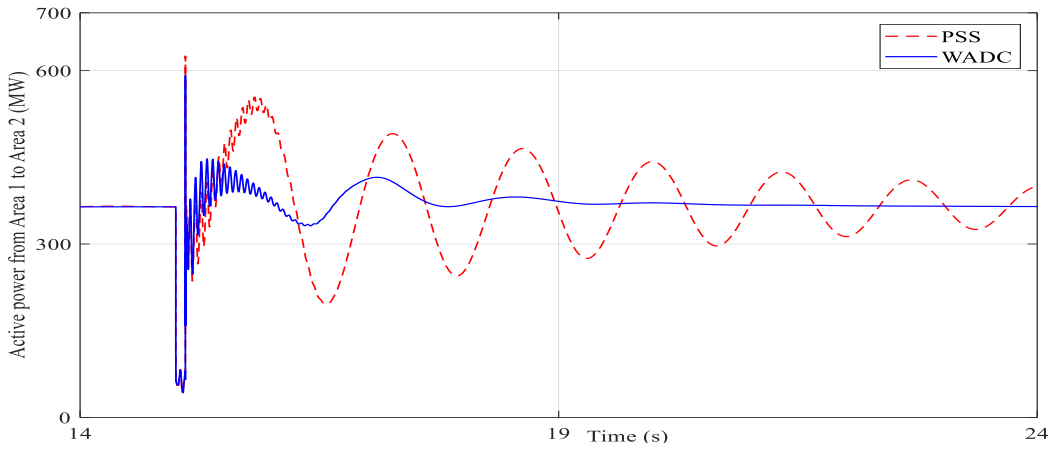

Figure 8. 12. Active power flow transmitted from Area 1 to area 2 after short circuit

In the second case, the aggregated WG replaces G3 in Area 2. Controller performance is tested with a three phase short circuit applied to Bus 7 for 100 ms. Figure 8. 13 shows robust stability and performance of the proposed controller in this case.

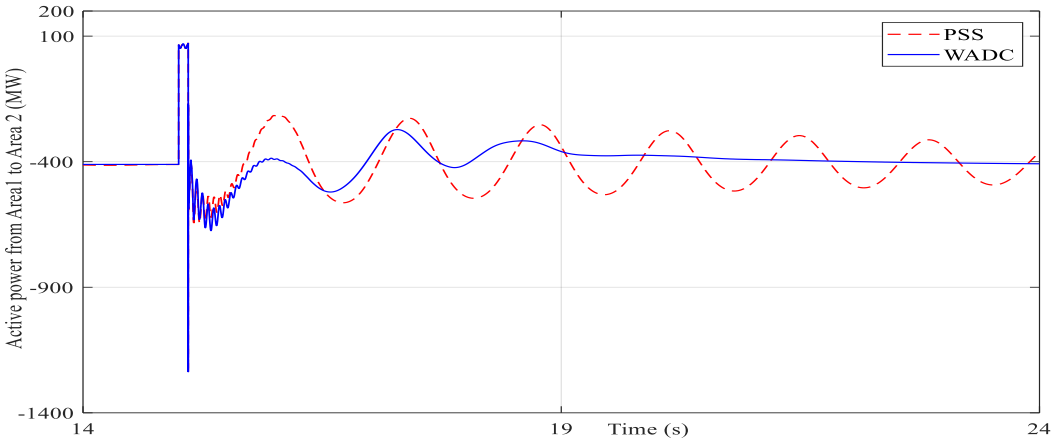

Figure 8. 13. Active power flow transmitted from Area 1 to Area 2 after short circuit

Figure 8. 14 shows the robust performance and stability of the proposed controller for the test grid without WGs for changed operating point.

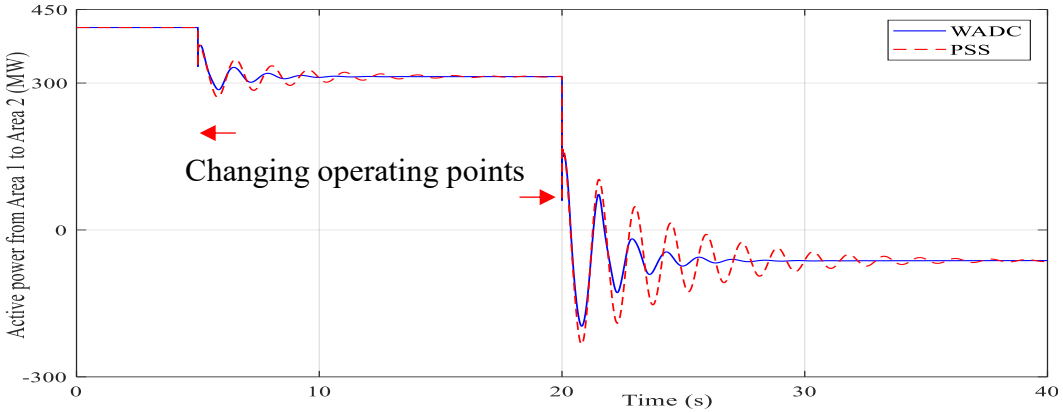

Figure 8. 14. Active power flow transmitted from Area 1 to Area 2 in response of changing operating points

It should be mentioned that in all cases propagated time delay was considered.

According to joint observability/controllability and Figure 8. 15, the centralized controller sends control signals to more controllable synchronous generators and WGs. In this case, one generator in any area and WG receive control signals. Figure 8. 15 shows the magnitude Bode diagram of control signals, which were considered for multi model of test grid. Large magnitude of dashed curves belongs to the synchronous generators in proposed controller. The control signal to WG with solid curve can be ignored in comparison with the control signals to synchronous generators. It means, although WG has enough controllability, it has low contribution in comparison with synchronous generators.

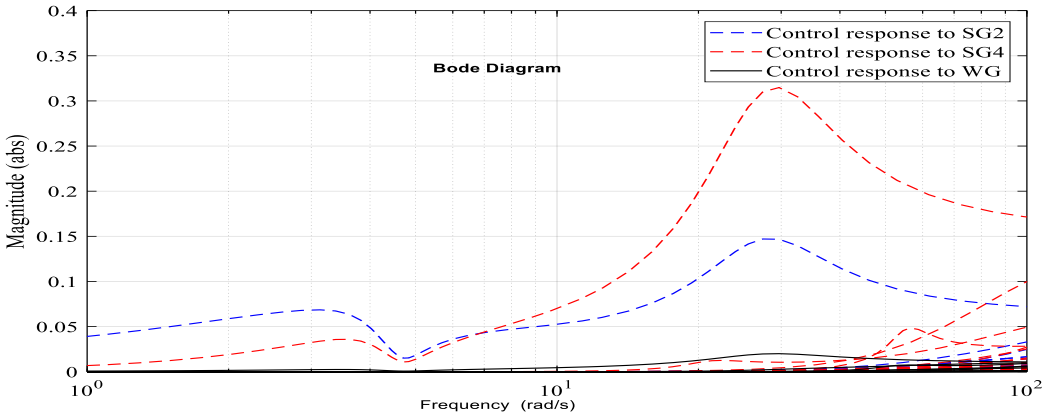

Figure 8. 15. Magnitude of control signals

8.5. Robust CWADC Design with Integration of Photovoltaic Plant

The impact of a PV plant on power system stability is minimal when deployed in small scale. However, when penetration level increases, the dynamic performance of the power system can be significantly affected [107] . Since PV plants are based on power electronics converters, there are primarily four mechanisms by which the EM modes can be affected. These are as follows;

- Redispatch of conventional generators with PSSs due to PV power.
- By affecting the major line flows in the system.
- Controller interaction between PV plant controls and nearby generators.
- The physical difference between the generators and PV generators, i.e., inertial contribution of rotating mass.

For power system with large scale PV penetration, due to the aforementioned mechanisms, the damping of EM and other lightly damped modes can be affected negatively as reported in [107] , [108] and [109] . Tuning of a PSS could help to improve the damping of EM modes. But, it requires coordinated tuning of PSSs; otherwise, a tuned PSS could have a detrimental effect on

system transient stability. Moreover, retuning of a PSS can be time consuming with high computational burden, which limits optimal real time operation. On the contrary, the centralized damping controller at a PV plant can ensure the required system performance without retuning of other system controllers. This type of a controller at the PV plant would allow a flawless integration. [110]

8.5.1. Controller Model, Inputs and Outputs

In this study, the 2 area 4 machine power system has been modified to assess the impact of a PV power plant on inter-area oscillations. A single equivalent model (aggregated model) was used to represent all individual units within the power plant in order to avoid increased computation time. The impact of PV plant is considered in two scenarios: the penetration by PV plants (in range of 50 to 200 MW) at Bus 7 and 9 or replacing of G1 or G3 with PV as shown in Figure 8. 16 is used. Table 8. 3 shows the eigenvalue analysis.

In case of PV power penetration, inertia of whole grid does not change and regarding frequency of inter-area and local modes, variation is not significant and is predictable. Replacing one generator by PVs, one local modes disappears. In the area that synchronous generator is represented by PV, any EM oscillation happens between synchronous generator and PV evoking local mode. Total grid inertia decreases which effects on frequency of inter-area and local modes as it is shown in Table 8. 3 and makes the grid more unstable.

Table 8. 3. Eigenvalue analysis

Mode type	**Eigenvalue** $\sigma \pm j\omega$	**Damping Ratio (%)** $-\sigma/\sqrt{\sigma^2+\omega^2}$	**Frequency(Hz)** $\omega/2\pi$
Power grid without PV			
Inter-area	$0.13 \pm j4.14$	-3.13	0.66
Local	$-0.55 \pm j7.1$	7.72	1.13
Local	$-0.64 \pm j7.29$	8.68	1.16
Power grid with penetrating 200MW PV			
Inter-area	$-0.063 \pm j3.85$	1.63	0.61
Local	$-0.9 \pm j6.97$	13.4	1.07
Local	$-.98 \pm j6.96$	14	1.18
Power grid with replacing G by PV			
Inter-area	$0.11 \pm j4.62$	-2.31	0.73
Local	-0.64 ± 7.25	8.8	1.15

According to modal analysis and geometric observability/controllability for inter-area mode as mentioned in chapter 6, G2, G4 and PV plant (the PV is shown in Figure 2. 11 and is modeled as a current source) have the best controllability and are chosen as the control locations. Real power of tie line from Bus 7 to Bus 8 has the best observability and is selected as stabilizing signal for controller. Centralized control system is shown in Figure 8. 16.

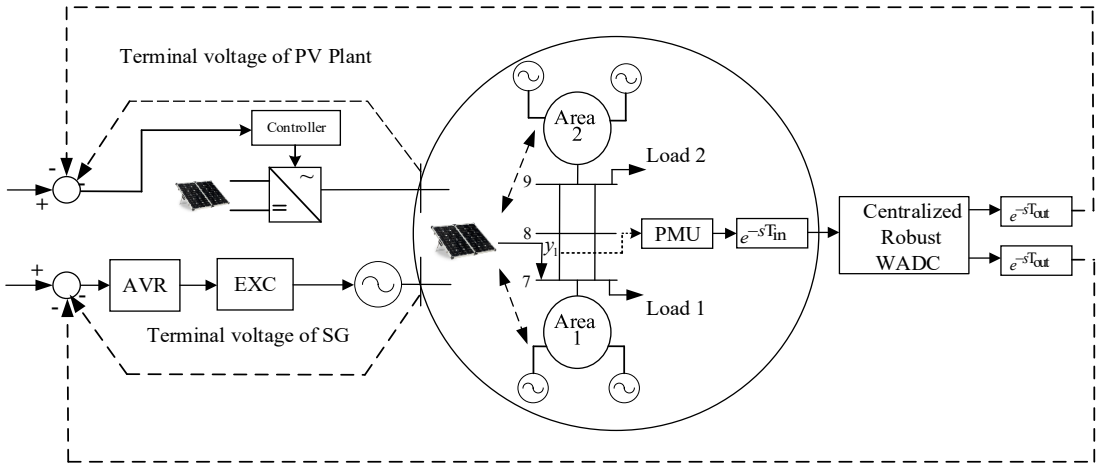

Figure 8. 16. Proposed WADC for 2 areas 4 machine system and PV power integrated

8.5.2. Model and Controller Order

Model reduction is considerable like chapter 7 emphasizes on reduced order models obtained by residualizing the less controllable and observable states of a balanced realization. The controller design technique can use the full order as well as reduced order system for designing a robust loop shaping controller. The proposed approach can also use reduced order systems:

- 3rd order controller applied to full 56th order model.
- 1st order controller applied to reduced 3rd order model.

Time responses are compared in Figure 8. 17 for a three phase short circuit fault, which is applied to Bus 7 for 100 ms. According to Figure 8. 17, the 1st order controller for 3rd order model does not have the same behaviour as the full order model but it is acceptable for evaluation. Therefore, the 1st order controller was chosen in this study. It should be mentioned that the performance of the designed fixed order robust H_∞ controllers is considered without PSS.

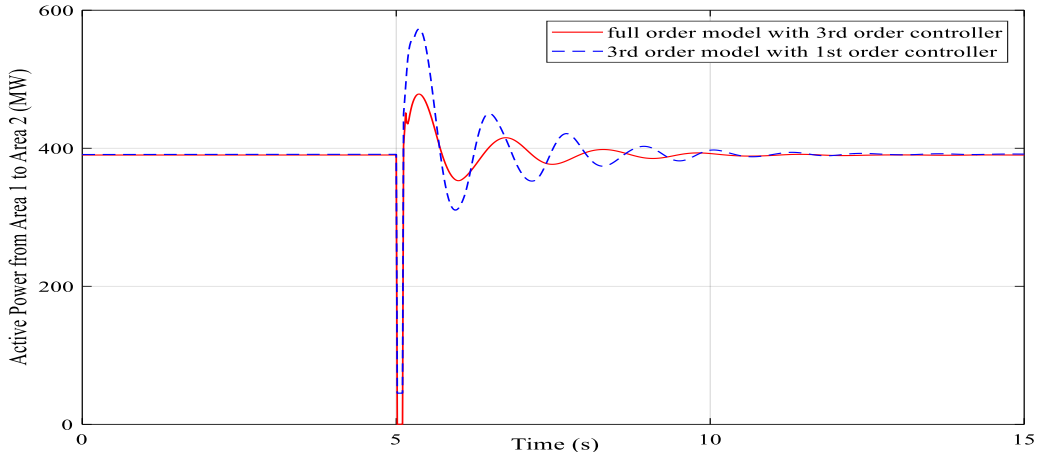

Figure 8. 17. Time domain response comparison of models and controllers of different orders

8.5.3. Nonlinear Time Domain Simulation and Centralized Controller Robustness

A robust 1st order WADC with one input and four outputs without PSS was designed. This controller can handle different uncertainties like different percentage of PV penetration, replacing of synchronous generator by PV, different topologies and operating points. The PV power uncertainties are considered as two scenarios:

- *Scenario 1: penetration by PV plant*

In this scenario, in the first case one aggregated PV with 200 MW capacity penetrates the grid. Figure 8. 18 shows the robust performance and stability of the proposed controller for changing operating point.

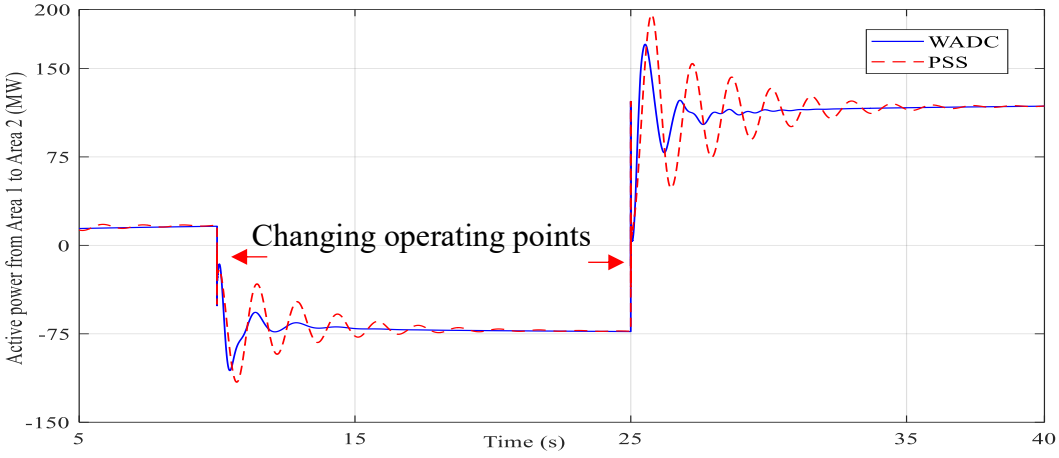

Figure 8. 18. Active power flow transmitted from Area 1 to Area 2 in response of changing operating points

In the second case, a 200 MW PV penetrates the test grid. The operating point changes to 500 MW active power transfer from Area 1 to Area 2. Controller performance is tested with

removing line 8-9. Figure 8. 19 shows robust stability and performance of the proposed controller; in comparison with PSS oscillation damping faster.

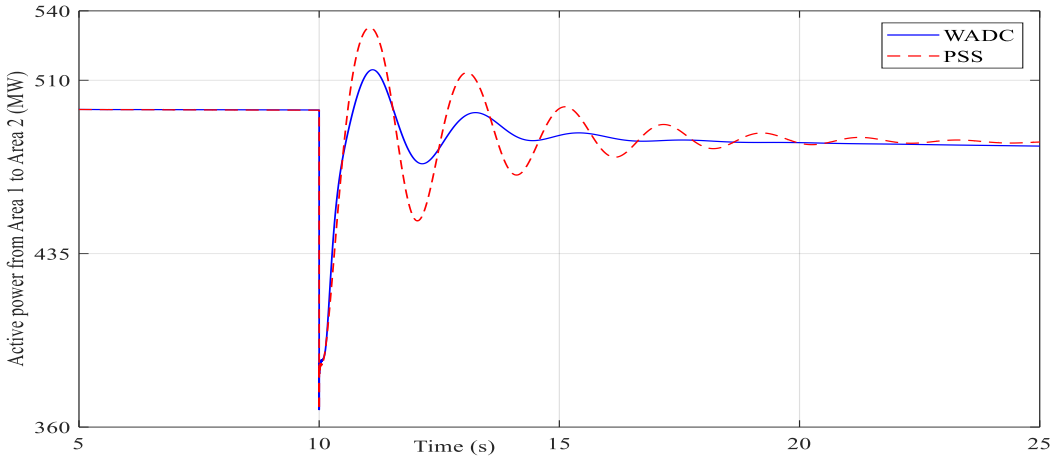

Figure 8. 19. Active power flow transmitted from Area 1 to Area 2 after removing line

- *Scenario 2: replacing of synchronous generator by PV*

In this scenario, in first case one aggregated PV with 700 MW active power capacity replaces G3. A three phase short circuit was applied to Bus 8 for 100 ms. Figure 8. 20 shows the active power flow from Area 1 to Area 2 with only PSS, and with the proposed fixed order WADC without PSS.

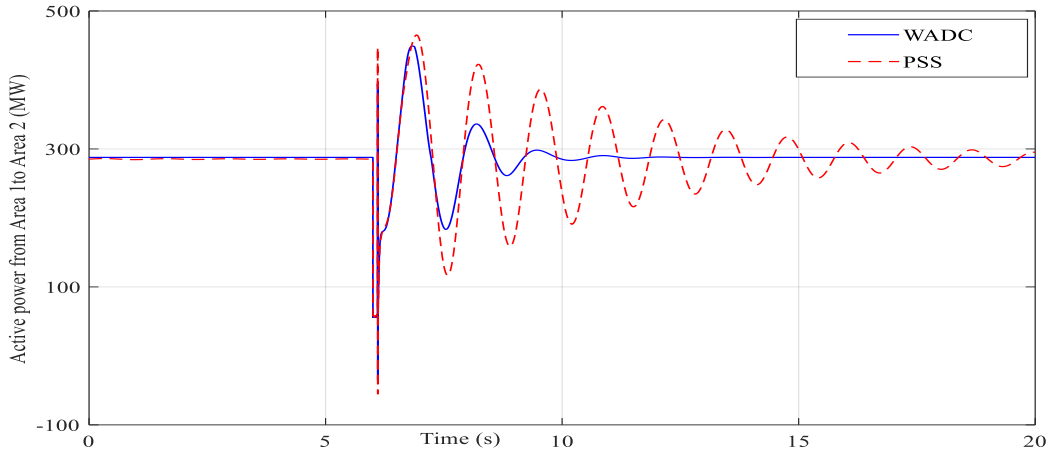

Figure 8. 20. Active power flow transmitted from Area 1 to Area 2 after short circuit

It is evident that with conventional PSS, the system is not well damped and the proposed controller stabilizes the system almost perfectly.

In the second case, the aggregated PV replaces G1 in Area 2. Controller performance is tested with a three phase short circuit applied to Bus 7 for 200 ms. Figure 8. 21 shows robust stability and performance of the proposed controller in this case, while conventional PSS tends to increase of oscillation.

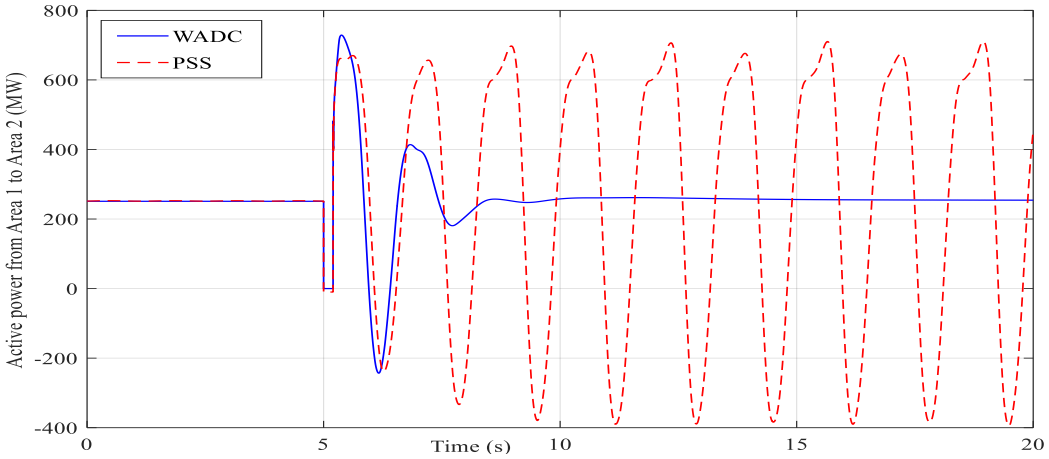

Figure 8. 21. Active power flow transmitted from Area 1 to Area 2 after short circuit

It should be mentioned that in all cases propagated time delay was considered.

CHAPTER 9 .CONCLUSIONS AND FUTURE WORK

9.1. Conclusion

Small signal oscillations in power systems are constantly present, because of the random load movements followed by generation reactions, reconfiguration of transmission network, and disturbances affecting the system. Since this phenomenon cannot be eliminated, the best approach power engineers can take is to introduce damping to those modes that compromise the system's operation and integrity.

Nowadays this task is performed to a great extent by the use of PSSs that are installed on specific generation plants and tuned to tackle particular oscillation modes. The fact is that the overall system damping cannot be improved by using the traditional approach such as local PSS with lack of general observability; wide area measurement and control are noticed as remedy.

Because of different uncertainty sources on power system such as variations in generation and load patterns and changes in the topology of networks, as well as uncertain renewable generation sources, power systems experience changes in operating conditions. The stabilizer needs to be adjusted for the frequency of interest for different operating points, then robust control is considered to overcome it.

Different robust control syntheses were designed and their robustness was proved in face of different uncertainties. The notable problem, which has ignored, is the order of controller state. Order of controller states has been reduced for acceptable computation time and memory during the implementation time. Reducing the order of the controller and introducing fixed order Lagrange parameter based controller were the solution to cope with mentioned problem. Risk of instability of reduced order control with different methods and square plant model (with same inputs and outputs) are the deficiency of recent solutions. Nonsmooth robust fixed order controller that in this thesis was introduced has dealt with the recent scarcities. This proposed approach avoids Lyapunov variables. The method supports even very large systems by moderating the size of optimization programs but the cost functions are nonsmooth and require special optimization techniques. The approach is effective in stability enhancement in transmission grids.

The sources of uncertainty in power system are studied and are classified to two major groups: Structured and unstructured uncertainties; both are modelled in this work. Unstructured uncertainty is known as frequency dependent and has important role to presenting uncertainty. It has been considered by transfer weighting function in frequency domain. In other works, this type of uncertainty is considered as PCM that cannot be as accurate as uncertain weighting function method.

Time delay as parametric uncertainty has been noticed. Propagated and fixed time delays have been considered to design the controller.

Centralized and decentralized architectures have been implemented to evaluate the efficient and reasonable performance of controllers. It has been proven that decentralized controller has better performance and stability in comparison with centralized one, due to special nominal model selection for decentralized controller and specific stability and performance criteria which have been considered in overall. Furthermore, for the centralized controller some reserve input and output channels were considered to deal with possible communication dropouts.

The advantage of the proposed approach is that it can be designed for full order model and is capable of considering both structured and unstructured uncertainties. Additionally, results show that the designed controller is robust following small and large disturbances and helps to stabilize the system, where local controllers, PSSs, fail to damp inter-area oscillations. The proposed robust controller can also guarantee rotor angle stability without local PSS.

9.2. Future Works

Although this research achieved promising results in applying wide area measurements and robust control techniques to the design of wide area control systems for the damping of power system oscillations, the work doesn't end here. The following aspects should be studied further:

1. Application of FACTS devices in the design of wide area damping control systems: The approach used in this research is to design wide area measurements based controllers that provide control actions through generator excitation systems supplemental to the action of local PSSs. For inter-area oscillations, FACTS devices may be preferred because they can change the power flow on tie lines directly and thus damp power oscillations more efficiently.

2. Coordination with protection and other control systems: In present transient stability programs, the existing protection systems and other control systems are not modeled. Therefore, the interactions between the designed control system and existing protection and other control systems were not studied in this research.
3. Design of fixed order μ synthesis robust controller: μ synthesis robust controller has merits because of simultaneous optimization of stability and performance criteria. Same structural constraints can be applied for this method and design of noticeable robust controller achieved.
4. Robustness evaluation to other unconsidered sources of uncertainty: every robust controller is designed for a subset and valid uncertainty sources. Uncertainty that is not considered in this research like wide area damping controller's error performance can be considered and tested.
5. Consideration of other nonsmooth optimization methods: This research used steepest decent for optimization. Other optimization methods like Mean Variance Mapping Optimization (MVMO), Genetic or Evolutionary Algorithms etc. can be of interest.

BIBLIOGRAPHY

[1] P. Kundur, “Power System Stability and Control”. New York: Mc Graw Hill, 1994.

[2] W. Mittelstadt, P. Krause, P. Overholt, J. Hauer, R. Wilson, and D. Rizy, “The DOE Wide Area Measurement System (WAMS) Project - Demonstration of dynamic information technology for the future power system”, in Proc. Fault and Disturbance Analysis/Precise Measurements in Power Syst. Conf., 1995,

[3] B. Chaudhuri and B. C. Pal, “Robust damping of multiple swing modes employing global stabilizing signals with a TCSC”, IEEE Transactions on Power Systems, vol. 19, pp. 499-506, 2004.

[4] B. Chaudhuri, R. Majumder and B. C. Pal, “Wide-area measurement based stabilizing control of power system considering signal transmission delay”, IEEE Transactions on Power Systems, vol. 19, pp. 1971-1979, 2004.

[5] D. Dotta , A. e Silva, and I. Decker, “Wide-area measurements-based two-level control design considering signal transmission delay”, IEEE Transactions on Power Systems, vol. 24, pp. 208-216, 2009.

[6] X. M. Mao, Y. Zhang, L. Guan, X. C. Wu and N. Zhang, “Improving power system dynamic performance using wide-area high-voltage direct current damping control”, IET Generation, Transmission & Distribution, vol. 2, pp. 245-251, 2008.

[7] P. Korba, M. Larsson and C. Rehtanz, “Detection of oscillations in power systems using Kalman filtering techniques”, Proceedings of IEEE Conference on Control Applications (CCA), 2003, pp. 183-188.

[8] J. F. Hauer, “Application of Prony analysis to the determination of modal content and equivalent models for measured power system response”, IEEE Transactions on Power Systems, vol. 6, no. 3, pp. 1062- 1068, Aug 1991.

[9] J. C. -H. Peng and N. -K. C. Nair, “Comparative assessment of Kalman Filter and Prony Methods for power system oscillation monitoring”, IEEE Power & Energy Society General Meeting, 26-30 July 2009, pp.1-8.

[10] D. S. Laila, M. Larsson, B. C. Pal and P. Korba, “Nonlinear damping computation and envelope detection using Hilbert transform and its application to power systems wide area monitoring”, IEEE Power & Energy Society General Meeting, 26-30 July 2009, pp.1-7.

[11] P. Tripathy, S.C. Srivastava, S.N Singh, “A modified TLS-ESPRIT-based method for low-frequency mode identification in power systems utilizing synchrophasor measurements”, IEEE Trans. Power Syst. 2011, 26, 719–727.

[12] A.J.Allen, M. Singh, E.Muljadi, S. Santoso, “Measurement-based investigation of inter-and intra-area effects of wind power plant integration”, Int. J. Elect. Power Energy Syst. 2016, 83, 450–457.

[13] J. Turunen, J. Thambirajah, M. Larsson, B.C. Pal, N.F. Thornhill, L.C. Haarla, W.W. Hung, A.M. Carter, and T. Rauhala, “Comparison of three electromechanical oscillation damping estimation methods”, IEEE Trans. Power Syst. 2011, 26, 2398–2407.

[14] S.N. Sarmadi., V. Venkatasubramanian, “Electromechanical mode estimation using recursive adaptive stochastic subspace identification”, IEEE Trans. Power Syst. 2014, 29, 349–358.

[15] G. Rogers, “Power system oscillations, Kluwer Academic”, 2000.

[16] M. Parsa and J. Toyoda, “Implementation of a hybrid power system stabilizer”, IEEE Transactions on Power Systems, vol. 4, no. 4, pp. 1463- 1469, 1989.

[17] H. Quinot, H. Bourles and T. Margotin, “Robust coordinated AVR PSS for damping large scale power systems”, IEEE Transactions on Power Systems, vol. 14, no. 4, pp. 1446-1451, 1999.

[18] G. J. Rogers, “The application of power system stabilizers to a multi generator plant”, IEEE Transactions on Power Systems, vol. 15, no. 1, pp. 350-355, 2000.

[19] N. Yang, Q. Liu and J.D. McCalley, “TCSC controller design for damping inter area oscillations”, IEEE Transactions on Power Systems, vol. 13, no. 4, pp. 1304-1310, 1998.

[20] W. Juanjuan, F. Chuang and Z. Yao, “Design of WAMS-based multiple HVDC damping control system”, IEEE Transactions on Smart Grid, vol. 2, pp. 363-374, 2011

[21] T. Knu¬ppel, J.N. Nielsen, K.H. Jensen, A. Dixon and J. Ostergaard, “Small-signal stability of wind power system with full-load converter interfaced wind turbines”, IET Renewable Power Generation, vol. 6, no. 2, pp. 79-91, 2012.

[22] Z. Miao, L. Fan, D. Osborn and S. Yuvarajan, “Control of DFIG based wind generation to improve inter area oscillation damping”, IEEE Transactions on Energy Conversion, vol. 24, no. 2, pp. 415-422, 2009.

[23] R. Preece, A. M. Almutairi, O. Marjanovic and J. V. Milanovic, “Damping of inter-area oscillations using WAMS based supplementary controller installed at VSC based HVDC line”, IEEE Trondheim PowerTech, 2011, pp. 1-8.

[24] R. Preece, J. V. Milanovic, A. M. Almutairi and O. Marjanovic, “Damping of Inter-Area Oscillations in Mixed AC/DC Networks Using WAMS Based Supplementary Controller”, IEEE Transactions on Power Systems, to be published.

[25] R. Preece, J. V. Milanovic, A. M. Almutairi and O. Marjanovic, “Probabilistic Evaluation of Damping Controller in Networks With Multiple VSC-HVDC Lines”, IEEE Transactions on Power Systems, vol. 28, no. 1, pp. 367-376, Feb. 2013.

[26] “IEEE Recommended Practice for Excitation System Models for Power System Stability Studies”, IEEE Std 421.5-2005 (Revision of IEEE Std 421.5-1992), pp.1-85, 2006

[27] M. Noroozian, L. Angquist, M. Gandhari, and G. Andersson, “Improving power system dynamics by series-connected FACTS devices”, IEEE Transaction on Power Delivery, vol. 12, pp. 1635–1641, 1997.

[28] X. M. Mao, Y. Zhang, L. Guan, X. C. Wu and N. Zhang, “Improving power system dynamic performance using wide-area high-voltage direct current damping control”, IET Generation, Transmission & Distribution, vol. 2, pp. 245-251, 2008.

[29] A. E. Leon, J. M. Mauricio, A. Gomez-Exposito and J. A. Solsona, “Hierarchical Wide-area Control of Power Systems Including Wind Farms and FACTS for Short-term Frequency Regulation”, IEEE Transactions on Power Systems, vol. 27, pp. 2084-92, 2012

[30] S. Zhang and V. Vittal, “Design of Wide-area Damping Control Robust to Transmission Delay using μ-Synthesis approach”, IEEE PES General Meeting, National Harbor, MD, USA, July 2014 , pp 1-5

[31] J. Deng, C. Li, X. Zhang, “Coordinated design of multiple robust FACTS damping controllers: A BMI-based sequential approach with multi-model systems”, IEEE Trans Power Sys, 2015, 30, (6), pp 3150-59

[32] J. Deng, X. Zhang, “Robust damping control of power systems with TCSC: A multi-model BMI approach with H2 performance”, IEEE Trans Power Sys, 2014, 29, (4), pp 1512-21

[33] S. Tossaporn, I. Ngamroo, “Robust power oscillation damper design for DFIG-based wind turbine based on specified structure mixed H_2/H_∞ control”, Renewable Energy, 2014, 66, pp 15-24

[34] H.G. Far, H. Banakar, P. Li, C. Luo, and B.T. Ooi, "Damping inter-area oscillations by multiple modal selectivity method", IEEE Trans Power Sys, 2009, 24, (2), pp 766-775

[35] B. P. Padhy, S. C. Srivastava and N. K. Verma, "Robust wide-area TS fuzzy output feedback controller for enhancement of stability in multimachine power system", IEEE Systems Journal, vol. 6, pp. 426-435,

[36] M. Mokhtari, F. Aminifar, D. Nazarpour and S. Golshannavaz, "Wide-Area Power Oscillation Damping With a Fuzzy Controller Compensating the Continuous Communication Delays", IEEE Transactions on Power Systems, to be published.

[37] H. Chen, H. Bai, M. Liu and Z. Guo, "Wide-area robust H_∞ control with pole placement for damping inter-area oscillations", Power Systems Conference and Exposition (PSCE'06), IEEE PES, 2006, pp. 2101-2108.

[38] Y. Li, C. Rehtanz, S. Rüberg, L. Luo and Y. Cao, "Wide-area robust coordination approach of HVDC and FACTS controllers for damping multiple inter area oscillations", IEEE Transactions on Power Delivery, vol. 27, pp. 1096-1105, 201212.

[39] Y. Zhang and A. Bose, "Design of Wide-Area Damping Controllers for Inter area Oscillations", IEEE Transactions on Power Systems, vol. 23, pp. 1136-1143, 2008.

[40] S. Ray and G. Venayagamoorthy, "Real-time implementation of a measurement-based adaptive wide-area control system considering communication delays", IET Generation, Transmission & Distribution, vol. 2, pp. 62-70, 2008

[41] S. Islam, P. X. Liu and A. El Saddik, "Wide-area measurement based power system for smart transmission grid with communication delay", IEEE International Instrumentation and Measurement Technology Conference (I2MTC), 2012, pp. 138-143.

[42] B. Chaudhuri, R. Majumder and B. C. Pal, "Wide-area measurement based stabilizing control of power system considering signal transmission delay", IEEE Transactions on Power Systems, vol. 19, pp. 1971-1979, 2004.

[43] A. Heniche and I. Kamwa, "Assessment of two methods to select wide-area signals for power system damping control", IEEE Transactions on Power Systems, vol. 23, pp. 572-581, 2008

[44] B. Chaudhuri and B. C. Pal, "Robust damping of multiple swing modes employing global stabilizing signals with a TCSC", IEEE Transactions on Power Systems, vol. 19, pp. 499-506, 2004.

[45] X. M. Mao, Y. Zhang, L. Guan, X. C. Wu and N. Zhang, "Improving power system dynamic performance using wide-area high-voltage direct current damping control", IET Generation, Transmission & Distribution, vol. 2, pp. 245-251, 2008.

[46] M. M. Farsangi, Y. H. Song and K. Y. Lee, "Choice of FACTS device control inputs for damping inter area oscillations", IEEE Transactions on Power Systems, vol.19, no.2, pp. 1135- 1143, May 2004.

[47] N. R. Chaudhuri, A. Domahidi, R. Majumder, B. Chaudhuri, P. Korba, S. Ray and K. Uhlen, "Wide-area power oscillation damping control in Nordic equivalent system", IET Generation, Transmission and Distribution, vol. 4, pp. 1139-1150, 2010.

[48] A.A. Abdlrahem, R. Hadidi, A. Karimi, P. Saraf , E. Makram, "Fixed-order loop shaping robust controller design for parametric models to damp inter-area oscillations", Electrical Power and Energy Systems 88 (2017) 164–17

[49] IEEE Recommended Practice for Excitation System Models for Power System Stability Studies IEEE Std 421.5-2005, 2005.

[50] E. V. Larsen and D. A. Swann, "Applying power system stabilizers - Part I, II and III", IEEE Trans. Power Apparatus and Syst., vol. 100, no. 6, pp. 3017-3046, June 1981.

[51] H. Renmu, M. Jin and D. Hill, “Composite load modelling via measurement approach”, IEEE Trans Power Sys, 2006, 21, (2), pp 663–672,

[52] P.C. Krause, O. Wasynczuk and S.D. Sudhoff, “Analysis of Electric Machinery”, IEEE Press, 2002.

[53] H. F. Latorre, M. Ghandhari, and L. Söder, “Active and reactive power control of a VSC-HVDC”, Electric Power Systems Research, vol. 78, pp. 1756-1763, 2008.

[54] P. E. Bjorklund, K. Srivastava, and W. Quaintance, “HVDC Light® Modeling for Dynamic Performance Analysis”, in PSCE '06, 2006.

[55] M. Suwan, T. Neumann, C. Feltesa and I. Erlich, “Educational Experimental Rig for Doubly-Fed Induction Generator based Wind Turbine”, IEEE Power and Energy Society General meeting, San Diego, USA, 2012

[56] F. Shewarega, I. Erlich and J.L. Rueda, “Impact of large offshore wind farms on power system transient stability”, IEEE/PES Power Systems Conference and Exposition, Seattle, WA, USA (2009)

[57] S. Kouro, J. I. Leon, D. Vinnikov, L. G. Franquelo, “Grid-Connected Photovoltaic Systems: An Overview of Recent Research and Emerging PV Converter Technology”, IEEE Industrial Electronics Magazine (Vol. 9,Issue: 1, March 2015)

[58] M.G. Villalva, J.R. Gazoli and E.R. Filho, “Comprehensive Approach to Modeling and Simulation of Photovoltaic Arrays”, in IEEE Transactions on Power Electronics, 2009 , Page(s): 1198 – 1208

[59] B.-K. Choi and H.-D. Chiang, “Multiple solutions and plateau phenomenon in measurement-based load model development: Issues and suggestions”, IEEE Trans Power Sys, 2009, 24, (2), pp 824–831

[60] B.-K. Choi and H.-D. Chiang, “Multiple solutions and plateau phenomenon in measurement-based load model development: Issues and suggestions”, IEEE Trans Power Sys, 2009, 24, (2), pp 824–831

[61] J. Ma, D. Han, R.-m. He, Z.-Y. Dong and. D. Hill, “Reducing identified parameters of measurement-based composite load model”, Power Systems, IEEE Transactions on,2008, 23, (1), pp. 76–83

[62] M. Jin, H. Renmu and D. Hill, “Load modelling by finding support vectors of load data from field measurements”, Power Systems, IEEE Transactions on, 2006, 21, (2), pp. 726–735

[63] P. Kundur, J. Paserba, et al, “Definition and Classification of Power System Stability”, IEEE Transactions on Power Systems, vol. 19, no.2. May 2004, pp. 1387-1401

[64] P. Kundur, D. C. Lee, J. P. Bayne and P. L. Dandeno, “Impact of tur-bine generator controls on unit performance under system disturbance conditions”, IEEE Trans. Power Apparatus and Systems, vol. PAS-104, pp. 1262-1267, June 1985

[65] Q. B. Chow, P. Kundur, P. N. Acch ione, and B. Lautsch, “Improving nuclear generating station response for electrical grid islanding”, IEEE Trans. Energy Conversion, vol. EC-4, pp. 406–413, Sept. 1989.

[66] P. Kundur, “A survey of utility e experiences with power plant response during partial load rejections and system disturbances”, IEEE Transaction Power Apparatus and Systems, vol. PAS-100, pp. 2471–2475, May 1981

[67] J. Bucciero, and M. Terbrueggen, “Interconnected power systems dynamic tutorial”, Electric Power Research Institute Tutorial TR-107726-R1, 1998.

[68] G. Rogers, “Demystifying power system oscillations”, IEEE on Computer Applications Power1996; 9(3): 30–35.

[69] L. Vanfretti, J. Chow, “Computation and analysis of power system voltage oscillations from inter area modes”, Proceedings of the IEEE PES General Meeting, 2009.

[70] L. Vanfretti, J. Chow, “Analysis of power system oscillations for developing synchrophasor data applications”, accepted for 2010 IREP Symposium – Bulk Power System Dynamics and Control, 2010.

[71] C. C4.601, “Wide Area Monitoring and Control for transmission capability enhancement”, Report, August 2007

[72] A.G. Phadke, “Synchronized phasor measurements in power systems”, Computer Applications in Power, IEEE, vol: 6, Issue: 2, Year: 1993.

[73] P. Walter Cattaneo, “The anti-aliasing requirements for amplitude measurements in sampled systems”, Elesvier – ‘Nuclear instrumentation and methods in physics research section A: Accelerators, spectrometer, detectors and associated equipment’, vol: 481, Issue: 1-3, Year: 2002, page: 632-636.

[74] P. Walter Cattaneo, “The anti-aliasing requirements for area and timing measurements in sampled systems”, Elesvier - ‘Signal processing’, vol: 82, Issue:3, Year:2002, page: 407-416.

[75] T. McAleer, Harold, “A New Look at the Phase-Locked Oscillator”, Proceedings of the IRE, vol: 47, Issue: 6, Publication Year: 1959

[76] K.E. Martin, D. Hamai, M.G. Adamiak and others, “Exploring the IEEE Standard C37.118–2005 Synchro phasors for Power Systems”, IEEE Transactions on Power Delivery, vol: 23, Issue: 4, Publication Year: 2008

[77] I. Kamwa, J. Beland, G. Trudel, R. Grondin, C. Lafond and D. McNabb, “Wide-Area Monitoring and Control at Hydro-Que´bec: Past, present and future”, IEEE Power Engineering Society General Meeting 2006.

[78] J. Chow, J. Sanchez-Gasca, H. Ren Hand S. Wang, “Power system damping controller design using multiple input signals”, IEEE Control Systems Magazine 2000; 20(4): 82–90.

[79] I. Kamwa., A. Heniche, G. Trudel, M. Dobrescu, R. Grondin and D. Lefebvre, “Assessing the technical value of FACTS-based wide-area damping control loops”, IEEE Power Engineering Society General Meeting 2005.

[80] Y. Chompoobutrgool, L. Vanfretti*, M. Ghandhari, “Survey on power system stabilizers control and their prospective applications for power system damping using Synchro phasor-based wide-area systems”, Trans. Electr. Power 2011; Published online 14 February 2011 in Wiley Online Library

[81] I. Kamwa, R. Grondin and Y. Hebert, “Wide-Area Measurement based stabilizing control of large power systems – A decentralized/hierarchical approach”, IEEE Transactions on Power System 2001; 16(1): 136–153.

[82] I. Kamwa, L. Gerin-Lajoie and G. Trudel, “Multi-loop power system stabilizers using wide-area synchronous phasor measurements”, Proceedings of the American Control Conference 1998; 2963–2967.

[83] X. Xie and C. Lu, “Optimization and coordination of Wide-Area damping controls for enhancing the transfer capability of interconnected power systems”, Electric Power Systems Research 2008; 78: 1099–1108.

[84] X. Xie, J. Xiao, C. Lu and Y. Han, “Wide-Area stability control for damping inter area oscillations of interconnected power systems”, Proceedings of the IEEE Generation, Transmission and Distribution 2006; 153(5): 507–514.

[85] Duc-H. Nguyen, L. Dessaint, A. Okou, I. Kamwa, “A power oscillation damping control scheme based on bang-bang modulation of FACTS signals”, IEEE Transactions on Power System 2010; 25(4): 1918–1927.

[86] C. W. Taylor, D. C. Erickson, K. E. Martin, R. E. Wilson, and V. Venkatasubramanian, “WACS - Wide-area stability and voltage control system: R & D and online demonstration”, Proc. of the IEEE, vol. 93, no. 5, pp. 892-906, May 2005.

[87] V. Arcidiacono, E. Ferrari, R. Marconato, J. DosGhali, D. Grandez, “Evaluation and Improvement of Electromechanical Oscillation Damping by Means of Eigenvalue-Eigenvector Analysis. Practical Results in

the Central Peru Power System", IEEE trans. on power apparatus and System s, Vol. PAS-99, pp. 769-778, March/April 1980

[88] N. Martins and L. T. G. Lima, "Determination of suitable locations for power system stabilizers and Static VAR Compensators for damping electromechanical oscillations in large scale power systems", IEEE Trans. Power Syst., vol. 5, pp. 1455–1469, Nov. 1990.

[89] P. Pourbeik and M. J. Gibbard, "Damping and synchronizing torques induced on generators by FACTS stabilizers in mu ltimachine power systems", IEEE Trans. Power Syst., vol. 11, pp. 1920–1925, Nov. 1996.

[90] R. urramazan, S. Vaez-Zadeh, H. Nourzadeh, "Power system MIMO identification for coordinated design of PSS and TCSS controller", IEEE Power Engineering Society General Meeting2007

[91] A. M. A. Hamdan and A. M. Elabdalla, "Geometric measures of modal controllability and observability of power systems models", Electric Power System Research, vol. 15, pp. 147–155, 1988.

[92] K. Zhou,and C. Doyle, "Essentials of Robust Control', Prentice-Hall", (1998)

[93] S. Skogestad and I. Postlethwaite, "Multivariable Feedback control", 2nd ed., 2005.

[94] Ricardo S. Sánchez-Peña and Mario Sznaier, "Robust Systems: Theory and Applications", Wiley, New York, 1998,

[95] Kang-Zhi Liu, Yu Yao, "Robust Control: Theory and Applications", October 2016

[96] A. Pierre, N. Dominikus, "Nonsmooth H_∞ Synthesis", European IEEE Trans. Aut. Control, 51 (2006), pp. 71–86

[97] A. Pierre, N. Dominikus, "Nonsmooth Optimization for Multidisk H_∞ Synthesis", European Journal of Control, 2006, 12, (3), pp 229-244.

[98] L. Philipp, A. Mahmood, and B. Philipp, "An improved refinable rational approximation to the ideal time delay", IEEE Trans. Circuit Syst., vol. 46, no. 5, pp. 637-640, May 1999.

[99] H. Wu, K.S. Tsakalis and G. T. Heydt, "Evaluation of Time Delay Effects to Wide-Area Power System Stabilizer Design", IEEE Trans. on Power Syst., Vol. 19, NO. 4, pp 1935-1941, Nov. 2004

[100] B. Naduvathuparambil, M.C. Valenti, and A. Feliachi, "Communication Delays in Wide-area Measurement Systems", Proceedings of the Thirty-Fourth Southeastern Symposium on System Theory, pp.118- 122, 2002.

[101] B.-K. Choiand H.-D Chiang, "Multiple solutions and plateau phenomenon in measurement-based load model development: Issues and suggestions", IEEE Trans Power Sys, 2009, 24, (2), pp 824–831

[102] V. Krishnan, S. Srivastava, S. Chakrabarti, "A Robust Decentralized Wide Area Damping Controller for Wind Generators and FACTS Controllers Considering Load Model Uncertainties", IEEE Trans on Smart Grid, 360-372 (2018)

[103] M. S.Sadabadi, A. Karimi and H. Karimi, "Fixed-order decentralized/ distributed control of islanded inverter-interfaced micro grids", Control Engineering Practice, 45, 174-193.(2015)

[104] S. Dahal, N. Mithulananthan and T. Kumar Saha, "Assessment and Enhancement of Small Signal Stability of a Renewable- Energy- Based Electricity Distribution System", IEEE Trans on sustainable energy, vol.3, no.3, July 2012 407

[105] M. Maherani, I. Erlich, "Robust MIMO Centralized Fixed Order Wide Area Damping Controller", Proc. Int IEEE PES ISGT, Sarajevo, Bosnia and Herzegovina (2018)

[106] M. Maherani, I. Erlich, "Robust Decentralized Fixed Order Wide Area Damping Controller", Proc. Int. Conf. The 10th Symposium on Control of Power and Energy Systems (CPES2018), Tokyo, Japan(2018)

[107] Y. T.Tan, “Impact of power system with a large penetration of photovoltaic generation”, Ph.D. dissertation, Inst. of Sci. and Technol., The Univ. of Manchester, Manchester, U.K., 2004.

[108] W. Du, H. F. Wang, and L.-Y. Xiao, “Power system small-signal stability as affected by grid-connected photovoltaic generation”, Eur. Trans. Electr. Power, vol. 21, no. 5, pp. 688–703, Jul. 2011.

[109] R. Shah, N. Mithulananthan, A. Sode-Yome, and K. Y. Lee, “Impact of large-scale PV penetration on power system oscillatory stability”, in Proc. IEEE Power Energy Soc. General Meeting, Minneapolis, MN, Jul.25–29, 2010, pp. 1–7.

[110] R. Shah, N. Mithulananthan, and K. Y. Lee, “Contribution of PV systems with ultra-capacitor energy storage on inter-area oscillation”, in Proc. IEEE Power Energy Soc. General Meeting, Detroit, MI, Jul. 24–28, 2011, pp. 1–8.

APPENDIX A

Two Area, Four Machine System Parameters

The system consists of two similar areas connected by a weak tie. E ach area consists of two coupled units, each having a rating of 900 MVA and 20 kV. The generator parameters in per unit on the rated MVA and kV base are as follows:

x_d = 1.8 [p.u.]

x_q =1.7 [p.u.]

$x_{d'}$ = 0.3 [p.u.]

$x_{q'}$ =0.55 [p.u.]

r_a = 0.0025 [p.u.]

$T_{d'}$ = 8.0 [s]

$T_{q'}$ = 0.4 [s]

H = 6.5 for G1 and G2 [kg m^2]

H = 6.175 for G3 and G4 [kg m^2]

K_D = 0

Each step up transformer has an impedance of 0+j0.15 per unit on 900 MVA and 20/30 kV base, and has an off nominal ratio of 1.0.

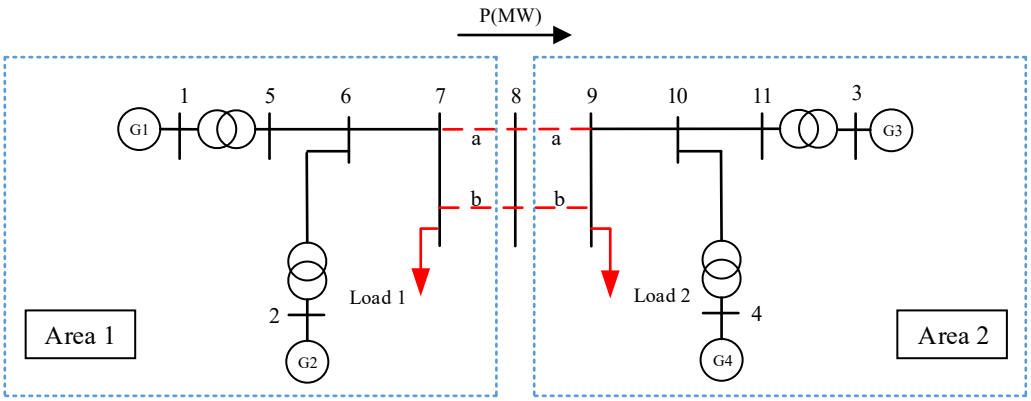

Figure A. 1. Two area, four machine test system

The transmission system nominal voltage is 230 kV. The line lengths are identified in Figure A. 1. The parameters of the lines in per unit on 100 MVA, 230 kV base are:

r = 0.0001 [p.u./km]

x_l = 0.001 [p.u./km]

b_c = 0.00175 [p.u./km]

The system is operating with Area 1 exporting 400 MW to Area 2, and the generating units are loaded as follows:

G1: P = 700 MW, Q = 185 Mvar, E_t = 0 1.03∠20.2

G2: P = 700 MW, Q = 235 Mvar, E_t = 1.01∠10.5

G3: P = 719 MW, Q = 176 Mvar, E_t = 1.03∠-6.8

G4: P = 700 MW, Q = 202 Mvar, E_t = 1.01∠-17.0

The loads and reactive power supplied (Q_c) by the shunt capacitors at Buses 7 and 9 area as follows:

Bus 7: P_l = 976 MW, Q_l = 100 Mvar, Q_c = 200 Mvar

Bus 9: P_l = 1767 MW, Q_l = 100 Mvar, Q_c = 350 Mvar

Self-excited dc exciter

K_A = 20.0

T_A = 0.055

T_E = 0.36

K_F = 0.125

T_F = 1.8

A_{ex} = 0.0056

B_{ex} = 1.075

T_R = 0.05

APPENDIX B

IEEE 39 Bus System Parameters

Power Flow Data

The power flow data for this system is divided in:

- Bus Data
- Load Data
- Generation Data
- Branch Data

Bus Data

Table B. 1 represents the bus data. The nomenclature for the table headings is:

Bus Number	Number of the bus
Bus Name	Alphabetic identifier for each bus
Bus Base kV	Bus base voltage, in [kV]
Bus Type	Bus type code: (1) Load Bus, PQ bus (2) Generator Bus, PV bus (3) Swing Bus
Bus Voltage	Voltage magnitude, in [p.u.]
Bus Angle	Voltage angle, in [deg]

Table B. 1. IEEE 39-Bus Test System: Bus Data

Bus Number	Bus Base [kV]	Bus Type	Bus Voltage [p.u.]	Bus Angle [deg]
1	345	1	1.048	-9.426
2	345	1	1.050	-6.885
3	345	1	1.034	-9.728
4	345	1	1.011	-10.529
5	345	1	1.016	-9.376
6	345	1	1.017	-8.681
7	345	1	1.006	-10.841
8	345	1	1.005	-11.337
9	345	1	1.032	-11.151
10	345	1	1.023	-6.314
11	345	1	1.020	-7.123
12	345	1	1.007	-7.135
13	345	1	1.020	-7.018
14	345	1	1.018	-8.662
15	345	1	1.019	-9.059
16	345	1	1.034	-7.655
17	345	1	1.036	-8.647
18	345	1	1.034	-9.485
19	345	1	1.050	-3.039
20	345	1	0.991	-4.447
21	345	1	1.033	-5.257
22	345	1	1.050	-0.818
23	345	1	1.045	-1.016
24	345	1	1.039	-7.536
25	345	1	1.058	-5.513
26	345	1	1.053	-6.774
27	345	1	1.039	-8.784
28	345	1	1.050	-3.266
29	22	2	1.050	-0.509
30	22	2	1.047	-4.469
31	22	3	0.982	0.000
32	22	2	0.983	1.632
33	22	2	0.997	2.176
34	22	2	1.012	0.741
35	22	2	1.049	4.138
36	22	2	1.063	6.829
37	22	2	1.027	1.265
38	22	2	1.026	6.55
39	22	2	1.030	-10.956

Load Data

Table B. 2 represents the load data. The nomenclature for the table headings is:

Bus Number — Number of the Bus

P — Real component of the load, in [MW]

Q — Reactive component of the load, in [Mvar]

Table B. 2. IEEE 39 Bus Test System: Load Data

Load	Bus	*P* [MW]	*Q* [Mvar]
Load 03	Bus 03	322.0	2.4
Load 04	Bus 04	500.0	184.0
Load 07	Bus 07	233.8	84.0
Load 08	Bus 08	522.0	176.0
Load 12	Bus 12	7.5	88.0
Load 15	Bus 15	320.0	153.0
Load 16	Bus 16	329.0	32.3
Load 18	Bus 18	158.0	30.0
Load 20	Bus 20	628.0	103.0
Load 21	Bus 21	274.0	115.0
Load 23	Bus 23	247.5	84.6
Load 24	Bus 24	308.6	-92.2
Load 25	Bus 25	224.0	47.2
Load 26	Bus 26	139.0	17.0
Load 27	Bus 27	281.0	75.5
Load 28	Bus 28	206.0	27.6
Load 29	Bus 29	283.5	26.9
Load 31	Bus 31	9.2	4.6
Load 39	Bus 39	1104.0	250.0

Generation Data

Table B. 3 represents the generation data. The nomenclature of the table headings is:

Bus Number — Number of the bus

P — Generator real power output, in [MW]

Q — Generator reactive power output, in [Mvar]

Table B. 3. IEEE 39-Bus Test System: Generation Data

Bus	*P* [MW]	*Q* [Mvar]
29	0	100
30	250	136.20
31	520.81	170.34
32	650	175.9
33	632	103.34
34	508	164.39
35	650	204.84
36	560	96.88
37	540	-4.43
38	830	-19.38
39	1000	-68.45

Branch Data

Table B. 4 represents the branch (transmission lines and transformers) data. The nomenclature for the table headings is:

Number — Number of the branch

From Bus — Branch starting bus number

To Bus	Branch ending bus number
Resistance (p.u.)	Branch resistance, in [p.u.]
Reactance (p.u.)	Branch reactance, in [p.u.]
Susceptance (p.u.)	Branch total charging susceptance, in [p.u.]

Table B. 4. IEEE 39-Bus Test System: Branch Data

From Bus	**To Bus**	***r* [p.u./m]**	***x* [p.u./m]**	***b* [p.u./m]**
1	2	0.0035	0.0411	0.6987
1	39	0.0010	0.025	0.7500
2	3	0.0013	0.0151	0.2572
2	25	0.0070	0.0086	0.1460
3	4	0.0013	0.0213	0.2214
3	18	0.0011	0.0133	0.2138
4	5	0.0008	0.0128	0.1342
4	14	0.0008	0.0129	0.1382
5	6	0.0002	0.0026	0.0434
5	8	0.0008	0.0112	0.1476
6	7	0.0006	0.0092	0.1130
6	11	0.0007	0.0082	0.1389
7	8	0.0004	0.0046	0.0780
8	9	0.0023	0.0363	0.3804
9	39	0.0010	0.0250	1.2000
10	11	0.0004	0.0043	0.0729
10	13	0.0004	0.0043	0.0729
13	14	0.0009	0.0101	0.1723
14	15	0.0018	0.0217	0.3660
15	16	0.0009	0.0094	0.1710
16	17	0.0007	0.0089	0.1342
16	19	0.0016	0.0195	0.3040
16	21	0.0008	0.0135	0.2548
16	24	0.0003	0.0059	0.0680
17	18	0.0007	0.0082	0.1319
17	27	0.0013	0.0173	0.3216
21	22	0.0008	0.0140	0.2565
22	23	0.0006	0.0096	0.1846
23	24	0.0022	0.0350	0.3610
25	26	0.0032	0.0323	0.5130
26	27	0.0014	0.0147	0.2396
26	28	0.0043	0.0474	0.7802
26	29	0.0057	0.0625	1.0290
28	29	0.0014	0.0151	0.0249

Dynamic Data

The dynamic data are classified as:

- Generator Dynamic Data
- Exciter Data
- Governor Data

Appendix B

Generator Dynamic Data

Table B. 5 represents the generator dynamic data.

The nomenclature for the table headings is:

x_d, x'_d Generator direct axis synchronous and transient reactance, in [p.u.];

x_q, x'_q Generator quadrature axis synchronous and transient reactance, in [p.u.];

r_a Generator armature resistance, in [p.u.];

T'_d, T'_q Direct and quadrature axis transient field winding time constants.

H Generator inertia constant in [kg m^2].

Table B. 5. IEEE 39-bus Test System: Generator Dynamic Data

No	H in [kg m^2]	r_a in [p.u.]	x'_d in [p.u.]	x'_q in [p.u.]	x_d in [p.u.]	x_q in [p.u.]	T'_{d0} in [s]	T'_{q0} in [s]	x_l in [p.u.]	x'' in [p.u.]	T''_{d0} in [s]	T''_{q0} in [s]
1	500	0.000	0.006	0.008	0.020	0.019	7.000	0.70	0.003	0.004	0.05	0.035
2	30.3	0.0000	0.0697	0.1700	0.2950	0.2820	6.560	1.500	0.0350	0.0500	0.050	0.035
3	35.8	0.0000	0.0531	0.0876	0.2495	0.2370	5.700	1.500	0.0304	0.0450	0.050	0.035
4	28.6	0.0000	0.0436	0.1660	0.2620	0.2580	5.690	1.500	0.0295	0.0350	0.050	0.035
5	26.0	0.0000	0.1320	0.1660	0.6700	0.6200	5.400	0.440	0.0540	0.0890	0.050	0.035
6	34.8	0.0000	0.0500	0.0814	0.2540	0.2410	7.300	0.400	0.0224	0.0400	0.050	0.035
7	26.4	0.0000	0.0490	0.1860	0.2950	0.2920	5.660	1.500	0.0322	0.0440	0.050	0.035
8	24.3	0.0000	0.0570	0.0911	0.2900	0.2800	6.700	0.410	0.0280	0.0450	0.050	0.035
9	34.5	0.0000	0.0570	0.0587	0.2106	0.2050	4.790	1.960	0.0298	0.0450	0.050	0.035
10	42.0	0.0000	0.0310	0.0500	0.1000	0.0690	10.200	0.000	0.0125	0.0250	0.050	0.035

Exciter Data

Table B. 6 represents the exciter data. The nomenclature for the table headings is:

K_A Amplifier gain, in [p.u.]

T_A Amplifier time constant, in [s]

T_E Exciter time constant, in [s]

K_F Regulator gain, in [p.u.]

T_F Regulator time constant, in [s]

A_{EX}, B_{EX} Derived saturation constants for rotating exciters

V_{Rmax} Regulator maximum output, in [p.u.]

V_{Rmin} Regulator minimum output, in [p.u.]

E_{fdmax} Maximum field voltage, in [p.u.]

E_{fdmin} Minimum field voltage, in [p.u.]

Table B. 6. IEEE 39-bus Test System: Exciter Data

Gen	**30**	**31**	**32**	**33**	**34**	**35**	**36**	**37**	**38**	**39**
K_A **[p.u.]**	40	19.576	15.596	40	20	40	25	25	30	8.5
T_A **[s]**	0.03	0.016	0.048	0.05	0.03	0.05	0.02	0.02	0.01	0.05

The following exciter parameter values were common for all the generators:

T_E 0.36

K_F 0.1

T_F 0.36

A_{EX} 0.0056

B_{EX} 1.07

V_{Rmax} 8.0

V_{Rmin} -8.0

E_{fdmax} 8.85

E_{fdmin} -8.8

Governor Data

Table B. 7 represents the governor data. The nomenclature for the table headings is:

R Turbine droop setting, in [%]

T_G Governor time constant, in [s]

Table B. 7. IEEE 39-bus Test System: Governor Data

Gen	**30**	**31**	**32**	**33**	**34**	**35**	**36**	**37**	**38**	**39**
R **[%]**	3.54	3.85	3.16	3.16	2.318	3.16	3.03	3.03	3.50	5.39
T_G **[s]**	1.82	6.66	5	5	20	5	2	2	10	25

DOI: 10.17185/duepublico/70718
URN: urn:nbn:de:hbz:464-20191112-150705-8